UNIVERSITY OF CINCINNATI

August 18, 19 95

I, ZHONGMING ZHANG,
hereby submit this as part of the requirements for the degree of:

Doctor of Philosophy

in Chemistry

It is entitled Computer Simulations of Solid Electrode Materials

Approved by:

COMPUTER SIMULATIONS OF SOLID ELECTRODE MATERIALS

A Dissertation submitted to the

Division of Graduate Studies and Research
of the University of Cincinnati

in partial fulfillment of the
requirements for the degree of

DOCTOR OF PHILOSOPHY

in the Department of Chemistry
of the College of Arts and Sciences

1995

by

Zhongming Zhang
B.S., Ocean University Of Qingdao, China, 1987

Committee:
Thomas L. Beck, Chair
Bruce S. Ault
Joseph A. Caruso

ABSTRACT

This dissertation focused on theoretical studies of the properties and mechanisms of electrode materials by using molecular dynamics and Monte Carlo methods.

In the first part of this work, we presented theoretical studies of finite systems which exhibit superionic behavior in the bulk. Molecular dynamics simulations were performed on $(Ag_2Se)_n$ ionic clusters to investigate microscopic mechanisms for the onset of diffusion. No dramatic superionic behavior was observed when the size of cluster was small. However, the $(Ag_2Se)_{41}$ cluster presented superionic bebavior above 200K. On the time scales from 50ps to 250ps, the van Hove self-correlation function showed that there was a jumping mechanism when silver ions diffused at 264K. The results also showed that the $(Ag_2Se)_{80}$ cluster displayed more distinguished bulk-like superionic bebavior than the $(Ag_2Se)_{41}$ cluster. But, no superionic behavior was exhibited in the $(AgI)_{60}$ cluster, while the AgI crystal is a superionic conductor.

The second part of my thesis focused on studying structural and dynamical properties of self assembled monolayers on metal surfaces. We

started by discussing the driving forces which lead to ordering behavior at the solid-liquid interfaces. Monte Carlo simulations on the origins of tilt behavior in self assembled model rigid oligomers were presented. Finally, extensive molecular dynamics simulations of organic thiol monolayers self assembled on gold were performed. Dynamics simulations of a 4-mercapto-phenyl-phthalimide (4-MPP) self assembled monolayer on a Au(111) surface were performed. The structure and dynamics of the interphase were simulated at several surface densities and for two bonding geometries, one with the sulfur atom sp hybridized and one with sp^3 hybridization. The computed tilt angle for a high density monolayer was 23° for the sp hybridized case, in good agreement with the experimental results. The nature of the sulfur-metal bond strongly affected the observed tilt angle, and the angle increased with decreasing surface density. The distribution of rotation angles of the imide ring was broad. The molecules of the interphase exhibited substantial thermal fluctuations at room temperature, but did not freely rotate.

DEDICATION

To Mom and Dad:

for your unconditional love and support.

ACKNOWLEDGMENTS

First and foremost, I would like to thank my advisor, Prof. Thomas L. Beck, for his guidance, enthusiasm, encouragement, especially his cool throughout this work. Working with him itself has been a true inspiration.

I would like to acknowledge Prof. F. J. Boerio of Department of Materials Science and Engineering for a very enjoyable collaboration on the last project. I also would like to thank Prof. Bruce Ault and Prof. Joseph Caruso for serving on my committee.

I am grateful to all my friends: Qing Yu, Hebi Bai, Micheal Merrick, etc. for all the laughs and wouderful times that we shared. Especially, I thank Li Jun for your love from the other facet of the globe; and Dr. Yun Xiong for being a sister I always wanted to have.

And finally, I would like thank my brother, Zhongwei, for always being there for me.

Contents

List of Figures

List of Tables

Chapter 1

Introduction

The development of new materials and modification of known materials has always pioneered new technologies. Electrode materials have a wide range of applications in electrical/optical devices,[1-3] chemical and gas sensors,[4,5] surface protections, energy conversion and storage,[3] lubricants,[6] microelectronics, adhesion,[7] *etc.* In the last twenty years, they have been the subject of intensive research both experimantally and theoretically. Researchers have tried to understand the nature of diffusion mechanisms and phase transitions, as well as the driving forces which lead to such behavior. Studying their mechanisms and phenomena will provide us with the knoweledge of how electrodes work. This understanding will not only lead us to modify and optimize the properties of a given material, but will also help us to search for new structures and compounds that have useful properties. Most importantly, people will have the ability to design and construct the desired structure and properties of electrodes.

Crystal ionic conductors have been known for many years. But their applications have been limited due to their low ionic conductivity in the solid state. In 1914, Tubandt and Lorenz[8] discovered an unusually high ionic conductivity of α-AgI in the solid state. Later, many other ionic compounds were also found to have high ionic conductivity with high melting temperatures. These groups of ionic crystals are characterized by large

ionic conductivity and a small activation energy for one type of ion (either anion or cation) to move relatively freely in the stable sublattice of the other ion. Superionic conductors are well known good solid electrolytes. There have been lots of studies on their diffusion mechanisms in the crystal structures.[9-13] But superionic behaviors in glasses and highly disordered materials are not fully understood yet. Recently, besides trying to discover new materials for electrolytes, interest in chemically modified electrodes has grown rapidly due to their important applications. Especially, researchers have found that molecules can self assemble into monolayers on metal surfaces and form stable and dense structures.[14] These are called self-assembled monolayers (SAMs). They provide very exciting methods to generate special and unique properties on electrode surfaces. Although many experimental and theoretical efforts have been applied to study SAMs, there is still a lack of understanding of the underlying mechanism of the chemisorption process. My research has been focused on properties and mechanisms of both types of electrode materials, *i.e.* superionic conducters with short-ranged order and molecular monolayer modified metal electrodes.

Superionic conductors are also called fast-ion conductors(FIC). Besides AgI, many other ionic crystals have been found to have superionic behavior,

like Ag_2Se, Ag_2S, PbF_2, *etc.* More recently, superionic phenomena have also been observed in glassy materials and polymers.[15-17]

Different experimental methods have been used to study superionic behavior. They include: trace diffusion, X-ray powder diffraction,[18] NMR spectroscopic methods, neutron scattering,[19-21,15] Raman scattering,[22,17] extanded x-ray fine Structure (EXAFS),[12,23] etc. Single-Crystal Neutron Diffraction experiment performed by Cava and coworkers[24] and Quasielastic Neutron Scattering experiment conducted by Funke[20] have provided a wealth of information on structural and dynamical properties of superionic conductors.

Because superionic conductors combine phenomena that are observed in liquids and solids in an interesting way, there has been much theoretical work studying the mechanism of conduction and phase transitions. Over the past 20 years, molecular dynamics (MD) and Monte Carlo (MC) methods have been successfully used in studying superionic behaviors in bulk systems.[25,26,21,27,28] The results have been able to accurately reproduce the structural properties and dynamical properties of the real systems.

Intensive research has been conducted towards the most popular superionic conductor α-AgI. AgI has a body centered structure below its melting point. Above 420K, the I^- ions form a bcc sublattice and the Ag^+

ions become mobile and have a liquid-like diffusion constant. Both neutron inelastic scattering experiments and molecular dynamics[21] simulations confirmed that Ag^+ ions diffuse by jumps between tetrahedral sites. The mean residence time was predicted to be 2.97 psec.

Like α-AgI, α-Ag_2Se is another superionic conductor with a bcc structure. But the concentration or number of Ag^+ ions in each unit cell is doubled in α-Ag_2Se. Because diffusion corresponds to ions moving between occupied sites and empty sites, more Ag ions in each unit cell means less empty sites, but also means more ions are able to contribute to ionic conductivity. This feature makes α-Ag_2Se more unique to study its mechanism.

Rino, *et al.*[27] studied structural and dynamical correlations in superionic and molten Ag_2Se by using the molecular dynamics method. They found that the calculated temperature dependence of the self-diffusion constant of silver and the Haven's ratio were in good agreement with the experimental results.

Neutron scattering experments conducted by Dianoux and coworkers[15] found that small clusters of AgI with tetrahedral coordination existed in the $AgPO_3$ based glasses. The radii of the clusters are of the order of 4 Å to 20 Å.

It's our interest to investigate the microscopic mechanisms for the onset of diffusion in a finite system and gain insights into superionic conducting mechanisms in glassy materials. One advantage of studying the clusters is that the simulations are less computationally demanding than for the system with periodic boundary conditions.

The second part of my thesis involves studying structural and dynamical properties of self assembled monolayers on metal surfaces. Recently, attaching molecules to metal (Au, Ag, Pt,...) electrode surfaces has been an intensive research and exploration area.[14] By varying different molecules to modify electrodes, people have begun to design and control the molecular character of the electrode interface via attached molecular layers.[29]

Techniques that have been applied to construct organized, oriented assemblies of molecules include Langmuir-Blodgett (L-B) monolayer transfer and molecular self-assembly (SAM). Especially, SAM is probably the most promising method to construct stable, ordered, and oriented monolayers on electrode surfaces. Unique or special molecular functionality can be fabricated by special molecular architectures. The newest development in electrode materials is modification of electrode surfaces with polymer films.[30,31] Among the variety of these materials, 'conducting polymers' have generated the highest interest. These materials have unusual properties

from semi-conducting to near-metallic behavior.[29] These systems offer a whole new range of potential electrode materials. And in recent years, intensive research has been conducted to study their behavior in electrochemical systems. Also by using charged and ordered membrane assemblies deposited directly on glassy carbon electrodes by the Langmuir-Blodgett (L-B) method, ion-channel mimetic sensors were developed.[29]

It is well known that soaking gold in a solution containing long alkane chains can cause spontaneous chemisorption of molecules on the gold surface. Extensive study, both experimental and theoretical, has been focused on understanding molecular ordering of alkane chains on gold substrates. It is believed that the alkane chains form a dense and stable monolayer on gold surfaces with tilt angles of 20° to 30°.[32-35]

Until recently, little study has been conducted on monolayers with complex structures such as aromatic rings and imide rings. Miller and coworkers[36] performed an interesting experiment and found that more complex long rigid oligoimides can also self assemble on a gold surface and are surprisingly stable to electrochemical processes in the interphase. The average tilt angle was determined to be around 60° from the surface normal. The surface density was calcalated to be 175 $Å^2$ / molecule. According to the surface density and the tilt angle, a molecular structure of the monolayer

was proposed.

Professor Boerio, from Department of Materials Science and Engineering, University of Cincinnati, is interested in modifying metal surfaces with spontaneous adsorption of organosulfur monolayers. His particular interest is in using these monolayers as adhesion promoters for polyimide-to-metal bonding, while these systems are also of electrochemical relevance.[36] The molecule of interest is 4-MPP (4-mercapto-phenyl-phthalimide). By using surface-enhanced Raman scattering (SERS), reflection-absorption infrared spectroscopy (RAIR), and X-ray photoelectron spectroscopy (XPS), they found that 4-MPP molecules formed an oriented monolayer on the gold surface with a tilt angle of 21° from the surface normal. No preferred rotational angle for the imide ring was found. (See Appendix B)

Although many calculations have been performed on monolayers on surfaces, it is still not clear what are the driving forces for the orientation behavior in the monolayers. And there is no complete understanding of the chemisorption process on the metal surfaces. For example, to which site of the Au(111) lattice is the sulfur atom bonded? To answer these questions, the second part of my research will focus on self assembled monolayers on metal surfaces.

The organization of the thesis is as follows: in order to investigate the

microscopic mechanisms for the onset of diffusion, Chapter 2 will focus on the behavior of superionic clusters. The diffusion mechanism in a finite system with long-ranged forces is not yet well known. Because clusters have short ranged order like glasses, studying them will be helpful to gain insights into highly disordered materials and local behavior in glasses.

Chapter 3 will discuss the driving forces which lead to ordering behavior at solid-liquid interfaces. We present results of Monte carlo simulations on origins of tilt behavior in self assembled model rigid oligomers.

Chapter 4 includes preliminary results from a Potts model calculation, which will focus on domain structure and a long range ordering study of monolayers at solid surfaces by using large scale lattice calculations.

Chapter 5 will present extensive molecular dynamics simulations of organic thiol monolayers self assembled on gold. The molecule that we were interested in for this research is 4-mercapto-phenyl-phthalimide (4-MPP). The tilt angle calculated from my simlations is in very good agreement with experiment.

Chapter 6 concludes with discussion and possible future work.

Simulations of chain molecule-inorganic interphases are presented in Apppendix A. Appendix B will present the experimental study on molecular structure of monolayers from thiol-terminated polyimide model com-

pounds on the gold surface.

Methods used in each calculation will be presented in respective chapters.

Chapter 2

Molecular Dynamics Study of Superionic Behavior in Clusters

2.1 Introduction

It has been known for a long time that most crystals have relatively small conductivities in the solid state. They only become ionic conductors in the liquid state above certain transition temperatures. In 1914, experiments conducted by Tubandt and Lorenz found an extraordinarily high silver conductivity in AgI below its melting temperature.[8] Later, many other ionic compounds, such as Ag_2S, Ag_2Se, CaF_2, PbF_2, were discovered to possess a remarkable degree of ionic conductivity in the solid state. They are characterized by small activation energies for one type of ion, either anion or cation, to move relatively freely in the stable sublattice of the other ion. These kinds of ionic compounds are called superionic, or fast-ion conductors. More recently, superionic phenomena have also been observed in glassy materials and polymers.[16,37,38,37,39,40]

Because of their wide range of applications, superionic conducting materials have been the subject of intensive research, both experimentally as well as theoretically, in the last two decades. A major focus has been to understand the nature of diffusion mechanisms. Due to their high ionic conductivity in the solid state, they are good candidates for new materials for high-energy solid state batteries, energy-storage devices, optical memory, and chemical and gas sensors.[41,9,26,42] Studying the phenomena and

mechanism of high ionic mobility in the solid state will provide us with insights into how electrolytes work.

Many experimental methods have been applied to superionic conductors to investigate their structural and dynamical properties. Trace diffusion, X-ray powder diffraction,[18] NMR spectroscopic method, neutron scattering,[19–21,16,15,39,17] diffuse x-ray scattering, Raman scattering,,[22,17] *etc.* are among the most used measurements. Especially, the Single-Crystal Neutron Diffraction experiment performed by Cava and coworkers[24] and Quasielastic Neutron Scattering experiment conducted by Funke[20] have provided helpful information about the structural and dynamical properties of those compounds.

Because superionic conductors combine phenomena that are observed in liquid and solid in an interesting way, there has been much theoretical work studying the mechanism of conduction and phase transitions. Factors that affect diffusion in the solid state include order-disorder phenomena and crystal structure to glassy-disordered cluster transitions. Structures which allow fast ion transport are generally disordered, "channeled", or "layered". But high disorder does not necessarily translate into good ionic conductivity. Each of the mobile ions should have available more than one equivalent number of sites in the sublattice of another type of ion.

Catlow[43] classified three different types of mechanism: conventional but rapid highly correlated mechanism, liquid-like diffusion mechanism, and an intermediate mechamism. Two kinds of mechanism are more commonly known: continuous liquid-like motion or discrete hopping motion. The hopping model is the diffusion process of discrete jumps of a particle over the activation energy barrier. The average residence time of a particle at one site is much longer than the flight time between two sites. Examples of this type of diffusing mechanism include AgI, CaF_2, *etc.* If the diffusion of an ion is not represented by instantaneous jumps from one equilibrium site to another, but by a continuous motion in between, it is called a continuous model. The Ag^+ ions in Ag_2S are believed to diffuse through a continuous motion.

Over the past 20 years, molecular dynamics (MD) and Monte Carlo (MC) methods have been successfully used in studying superionic behaviors in bulk systems.[25,44–49,28,50] The results have been able to accurately reproduce the structural properties and dynamical properties of the real systems.

Rahman[25] pioneered the theoretical work in the superionic conductors by first using molecular dynamics in 1976. He studied the motion of ions in the superionic conductor CaF_2. The results showed that the F^-'s have

a constant of self-diffusion of $2.6 \times 10^{-5} cm^2 sec^{-1}$ while the Ca^{2+}'s form a stable lattice at 1590K and $2.525 g/cm^3$. Half of the F^-'s occupy the octahedral sites of the fcc Ca^{2+}'s lattice. The F^- ions diffuse through discrete jumps of anions between regular anion sites in CaF_2 with residence times of about 6 psec. Recently, a new shell-model molecular dynamics method has been developed and applied to CaF_2 by Lindan and Gillan.[51]

Later Vashishta and Rahman[44] performed MD simulations of the most popular superionic conductor α-AgI by constructing effective pair potentials using Pauling's ideas of ionic radii. Results showed that the diffusion constant and its temperature dependence were in good agreement with experiments. The silver density map obtained by their simulation was also very close to experiment.

Below 420K, AgI has a body centered crystal structure. Above 420K, Ag^+ ions become mobile and the diffusion coefficient is of the order of $10^{-5} cm^2/sec$, while I^- forms a bcc lattice. The I^- sublattice melts at 700K. Both neutron inelastic scattering experiments and molecular dynamics[21] simulations confirmed that Ag^+ ions diffuse by jumps between tetrahedral sites. The mean residence time was predicted to be 2.97 psec. An examination of the $\alpha \rightleftharpoons \beta$ phase transition showed that the calculated transition temperature and structural and dynamical properties were in

good agreement with experiments.[45]

Recently, O'Sullivan *et al.*[28] studied silver-ion disorder in α-AgI with MD simulation. Calculated diffuse x-ray scattering and Raman spectra were compared sucessfully with experimental data.

Like α-AgI, α-Ag_2Se is another superionic conductor with the bcc structure. But the concentration or number of Ag^+ ions in each unit cell is doubled in α-Ag_2Se which makes it more unique to study its mechanism. The structure of Ag_2Se has been studied by both X-ray diffraction and neutron diffraction. At low temperatures Ag_2Se forms an orthorhombic structure with $P2_12_12_1$ space symmetry (β-Ag_2Se).[52] Above 406K, the system undergoes structural transformation from β nonsuperionic phase to α superionic phase. The Se^{2-} transforms into a bcc sublattice and the Ag^+ sublattice undergoes a melting transition. Silver ions diffuse like a liquid through the lattice of Se^{2-} ions. The diffusion constant of Ag^+ is measured to be on the order of 10^{-5} cm^2/sec.[53] At 1170K, the Se^{2-} sublattice melts.

Funke[20] performed quasielastic neutron scattering measurements on a single crystal of α-Ag_2Se. By interpretation of the spectra, it was concluded that silver ions diffuse in a continuous diffusion model with the ions in the network along $\langle 100 \rangle$ channels. Neutron diffraction studies also showed that the distribution of the Ag^+ probability density was homogeneous along the

⟨100⟩ channel.

Ag_2S is another superionic conductor. It's microscopic dynamics of Ag^+ ions is essentially the same as Ag_2Se. X-ray powder diffraction data had determined the distribution of silver ions in β-Ag_2S.[18] Single-crystal neutron diffraction[24] showed that the distribution of mobile ions differs greatly in α-AgI and β-Ag_2S, despite similar anion arrays, reflecting the different silver ion concentrations characteristic of the bonding present in the respective low temperature phases.

Rino, *et al.*[27] studied structural and dynamical correlations in superionic and molten Ag_2Se by using the molecular dynamics method. The effective two-body interaction potentials, including Coulomb interactions, steric repulsions, and charge-dipole interactions due to the large electronic polarizability of the selenium ions, were used in the calculation. They found that the calculated temperature dependence of the self-diffusion constant of silver and the Haven's ratio were in good agreement with the experimental results. In the bcc lattice, there are 12 tetrahedral (t) sites (1/4, 0, 1/2), 6 octahedral (o) sites (0, 1/2, 1/2), and 24 triangularly coordinated sites (0, x, x). From the Se-Ag-Se bond angle distribution, it was concluded that Ag^+ mostly reside on *t* sites and also at occupancy slightly off *o* sites. The Ag^+ ions diffused through the bcc lattice of Se^{2-} ions.

The same kind of potentials were used to investigate the phase transition between a superionic phase (α) and a nonsuperionic phase (β) by Shimojo and Okazaki.[48] The low temperature structure was very similar to that observed in experiments. But this potential did not reproduce the structure of β-Ag_2Se with $P2_12_12_1$ space symmetry. The possible reason was suggested by variation of the covalent charactor of the potentials with temperature.

Recently, neutron scattering experments conducted by Dianoux and coworkers[15] found that small clusters of AgI with tetrahedral coordination existed in the $AgPO_3$ based glasses. The radii of the clusters are of the order of 4 Å to 20 Å.

A motivation for the work presented here is to investigate the microscopic mechanisms for the onset of diffusion. It is also interesting to study the diffusion mechanism in a finite system with long-ranged forces which is not yet well known.

The study of the physical and chemical properties of clusters of atoms and molecules has been a very active field of research in recent years. However, the majority of these researches have been focused on homogeneous clusters interacting through Lennard-Jones potentials. Heterogeneous clusters, especially ionic clusters are not well studied. Most of the studies

concerning ionic clusters are about the alkali halide clusters.[54-56] Because clusters often have short ranged order like glasses, studying them will be helpful to gain insights into highly disordered materials and local behavior in glasses. Because the diffusion of an ion is determined by its location and surrounding, each of the mobile ions should have more than one equivalent number of sites. For a cluster, many ions are located at the surface and have many empty sites available. By changing the size of the cluster, we can study surface effects on the diffusion constant and compare it with the bulk.

Molecular dynamics simulations have been performed on $(Ag_2Se)_n$ (n=1-5, 9, 41, 80), $(AgI)_{60}$, $(NaCl)_{108}$ ionic clusters. Because the effective two-body interaction potentials[27] had been successfully used in describing bulk Ag_2Se, we adopted their form in this study. Structural properties, such as pair-distribution functions and bond-angle distribution, as well as dynamical correlations, such as velocity autocorrelation functions and van Hove self-correlation functions were studied.

In section II, we will discuss the methodology of the MD simulations. We present the results of the simulations and discussion in section III, and summarize our findings in section IV.

2.2 Method

In order to reproduce structural and dynamical correlations which are observed in the experiment, potential functions have to be constructed correctly. As mentioned before, effective potentials constructed by Vashishta and Rahman[44] first introduced interionic potentials by using Pauling's ideas of ionic radii. Later, people used effective potentials in many calculations in different systems and were able to reproduce the structural perperties and dynamical properties successfully.[46,44,41]

The effective potential for $(Ag_2Se)_n$ clusters in this study were taken from Rino, *et al*,.[27] The same potentials were used to study phase transition in Ag_2Se.[48] They have the same form as in the other binary superionic conductors, such as AgI, Ag_2S, and CuI, which include Coulomb interactions, charge-dipole interactions and steric repulsions.

$$\varphi_{Ag-Ag}(r) = \frac{0.2408}{r^{11}} + \frac{0.2025}{r}, \tag{2.1}$$

$$\varphi_{Se-Ag}(r) = \frac{86.6614}{r^9} - \frac{0.405}{r} - 0.7088\frac{exp(-r/4.43)}{r^4}, \tag{2.2}$$

$$\varphi_{Se-Se}(r) = \frac{220.1905}{r^7} + \frac{0.81}{r} - 5.67\frac{exp(-r/4.43)}{r^4}. \tag{2.3}$$

The units are Å for the distance r between ions and $e^2/Å$=14.389 eV for the energies. The polarizability of silver is considered zero.

The molecular dynamics simulation method was performed on the clusters. Hamilton's equations of motion were solved for individual ions of the clusters with initial sets of positions and velocities.

$$H = \sum_{i=1}^{N} \frac{P_i^2}{2m_i} + V(r), \tag{2.4}$$

$$V(r) = \sum_{i<j}^{N} V(r_{ij}). \tag{2.5}$$

The system was simulated in the microcanonical ensemble. The Verlet algorithm was used to integrate the equations of motion. After choosing one initial configuration in the liquid state, the steepest-descent minimization method[57] was used to locate the potential surface minima of the cluster given an instantaneous location along the trajectory. The system was then heated to a melted state and cooled back to the solid state by uniformly scaling the velocities by a small amount. The heating-cooling rate was 400 steps/K. The equations of motion were then propagated to allow for proper relaxation with no total energy drift. The time step was taken to be 0.5×10^{-14} sec. Total energy, total linear momentum, and total angular

momentum were well conserved to ± 2.0 in 10^5 over several thousand time steps.

Normal mode analysis was performed on the $(Ag_2Se)_n$ (n=1-5) clusters to test the dynamics of our system. The frequencies are the square roots of the eigenvalues of the mass-weighed force constant matrix, ie. the Hessian matrix, where r is a point in the many-dimensional configuration space.

$$D_{ij}(r) = \sqrt{\frac{1}{m_i m_j}} \times \frac{\delta^2 V(r)}{\delta q_i \delta q_j}. \tag{2.6}$$

The dynamical matrix was computed at different points along the trajectory and then diagonlized. The resulting frequencies were then binned and averaged to obtain the harmonic density of states.

At low temperature, the cluster is considered a harmonic solid. The distribution of frequencies obtained by diagonalizing the matrix should correspond closely with its power spectrum. (defined below)

Other quantities that we computed here include n(r), ρ(r), the mean-square displacement (MSD), the normalized velocity auto-correlation function (VAF), the current-current correlation function, and the van Hove self-correlation function.

The n(r) is defined as the population of two kinds of particles at a distance r. The ρ(r) is the distribution of one kind of particle from the

center of mass of the cluster.

The mean-square displacement(MSD) is defined as,

$$\langle r^2(t)\rangle = \frac{1}{N}\sum_{i=1}^{N}\langle [r_i(t) - r_i(0)]^2\rangle, \tag{2.7}$$

where $\langle\rangle$ denotes an average over many independent time origins. The diffusion constant for that ion is determined from the slope of the mean square displacement versus time:

$$D = \frac{1}{6}\frac{d\langle r^2(t)\rangle}{dt}. \tag{2.8}$$

The normalized VAF is computed as:

$$C_i(t) = \frac{\langle V_i(t)\cdot V_i(0)\rangle}{\langle V_i^2(0)\rangle}. \tag{2.9}$$

where the averaging is over all the same kind of particles and over time origins. The power spectral density is computed by Fourier transformation of the VAF.

$$I_i(\omega) = 2\int_0^\infty C_i(t)\cos\omega t dt, \tag{2.10}$$

$I_i(\omega)$ represents the phonon density of states of particle i. The self-diffusion

coefficient is porportional to the zero frequency mode I(0).

The current-current correlation function for charge-current fluctuations is given as follows:

$$\psi(t) = \frac{\langle \mathbf{J(0)} \cdot \mathbf{J(t)} \rangle}{\langle \mathbf{J(0)^2} \rangle}, \tag{2.11}$$

where J(t) is the current-density defined by:

$$\mathbf{J(t)} = \sum_{\mathbf{i}} \mathbf{Q_i ev(t)}. \tag{2.12}$$

where v is velocity of the ion.

The freqency-dependent ionic conductivity $\sigma(\omega)$ is determined by Fourier transformation of the current-current correlation function $\psi(t)$:

$$\sigma(\omega) = \frac{2}{3\Omega kT} \int_0^\infty \psi(t) \cos \omega t dt. \tag{2.13}$$

The van Hove self-correlation function can describe a picture of the motion of an ion by monitoring its self-correlation function.

$$G_{s\alpha}(r,t) = \langle \delta [r_\alpha(t) - r_\alpha(0)] \rangle. \tag{2.14}$$

It defines the probability of finding how far an ion α has traveled r(t)

in time t, which was at the origin location r=0 at origin time t=0. The brackets denote an average over time origins and like ions. The results can tell us the mechanism of the diffusion. Its Fourier transform is the inelastic neutron scattering spectrum.

2.3 Results

2.3.1 Small Clusters

We performed MD calculations on the small clusters $(Ag_2Se)_n$ (n=1-5, 9) first. Along a dynamics trajectory in the liquid state, the clusters were quenched. As expected, many potential minima were located with small potential differences. Figure 2.1 shows six potential minima found for $(Ag_2Se)_3$.

In order to check the dynamics of our system, normal-mode analysis was performed on the quenched structure of $(Ag_2Se)_n$ (n=1-5, 9) clusters. Figures 2.2 and 2.3 show that the power spectrum at 47K is in very good agreement with normal mode analysis for $(Ag_2Se)_2$. For $(Ag_2Se)_9$, there were a total of 75 phonon states that were too close in frequency to yield distinguished individual lines. But the two peaks around $50cm^{-1}$ and $100cm^{-1}$ in the normal-mode spectrum matched the two peaks in the

corresponding power spectrum.

At low temperatures, the MSD for $(Ag_2Se)_9$ showed that sliver ions do not diffuse and have more oscillations than selenium ions while the clusters are in the solid glassy phase. With increasing temperatures, the Ag^+ ions showed larger mobility than the Se^{2-} ions. The diffusion constant of the Se^{2-} ions increased with temperature as for the Ag^+ ions, but with a smaller value. Figure 2.4 shows the MSD for $(Ag_2Se)_9$ with both the Ag^+ ions and the Se^{2-} ions at 195K. Table 2.1 displays the diffusion constants and ratios of diffusion constants between the Ag^+ and the Se^{2-} at different temperatures. The self-diffusion constant D was calculated from the slope of the MSD. The ratios between diffusion constants between the Ag^+ and the Se^{2-} ions for $(Ag_2Se)_9$ are all under 3.0, meaning that no clear distinguished superionic phase analogous to the bulk with Ag^+ ions diffusing through the Se^{2-} sublattice was observed.

The results suggest that small clusters, like $(Ag_2Se)_9$, are too small to show the distinguished superionic phase. Possible reasons are that the Se^{2-} ions were unable to form a bcc lattice that was detected in the bulk superionic phase, or the clusters were simply too small to show dramatic superionic behavior.

Previous studies on alkali halide clusters, such as NaCl, KCl, showed

that the behavior of the clusters depended strongly on the size.[55,58] In the case of the small Ag_2Se clusters, all the ions are considered on the surface. The question which we face is: if we increase the size of the cluster, will it show a significant superionic phase?

2.3.2 Medium Clusters

It has been demonstrated that the alkali halide cluster with sixty four ions is large enough to display bulklike properties.[54,56] We chose to study $(Ag_2Se)_{41}$ which contained distinct surface and interior ions.

Bulk Ag_2Se displays the superionic phase between 406K and 1170K. Below 406K, Ag_2Se has an orthorhombic structure. The Se sublattice melts at 1170K. For finite sized clusters, the freezing and melting transition temperatures are expected to be lower.

Dynamics simulations at different temperatures were conducted. The MSD for the Ag^+ ions and the Se^{2-} ions of $(Ag_2Se)_{41}$ at four temperatures are presented in Figures 2.5 and 2.6. Clearly, below 200K, the cluster showed a disordered glassy structure. Above 200K, the Ag^+ ions start to exhibit diffusion and the Se^{2-} ions remained in the solid state. Above 300K, the Se^{2-} ions diffused like a liquid, although with a smaller diffusion constant than the Ag^+ ions. We calculated the diffusion constants

and ratios of diffusion constants between the Ag^+ and the Se^{2-} at different temperatures and the results are presented in Table 2.2. The ratio differences in diffusion constants between the Ag^+ and the Se^{2-} become significantly larger than $(Ag_2Se)_9$.

The n(r) of Se-Ag at 160K had the nearest neighbor distance of 2.74Å which agrees with the bulk. (Figure 2.7) The peaks in $n_{SeSe}(r)$ are sharp. From the first peak, the nearest neighbor separation between Se-Se is found to be 4.41Å (bulk 4.30Å). The Se-Ag pair-distribution function has a giant first peak, which suggests that most silver ions and selenium ions have a separation distance of 2.74Å. The Ag-Ag pair-distribution function has broad peaks and is very similar to a glassy distribution.

The center of mass of the cluster was calculated at each time step along the dynamics trajectory. The distance between every ion and the center of mass of the cluster was calculated, then binned. Figure 2.8 shows $\rho(r)$ for Ag^+ and Se^{2-} ions at 160K. Se^{2-} ions displayed four individual layers from the center of mass, while Ag^+ ions concentrated nearer the middle of the cluster and then exhibited a disordered glassy-like distribution.

We calculated the bond-angle distribution functions for the $(Ag_2Se)_{41}$ cluster at 160K by choosing 4.2Å, 4.0Å, and 6.2Å as the cutoff distance for Ag-Ag, Ag-Se, and Se-Se, respectively. We determined the cutoff distances

by finding where the first peak in n(r) terminates. The distributions of the peaks are very close to the bulk. Those involving silver ions are fairly broad, indicating the glassy nature of silver. The bond-angle distribution of Se-Se-Se has three peaks at 57°, 107°, with a shoulder of a peak at around 160°. Figures 2.9 and 2.10 show the bond-angle distributions for Ag-Ag-Ag and Se-Se-Se. The bulk has three peaks centering at 70°, 110°, 180°, corresponding to a bcc lattice.[27] This may suggest that although the cluster is in glassy state, the Se^{2-} ions possess some bcc character.

The van Hove self correlation functions showed both Ag^{+} and Se^{2-} ions had solidlike distributions at 160K. Both kinds of ions exhibited thermal vibrations. At 50ps to 250ps $G_{*Ag}(r,t)$ had a peak at 0.43Å which means that the majority of the silver ions travel that distance as shown in Figure 2.11. The height of the peak decreases with time, but its position does not appear to move much. The mobility of the selenium ions at this temperature is extremely small. Its diffusion constant is 6.68×10^{-8} cm^2/cm.

When the temperature was increased to 251K, the Se^{2-} ions stayed in the solid state, while the Ag^{+} ions displayed liquid-like diffusion constants as shown in Figure 2.5. This is the characteristic of superionic behavior. The D of Ag^{+} is roughly $0.352 \times 10^{-5} cm^2/sec$ at 251K, while in the bulk, $D_{Ag} = 0.9 \times 10^{-5} cm^2/sec$ at 435K.[27]

The $\rho(r)$ showed that Se^{2-} ions formed two spherical shells from the center of mass and Ag^{+} ions diffused in between at 251K. (Fig. 2.12)

Figures 2.13, 2.14, 2.15, 2.16, 2.17, 2.18 display the six bond-angle distributions at 251K. The peaks of Se-Se-Se in the bond-angle distribution functions remained roughly the same. However, the Ag-Ag-Ag distribution became broader. (See Figure 2.9)

To further investigate the surface effect, we calculated the MSD for the interior ions and the surface ions separately. The cutoff distance was chosen as 4.8Å according to where the last shell of ions started in $\rho(r)$ and 6.0Å, in another run as which is the distance over which the system exhibits local charge neutrality.[27] Two kinds of methods were used. In method one, the surface ions and the interior ions were calculated at each time step. In method two, the surface ions and the interior ions were chosen at the first time step, and the same ions were tracked at the following steps. The results showed that interior Ag^{+} ions were somewhat more active than the surface Ag^{+} ions. The ratio of their diffusion constants is 1.28. Furthermore, the two methods reached essentially the same results which suggests that the ions stayed in their local region during the time scale of the MSD.

The velocity autocorrelation function for silver ions and selenium ions

and their Fourier transforms are shown in Figure 2.19, 2.20, 2.21, 2.22. As expected, the VAF for selenium showed significant oscillations and exihibited long time correlations, indicative of some degree of periodic behavior. The zero-frequency value of $I(\omega)$ is smaller than $I(\omega)$ of Ag^+, which suggests that the anions have significantly smaller diffusivity. The VAF for Ag^+ decayed after the first oscillation, which indicates liquidlike behavior and is very similar to the bulk system. $I(\omega)$ for Se^{2-} has more high frequency modes, while $I(\omega)$ for Ag^+ has more low frequency modes. The power spectrum of Se^{2-} has two peaks at around 45 cm^{-1} and 100 cm^{-1} which matched the spectrum in the bulk calculated by Rino, *et al.*[27] The frequency spectrum of Ag^+ has one peak at 40 cm^{-1} while in the bulk, the main peak was at 50.8 cm^{-1}. The current-current correlation function and its Fouier transform also matched the results calculated in the bulk.[27] The conductivity of the cluster $\sigma(\omega)$ had two peaks at 50 cm^{-1} and 100 cm^{-1}.

Both experiments and theory confirmed that Ag^+ ions in bulk AgI diffuse by jumps between tetrahedral sites of I^-'s bcc lattice.[21] The jump frequency was estimated at around 2.97 ps. Although Ag_2Se also has a bcc structure in the superionic phase, its diffusion mechanism is believed very different from AgI.[24] Ag_2S is another common superionic conductor. It is believed that the microscopic dynamics of Ag ions is very similar in the su-

perionic phase of Ag_2Se and Ag_2S.[27] The single-crystal neutron diffraction experiments performed by Cava and coworkers showed that Ag^+ ions exhibited large positional disorder in superionic phase of Ag_2S.[24] Funke studied quasielastic neutron scattering spectra from a single crystal of Ag_2Se.[20] By interpreting the data, he concluded that Ag^+ ions diffuse through continuous diffusion.

Figure 2.23 and 2.24 present the van Hove self-correlation function $G_{s\alpha}(r,t)$ for Ag^+ ions at 251K with time scale of 5ps to 25ps. This function discribes how far the number of ions travel from origin in a given time scale. The Ag ions showed diffusive motions and no jumps were observed. When the time scale increased to 50ps and 250ps, a jumping mechanism was observed for Ag^+ ions as indicated by peaks in G_{sAg}(r,t). (Figure 2.25, 2.26, 2.27, 2.28)

2.3.3 Larger Cluster

To compare our results more directly with the bulk, we increased the size of the cluster to $(Ag_2Se)_{80}$.

Figures 2.29, 2.30 show the MSD at four temperatures. Like $(Ag_2Se)_{41}$, the Ag^+ ions started to exhibit diffusive motions above 200K. Above 300K, the Se^{2-} 'sublattice' melts and both kinds of ions are free to move in the

cluster. At 275K, the MSD showed that the diffusion constant for Se^{2-} equalled zero and the Ag^{+} ions showed substantial diffusion constants. It is a more distinguished superionic phase than for the $(Ag_2Se)_{41}$ cluster. As expected, the cluster shows more bulk-like behavior with increasing size. The diffusion constants and the ratio between Ag^{+} and Se^{2-} are listed in Table 2.3. Note the large value for the ratio at T=275K.

For the van Hove function, at 199K with time scale from 50 ps to 250ps, both Se^{2-} and Ag^{+} ions had solidlike distributions with a sharp peak and a long tail. At 275K, as presented by Figures 2.31, 2.32, 2.33, 2.34, both the interior and the surface Ag ions diffused by jumps with time scales of 50 ps to 250 ps. The Se ions had solidlike distributions for both surface ions and interior ions. The ratio of diffusion constants between the interior Ag^{+} ions and the surface Ag^{+} ions was 1.21. When the temperature increased, the Ag^{+} and the Se^{2-} both displayed broad liquidlike distributions.

All the other structral and dynamical porperties were very similar to $(Ag_2Se)_{41}$.

2.3.4 Other clusters

In order to further understand the thermodynamics and kinetics of the solid-liquid transition in superionic clusters, we studied $(AgI)_{60}$ and $(NaCl)_{108}$

to compare with $(Ag_2Se)_n$ clusters.

As we mentioned before, α-AgI is one of most extensively studied superionic conductors. In the superionc phase, the Ag^+ ions diffuse by jumps between tetrahedral sites. The diffusion coefficient of Ag^+ is 2.0 $\times$ $10^{-5}cm^2/sec$ at 500K. It is interesting to investigate whether AgI also displays superionic behavior in a finite sized cluster.

The MSD shows that the Ag^+ and I^- ions in the $(AgI)_{60}$ cluster start to diffuse at about 200K. Figure 2.35 presents the MSD of the surface and the interior ions at 244K. It displays a much smaller difference in diffusion constants between Ag^+ and I^- ions than the larger Ag_2Se clusters. Below 200K , both Ag^+ and I^- ions were solidlike with close to zero diffusion constants. With increasing temperature, both kinds of ions start to show diffusion with similar diffusion constants. The $(NaCl)_{108}$ cluster behaved very much like $(AgI)_{60}$. Table 2.4 presents the diffusion constants and the ratios between Ag^+ and I^- ions at different temperatures.

For the power spectra, both the Ag^+ and I^- cases had significant spectral densities under 100 cm^{-1}. The same was true for the current-current spectrum, further indicating the overall liquidlike properties and lack of superionic behavior.

Neutron scattering experiments showed that there are AgI clusters

formed inside superionic conductor glasses.[15] The size of AgI is believed around 4Å. From our results, it appears that free AgI clusters do not exhibit superionic behavior.

2.4 Conclusions

Finite systems which exhibit superionic behavior in the bulk were investigated. Molecular dynamics simulations were performed on $(Ag_2Se)_n$ ionic clusters to investigate the microscopic mechanisms for the onset of diffusion. The potential model was taken from Rino *et al.*[27] which successfully reproduced many structral properties and dynamical properties of bulk system. Structural properties, such as pair-distribution functions and bond-angle distributions, as well as dynamical correlations, such as the velocity autocorrelation functions, were studied. At low temperature, the power spectra $(Ag_2Se)_n$ (n=1-5, 9) showed good agreement with normal-mode analysis. When the cluster was small, no dramatic superionic behavior was observed. As the size of the cluster increased, silver ions showed more mobility than selenium ions and presented superionic behavior like in the bulk. The Ag^+ ions that were on the surface of the cluster were less active than the Ag^+ ions in the interior of the cluster. For $(Ag_2Se)_{41}$ and $(Ag_2Se)_{80}$, the van Hove self-correlation function showed that there was a

jumping mechanism when silver ions diffused with time scale from 50ps to 250ps in the 'superionic phases'. To compare the properies of $(Ag_2Se)_n$ with other ionic clusters, MD calculations were also performed on $(AgI)_{60}$ and $(NaCl)_{108}$. The results showed that AgI clusters do not exhibit corresponding superionic behavior.

2.5 Tables

Temperature(K)	$D_{Ag}(cm^2/sec)$	$D_{Se}(cm^2/sec)$	D_{Ag}/D_{Se}
123	5.56×10^{-7}	3.56×10^{-7}	1.56
148	8.39×10^{-7}	4.69×10^{-7}	1.79
200	1.88×10^{-6}	8.89×10^{-7}	2.11
230	3.06×10^{-6}	1.20×10^{-6}	2.55
260	4.00×10^{-6}	1.89×10^{-6}	2.12
310	7.09×10^{-6}	3.01×10^{-6}	2.36

Table 2.1: Diffusion constants and the ratios of the Ag^+ and the Se^{2-} at different temperatures for $(Ag_2Se)_9$.

Temperature(K)	$D_{Ag}(cm^2/sec)$	$D_{Se}(cm^2/sec)$	D_{Ag}/D_{Se}
160	3.35×10^{-7}	6.68×10^{-8}	5.01
195	8.06×10^{-7}	1.35×10^{-7}	5.97
251	3.02×10^{-6}	5.63×10^{-7}	5.36
338	7.76×10^{-6}	1.14×10^{-6}	6.81
394	1.69×10^{-5}	5.06×10^{-6}	3.34

Table 2.2: Diffusion constants and the ratios of the Ag^+ and the Se^{2-} at different temperatures for $(Ag_2Se)_{41}$.

Temperature(K)	$D_{Ag}(cm^2/sec)$	$D_{Se}(cm^2/sec)$	D_{Ag}/D_{Se}
199	9.32×10^{-7}	1.91×10^{-7}	4.88
275	3.52×10^{-6}	3.58×10^{-7}	9.83
310	6.79×10^{-6}	1.32×10^{-6}	5.14
353	1.14×10^{-5}	2.32×10^{-6}	4.91

Table 2.3: Diffusion constants and the ratios of the Ag^+ and the Se^{2-} at different temperatures for $(Ag_2Se)_{80}$.

Temperature(K)	D_{Ag}(cm^2/sec)	D_I(cm^2/sec)	D_{Ag}/D_I
160	2.37×10^{-7}	2.32×10^{-7}	1.02
244	1.62×10^{-6}	1.16×10^{-6}	1.40
290	4.23×10^{-6}	3.90×10^{-6}	1.08
422	2.58×10^{-5}	2.53×10^{-5}	1.02

Table 2.4: Diffusion constants and the ratios of the Ag^+ and the I^- at different temperatures for $(AgI)_{60}$.

2.6 Figures

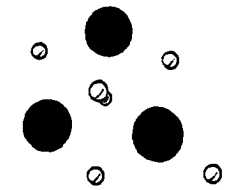

a) E= -0.91513 eV

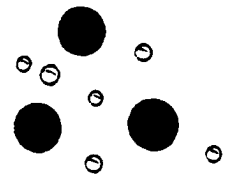

b) E= -0.91446 eV

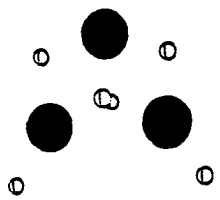

c) E= -0.90992 eV

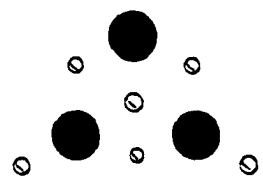

d) E= -0.90793 eV

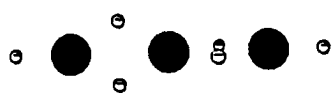

e) E= -0.90676 eV

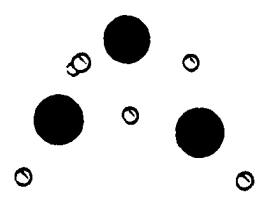

f) E= -0.90627 eV

Figure 2.1: Six potential minima for $(Ag_2Se)_3$.

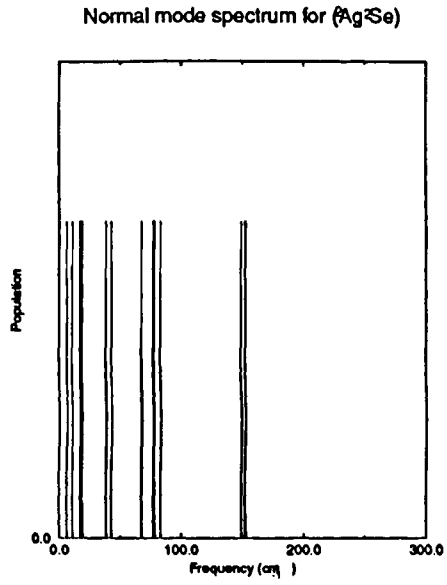

Figure 2.2: Normal modes for $(Ag_2Se)_2$.

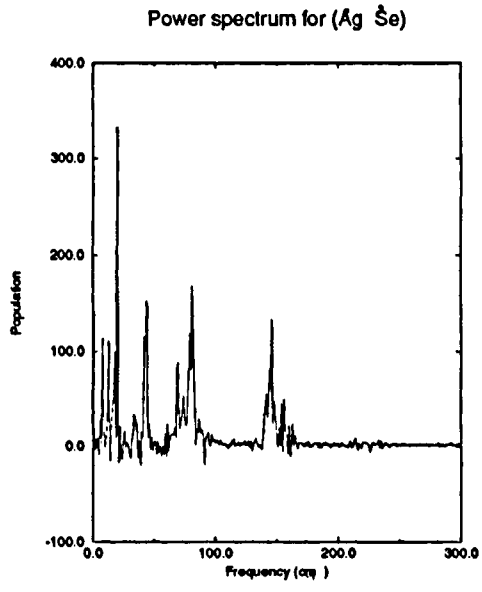

Figure 2.3: Power spectrum for $(Ag_2Se)_2$ at 47K.

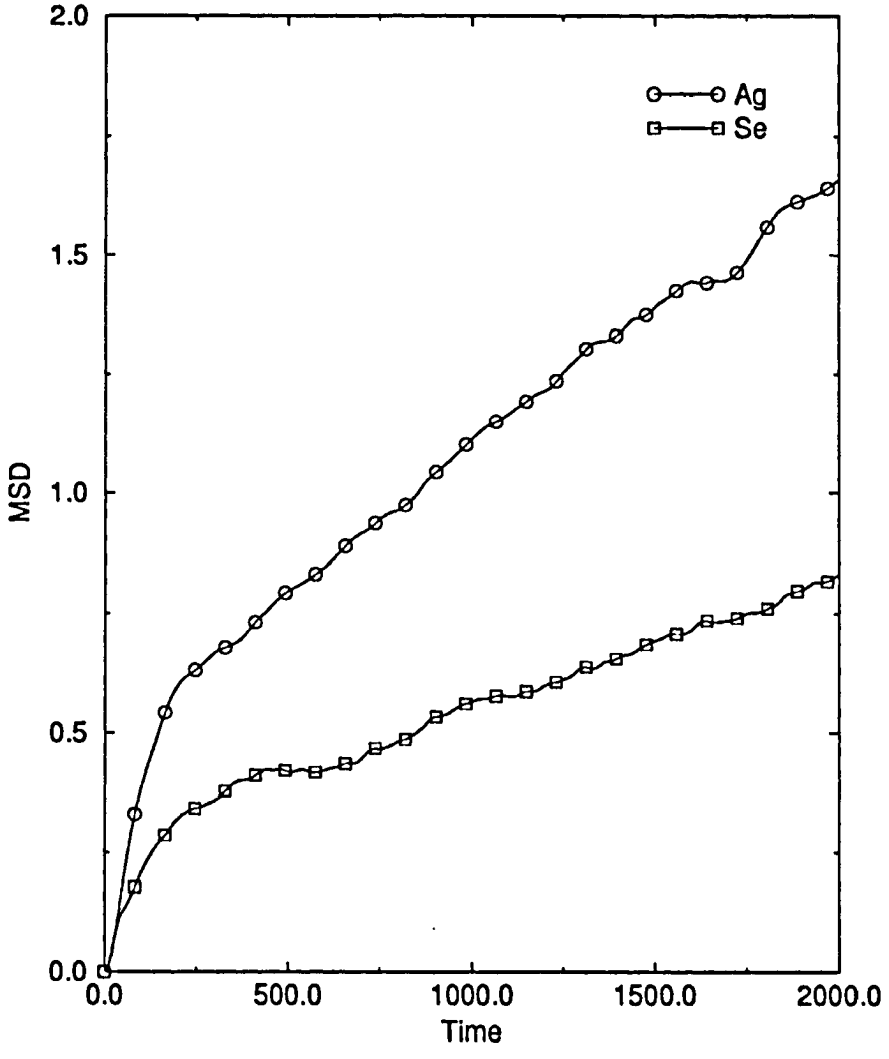

Figure 2.4: The MSD for $(Ag_2Se)_9$ at 200K.

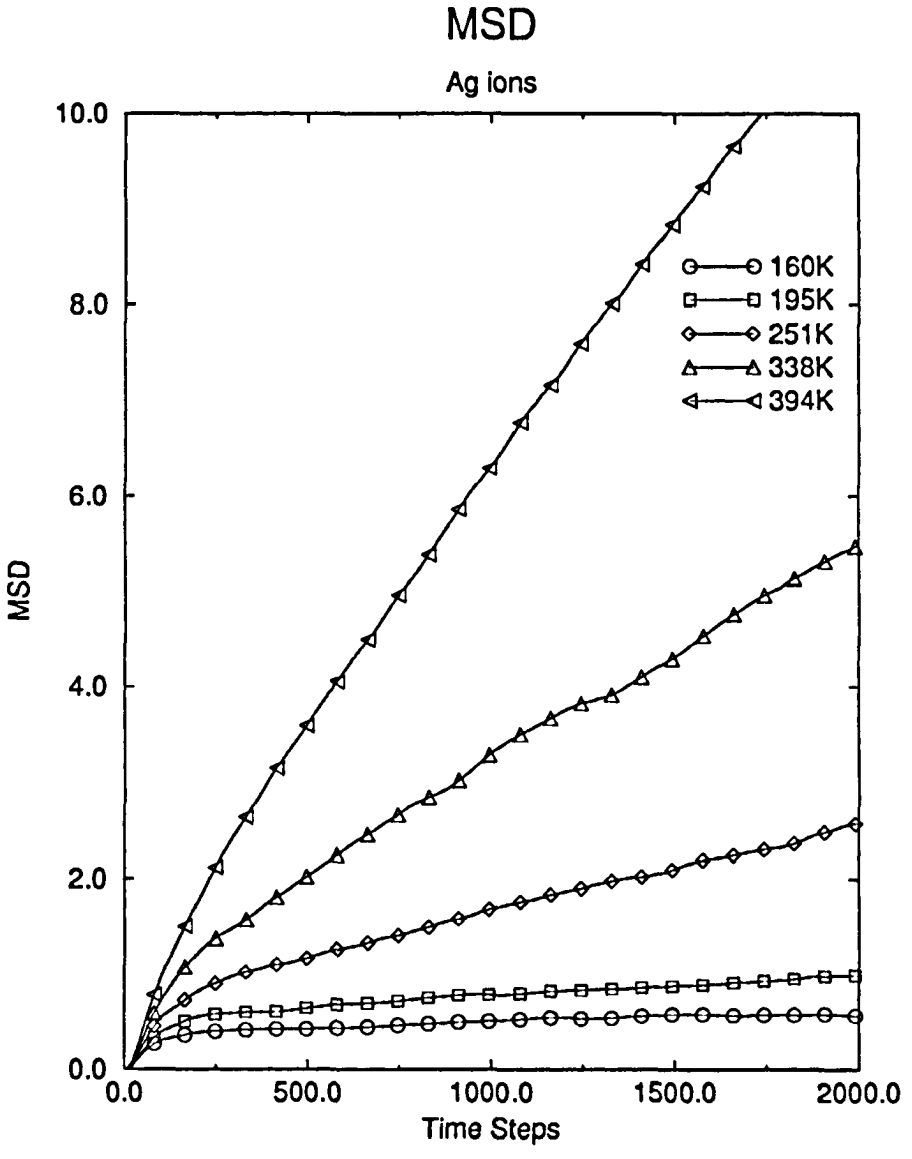

Figure 2.5: The MSD for Ag^+ ions for $(Ag_2Se)_{41}$ at different temperatures.

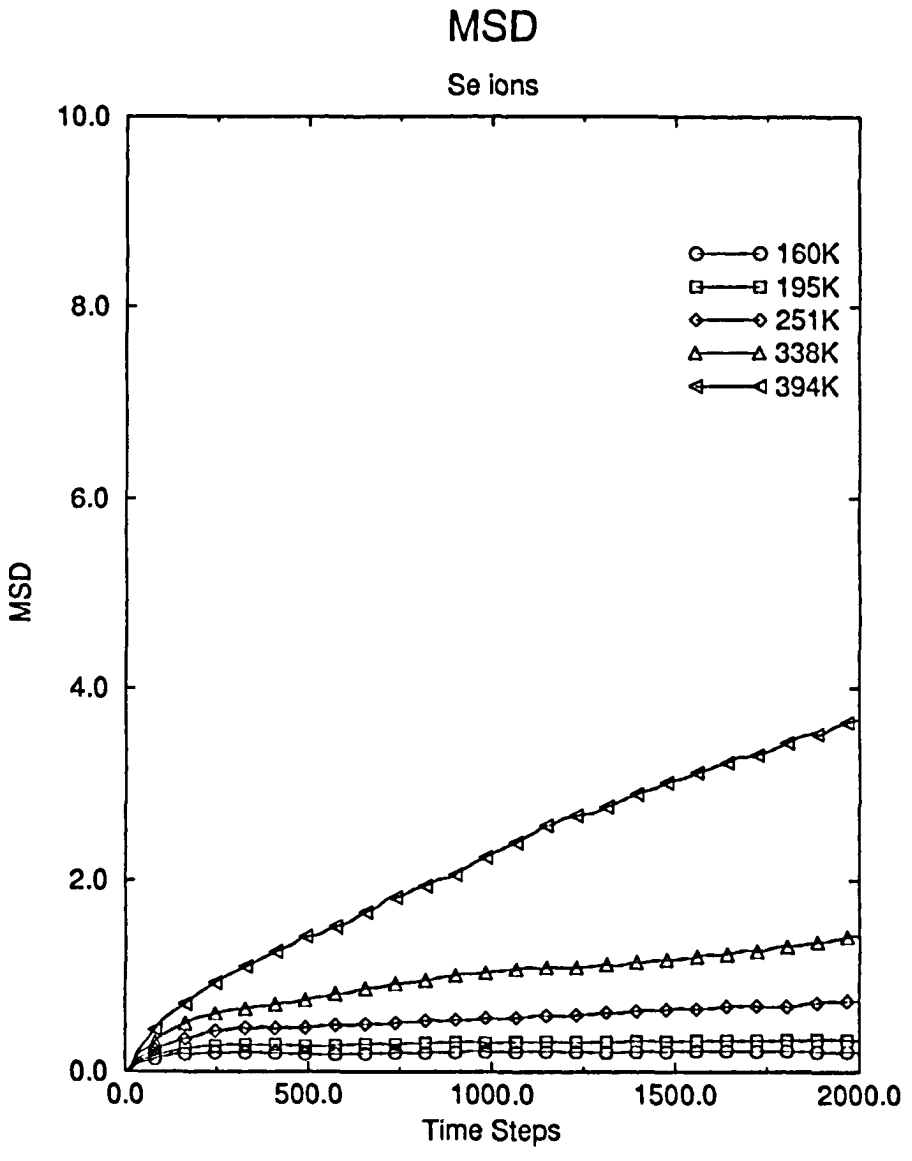

Figure 2.6: The MSD for Se^{2-} ions for $(Ag_2Se)_{41}$ at different temperatures.

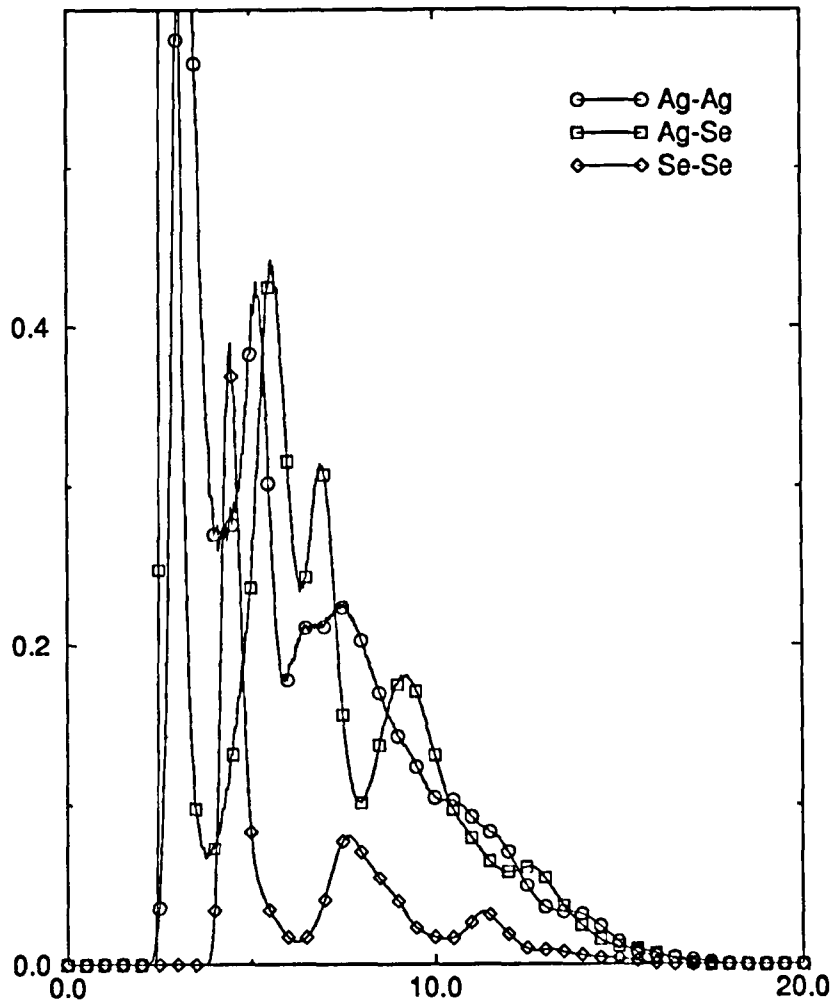

Figure 2.7: The n(r) for $(Ag_2Se)_{41}$ at 160K.

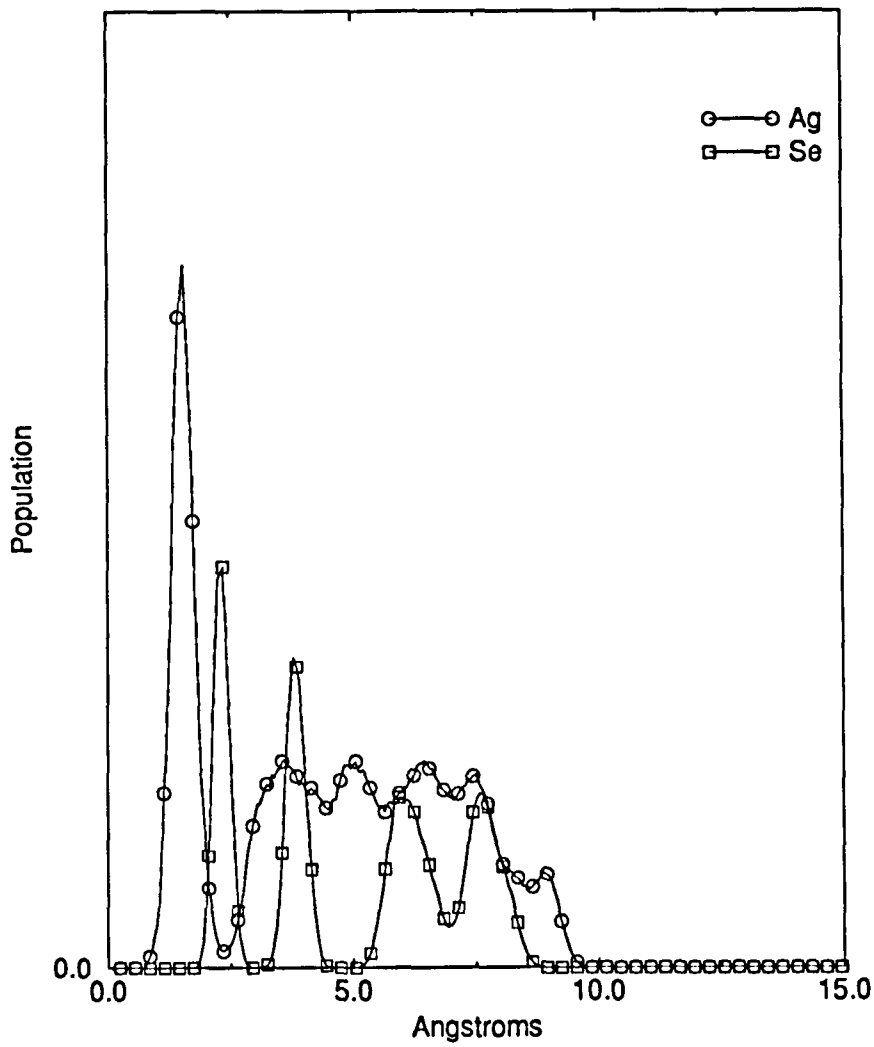

Figure 2.8: The $\rho(r)$ for $(Ag_2Se)_{41}$ at 160K.

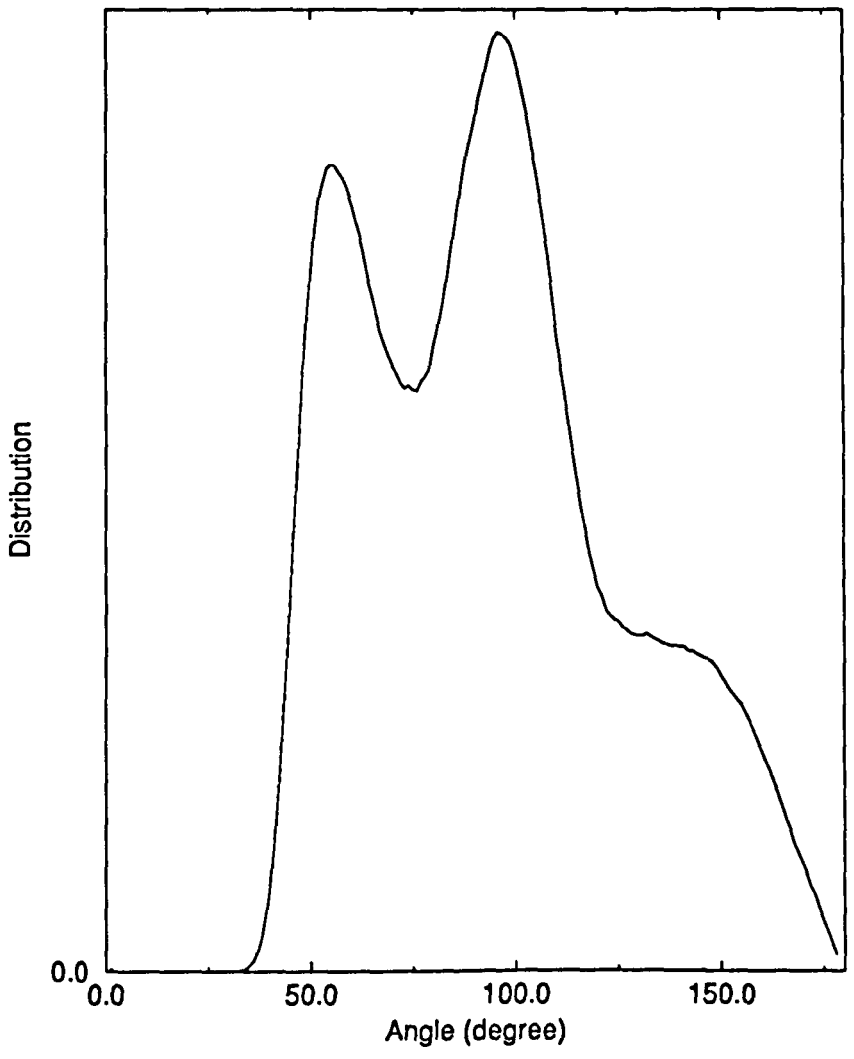

Figure 2.9: The Ag-Ag-Ag angle distribution for $(Ag_2Se)_{41}$ at 160K.

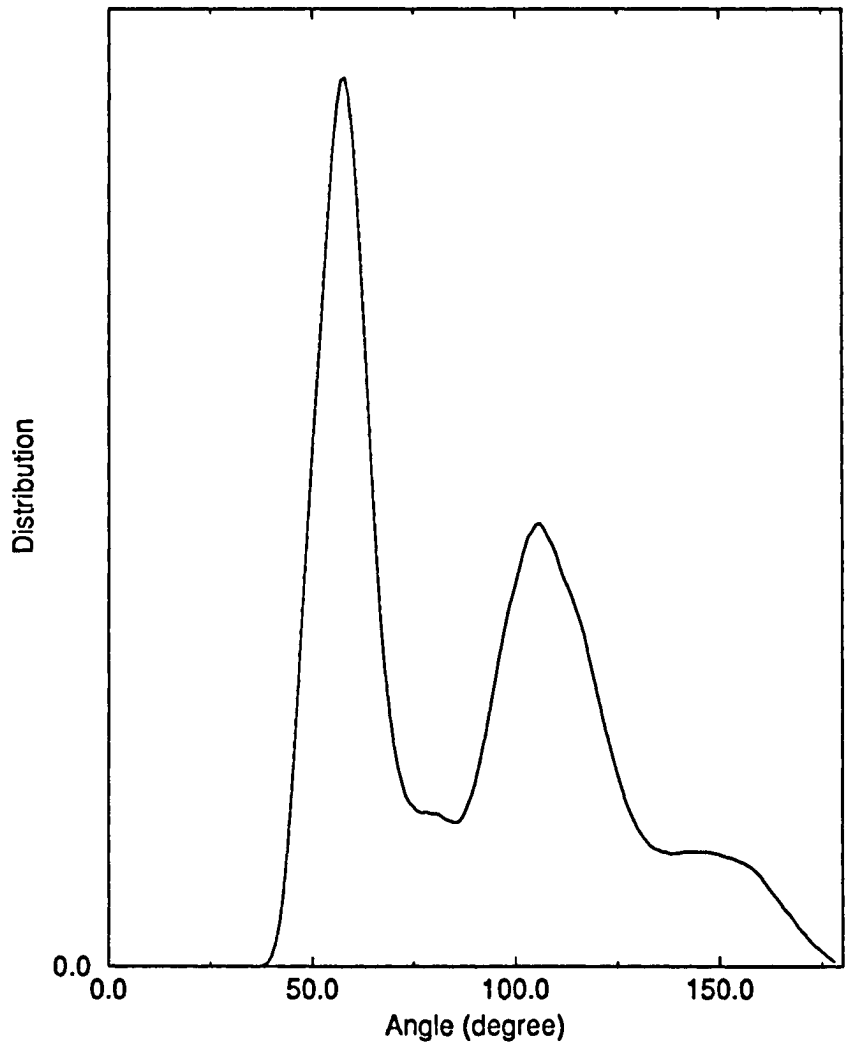

Figure 2.10: The Se-Se-Se angle distribution for $(Ag_2Se)_{41}$ at 160K.

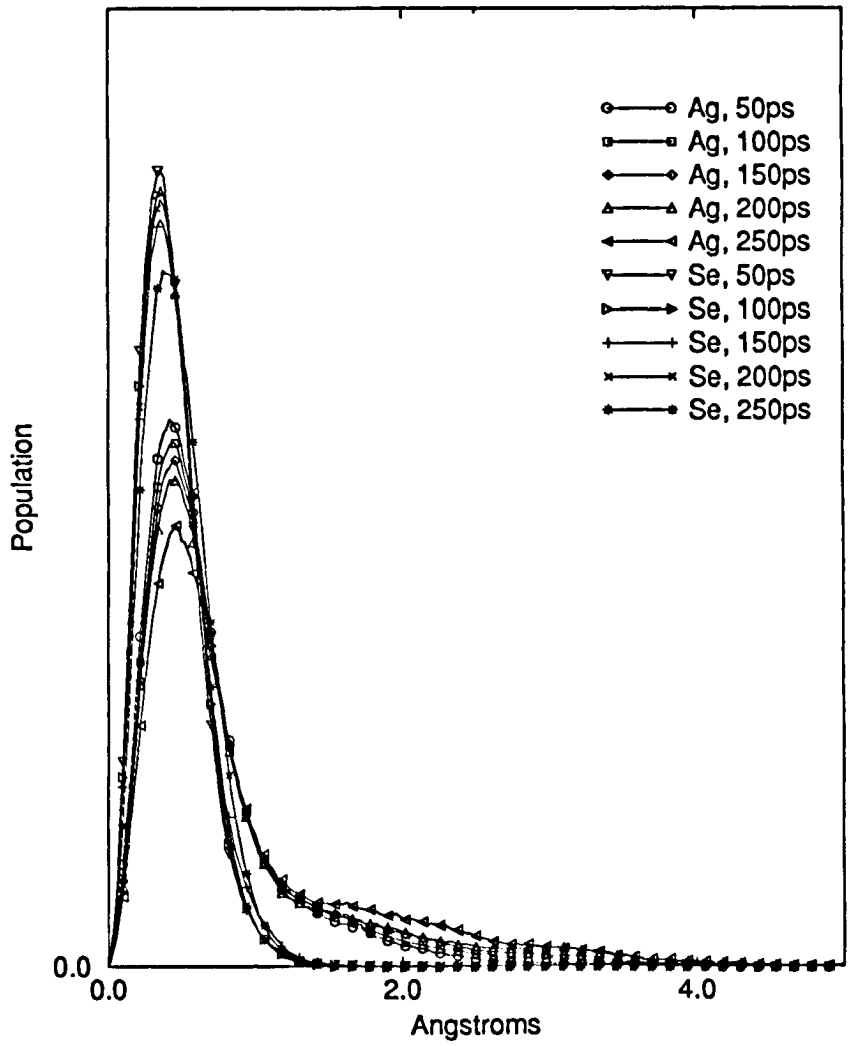

Figure 2.11: The van Hove self-correlation function for $(Ag_2Se)_{41}$ at 160K.

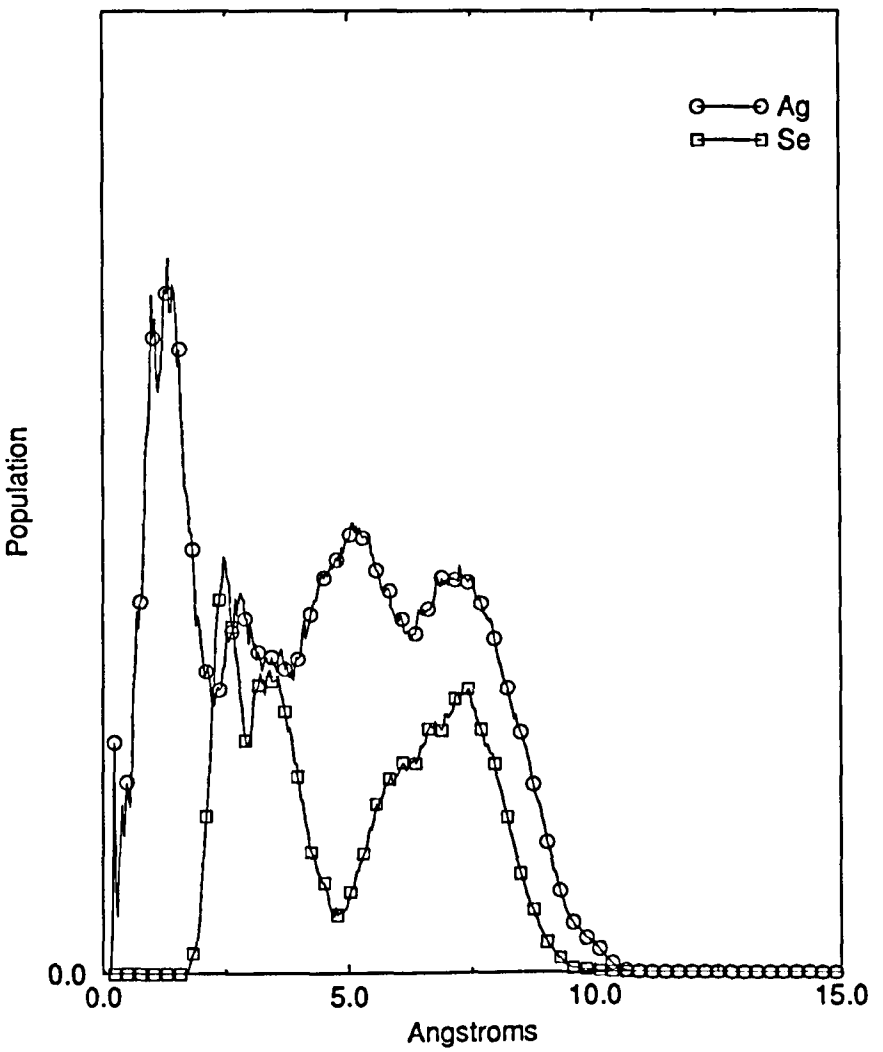

Figure 2.12: The $\rho(r)$ for $(Ag_2Se)_{41}$ at 251K.

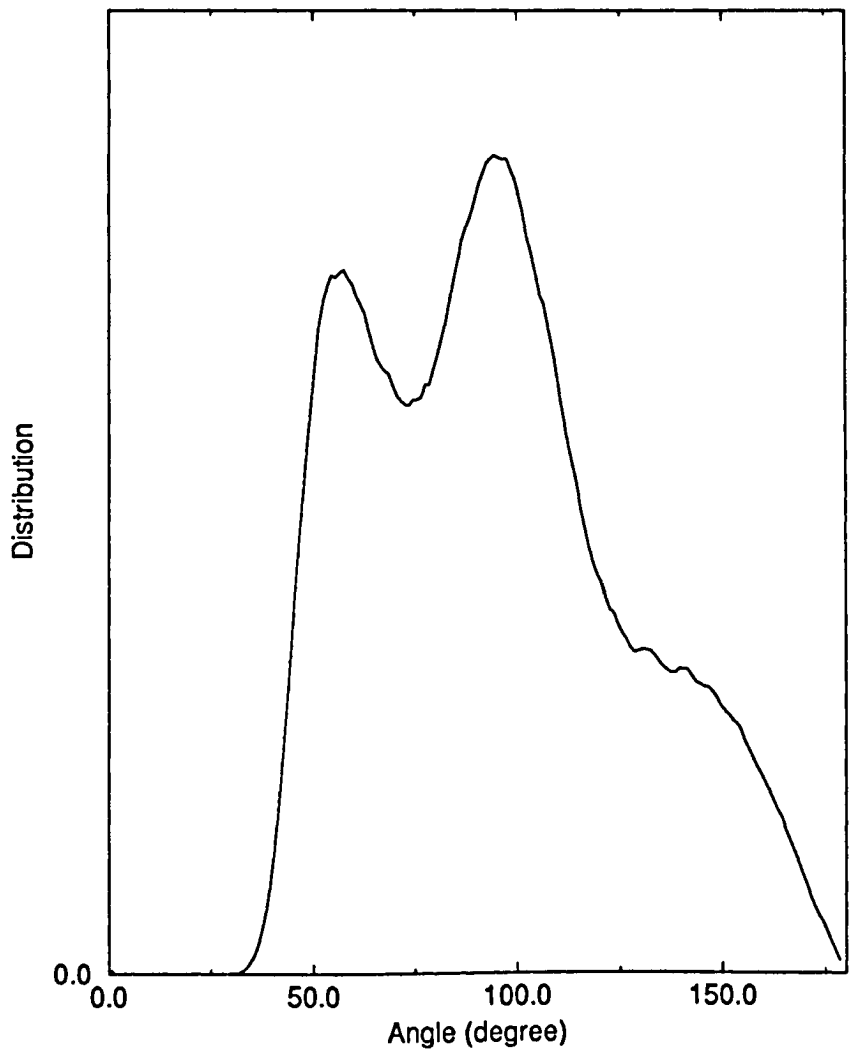

Figure 2.13: The Ag-Ag-Ag angle distribution for $(Ag_2Se)_{41}$ at 251K.

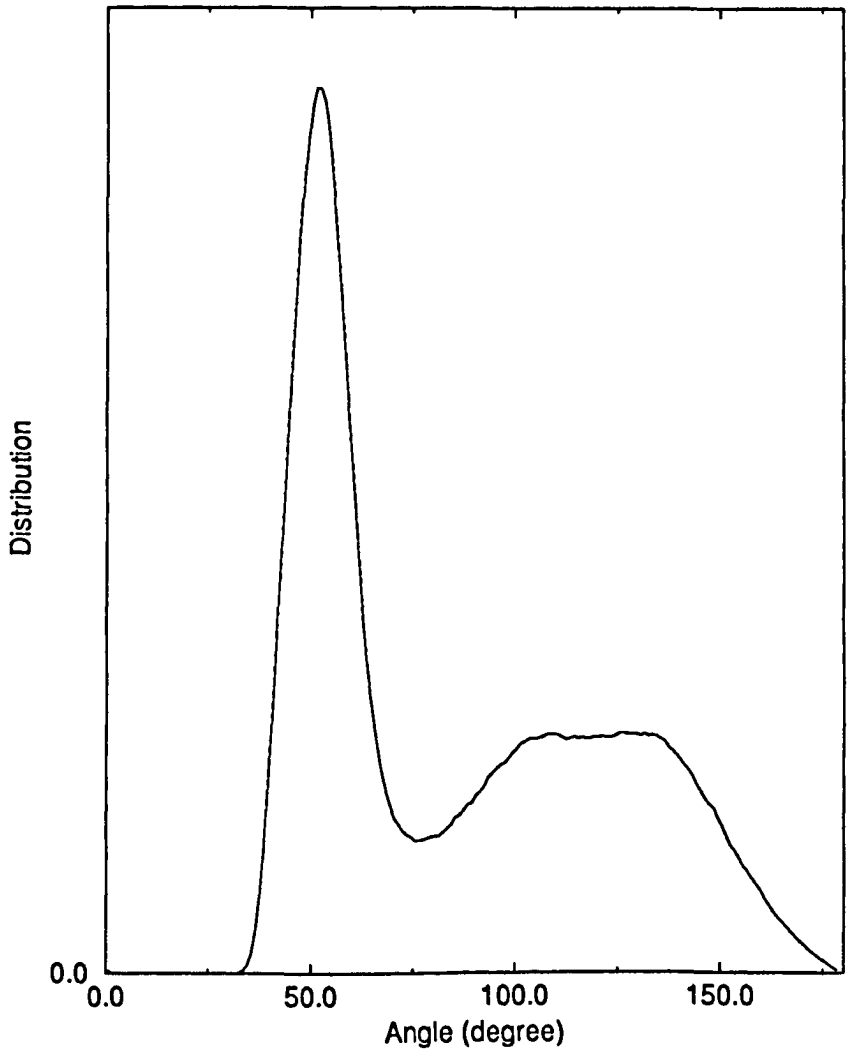

Figure 2.14: The Ag-Ag-Se angle distribution for $(Ag_2Se)_{41}$ at 251K.

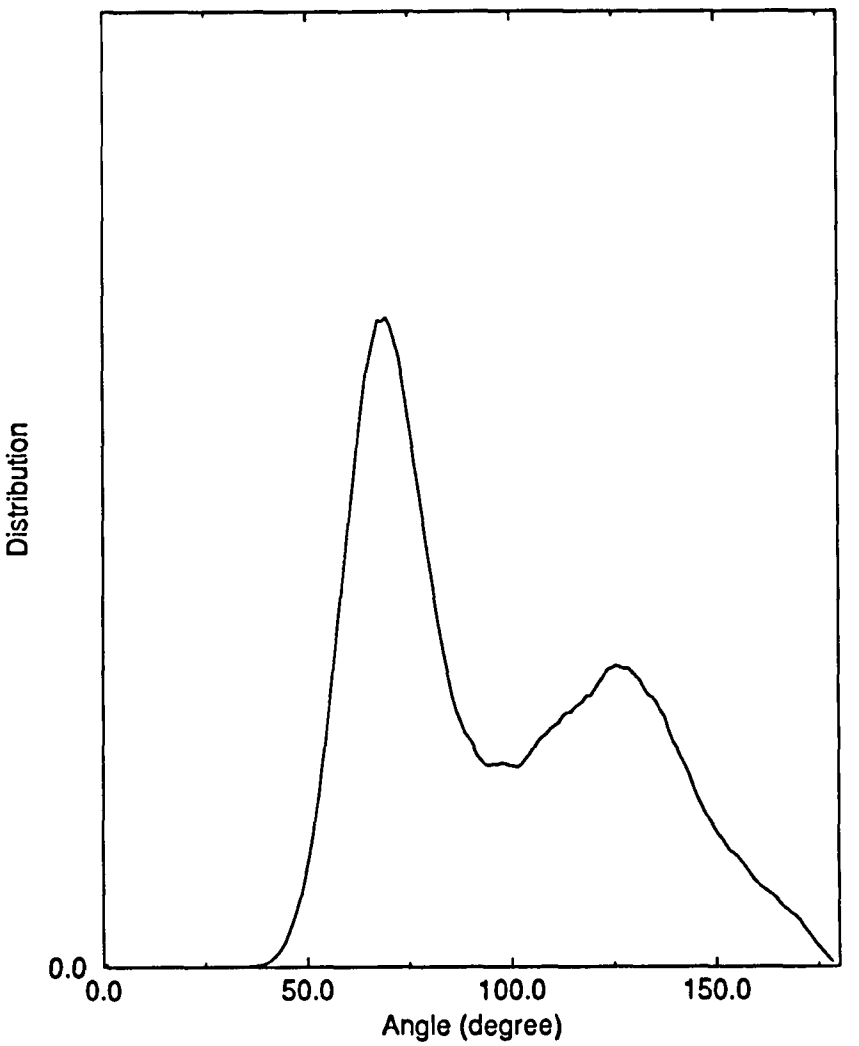

Figure 2.15: The Ag-Se-Ag angle distribution for $(Ag_2Se)_{41}$ at 251K.

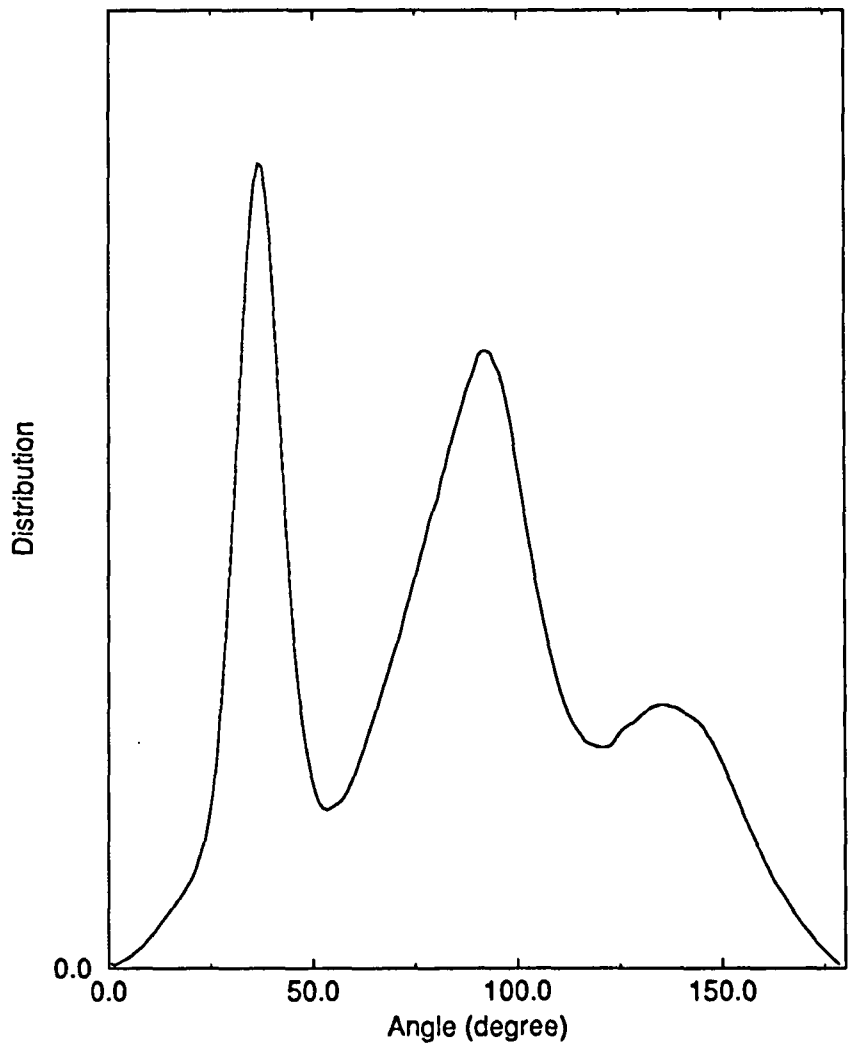

Figure 2.16: The Ag-Se-Se angle distribution for $(Ag_2Se)_{41}$ at 251K.

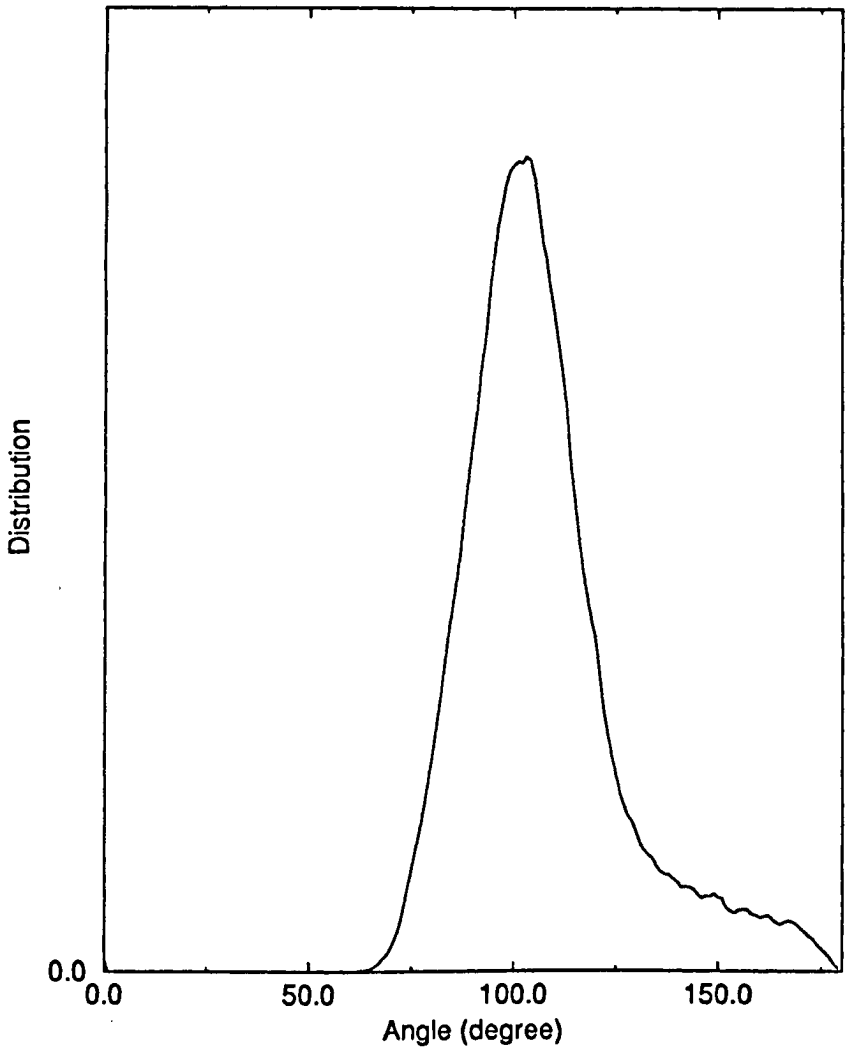

Figure 2.17: The Se-Ag-Se angle distribution for $(Ag_2Se)_{41}$ at 251K.

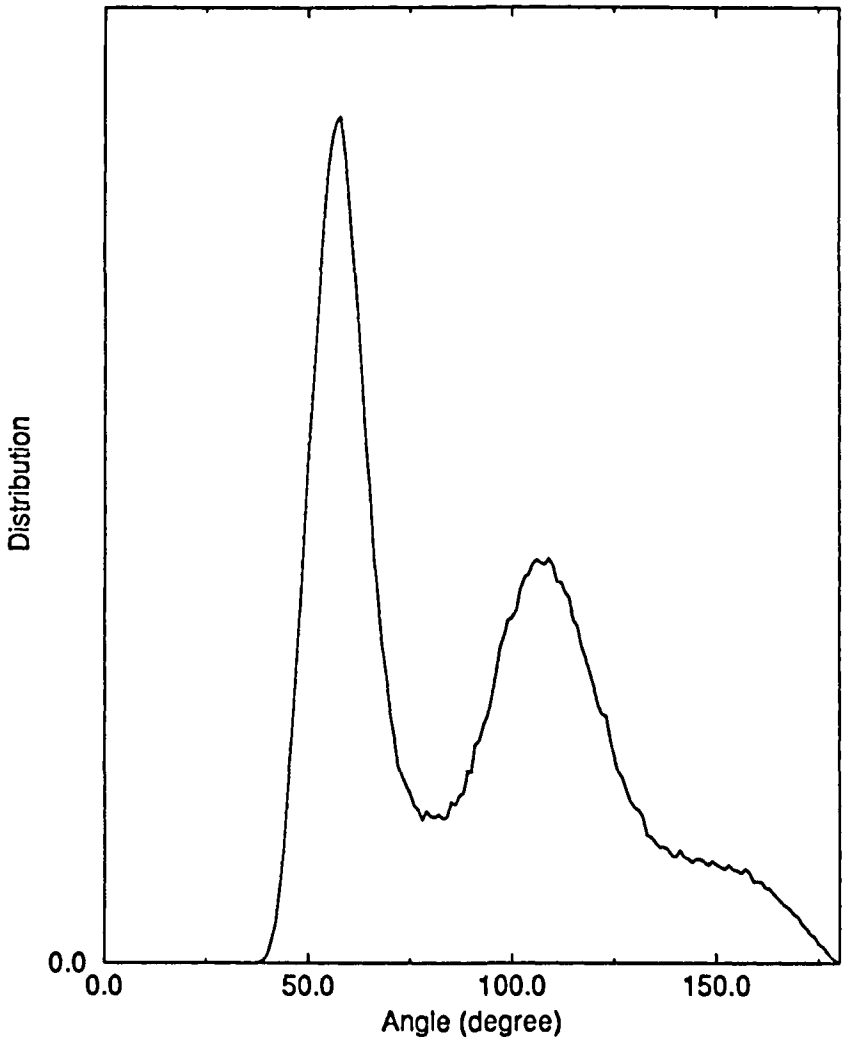

Figure 2.18: The Se-Se-Se angle distribution for $(Ag_2Se)_{41}$ at 251K.

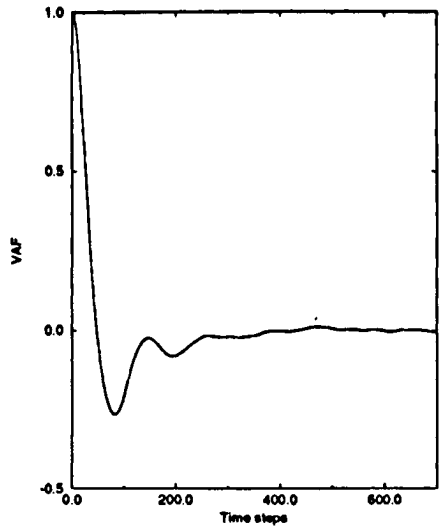

Figure 2.19: The VAF of Ag^+ for$(Ag_2Se)_{41}$ at 251K.

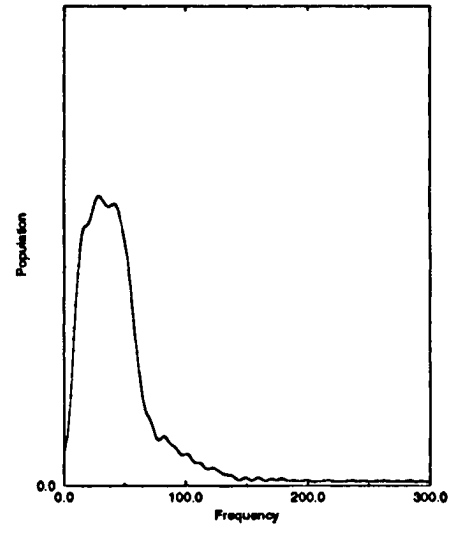

Figure 2.20: The power spectrum of Ag^+ for $(Ag_2Se)_{41}$ at 251K.

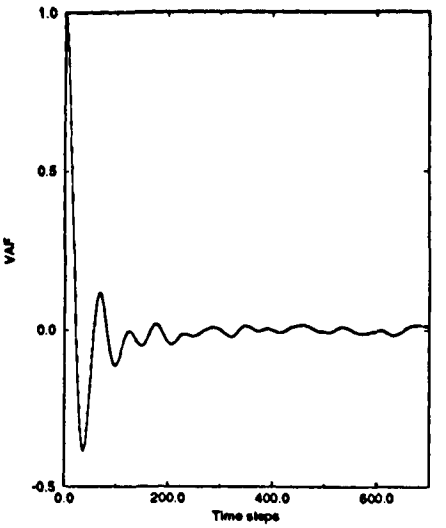

Figure 2.21: The VAF of Se^{2-} for $(Ag_2Se)_{41}$ at 251K.

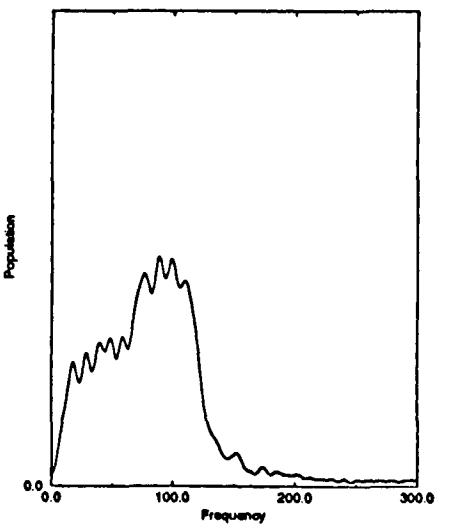

Figure 2.22: The power spectrum of Se^{2-} for $(Ag_2Se)_{41}$ at 251K.

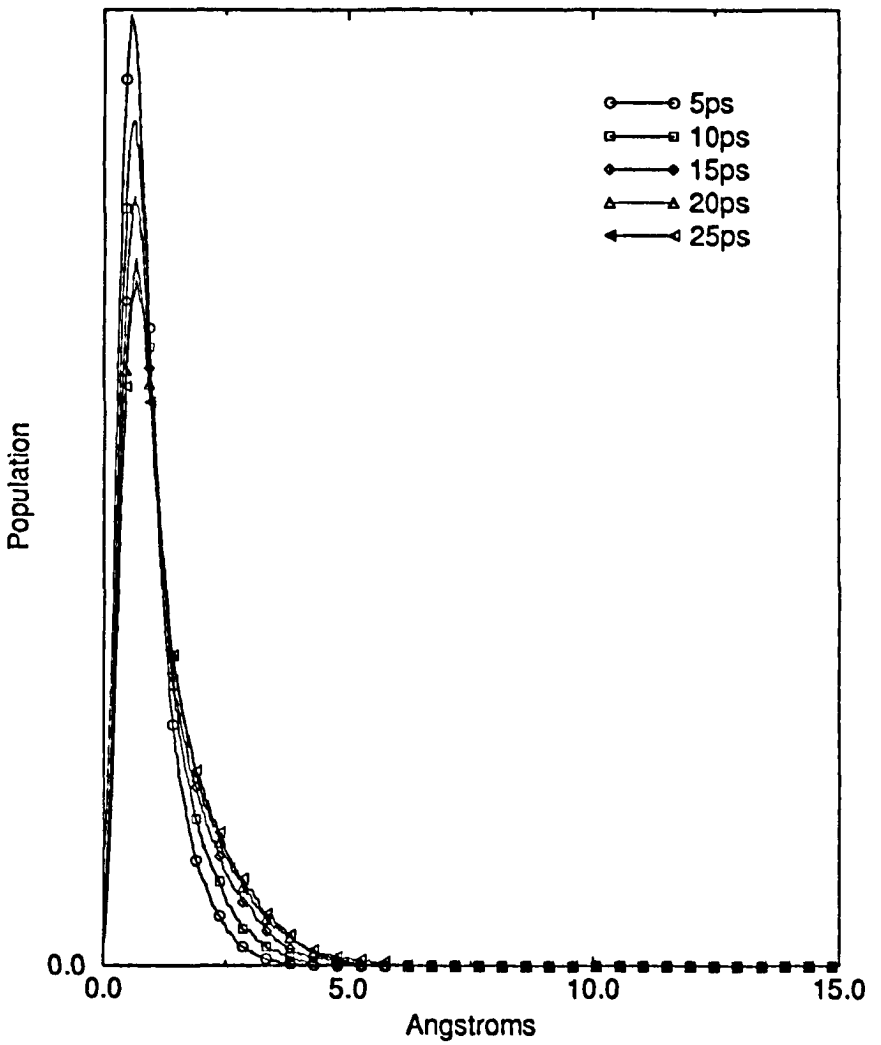

Figure 2.23: The van Hove self correlation function of Ag^+ for $(Ag_2Se)_{41}$ at 251K, time scale=5, 10, 15, 20, 25ps.

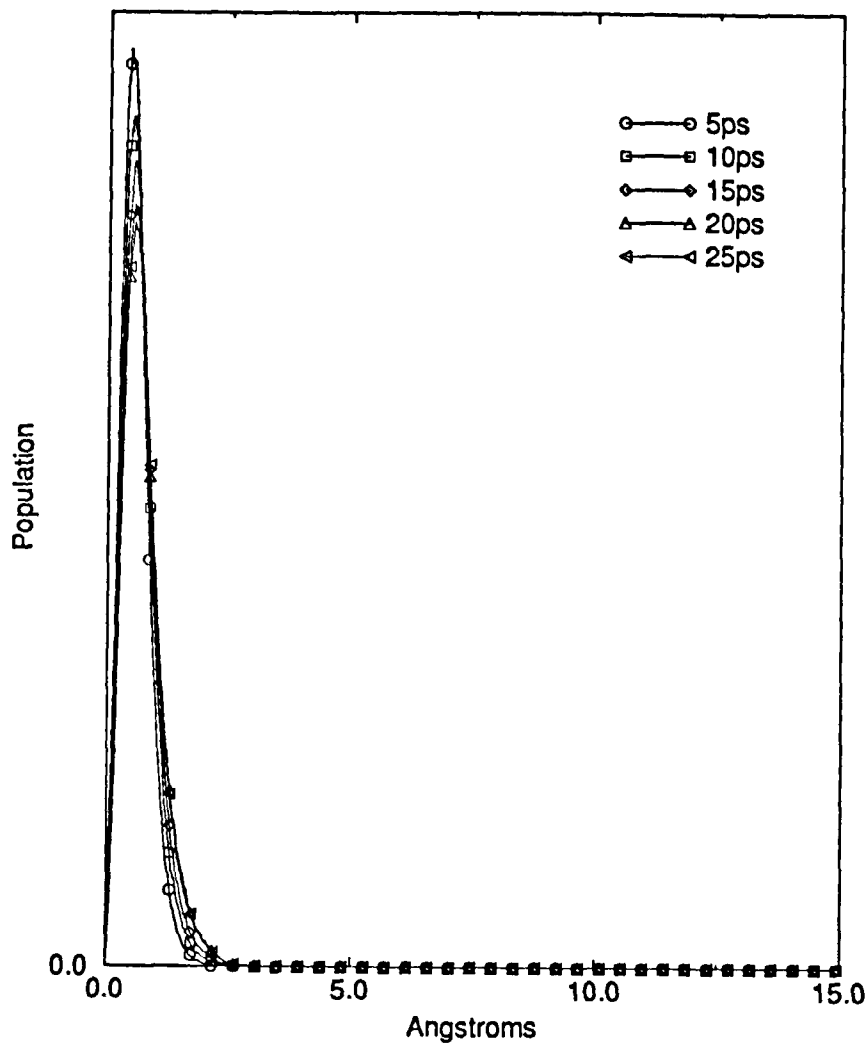

Figure 2.24: The van Hove self correlation function of Se^{2-} for $(Ag_2Se)_{41}$ at 251K, time scale=5, 10, 15, 20, 25ps.

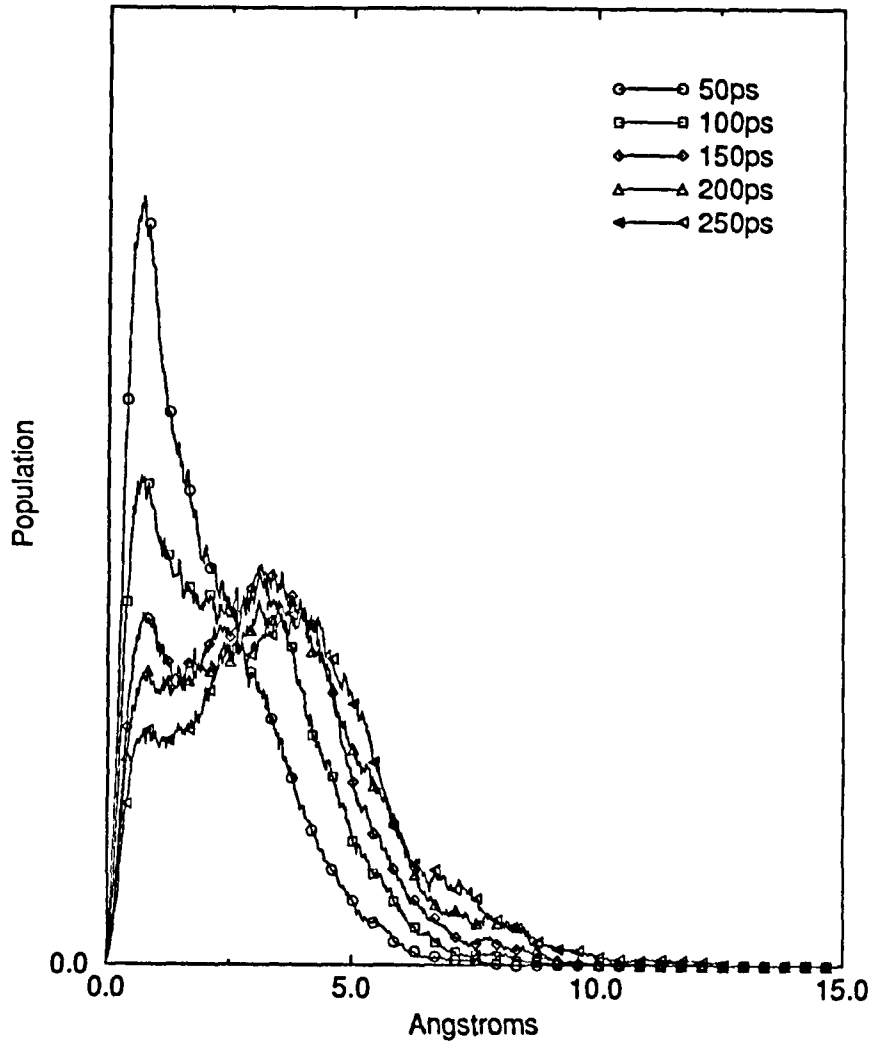

Figure 2.25: The van Hove self correlation function of the interior Ag^+ for $(Ag_2Se)_{41}$ at 251K, time scale=50, 100, 150, 200, 250ps.

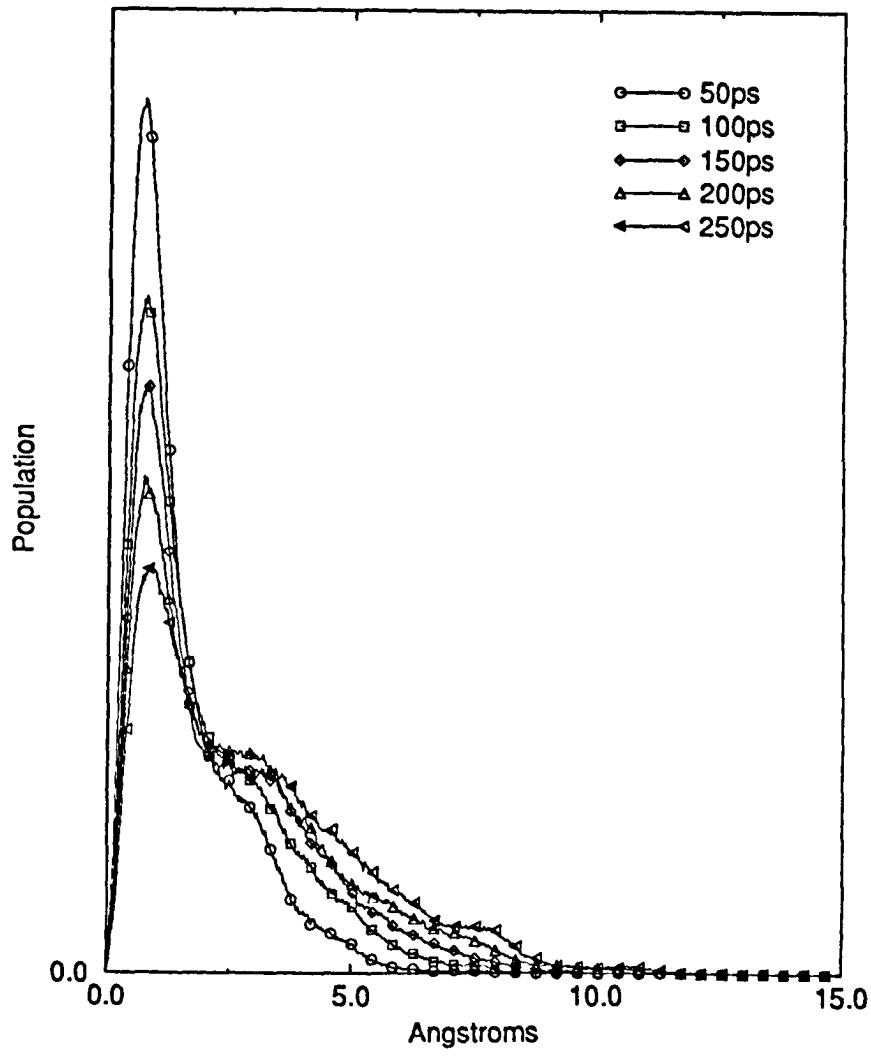

Figure 2.26: The van Hove self correlation function of the surface Ag^+ for $(Ag_2Se)_{41}$ at 251K, time scale=50, 100, 150, 200, 250ps.

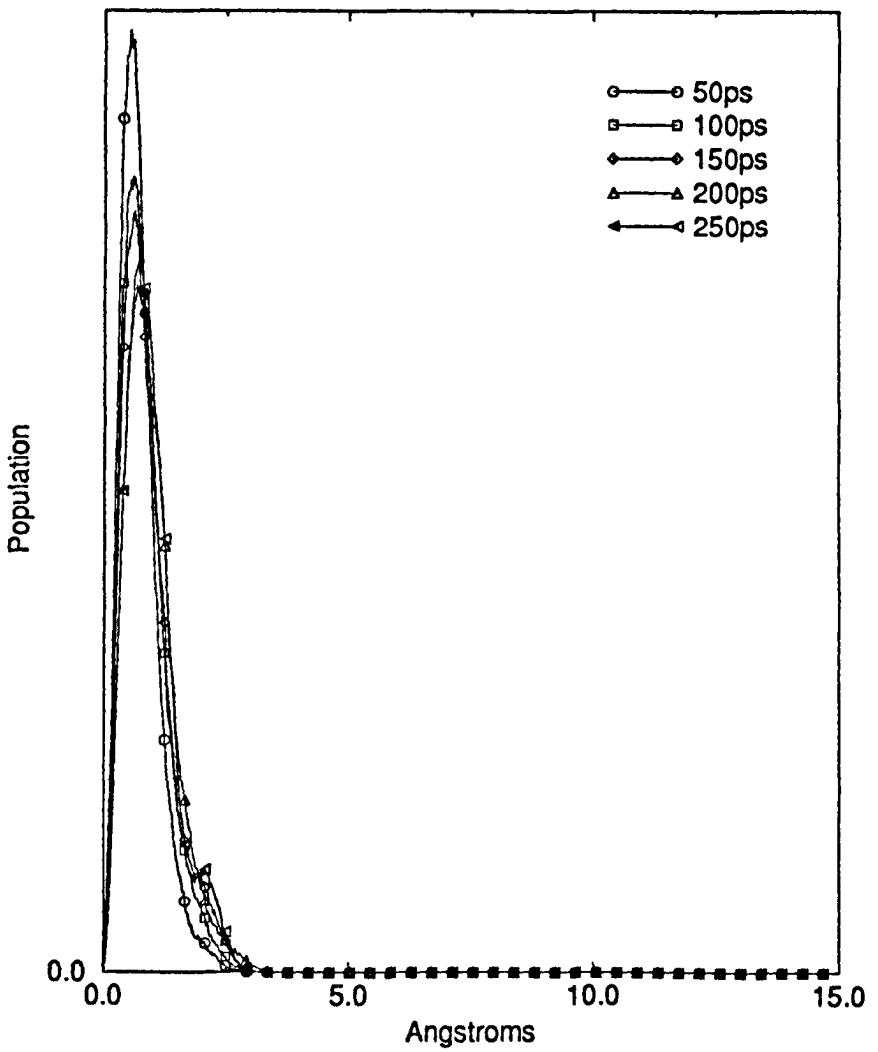

Figure 2.27: The van Hove self correlation function of the interior Se^{2-} for $(Ag_2Se)_{41}$ at 251K, time scale=50, 100, 150, 200, 250ps.

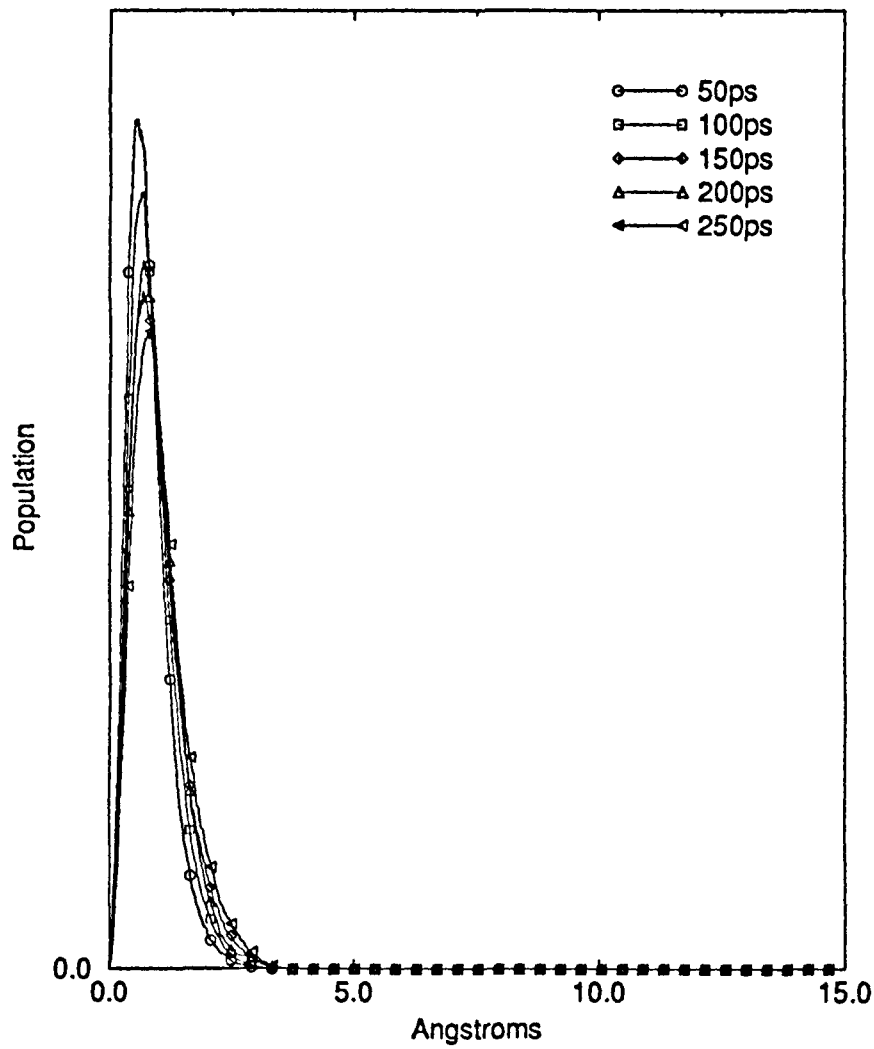

Figure 2.28: The van Hove self correlation function of the surface Se^{2-} for $(Ag_2Se)_{41}$ at 251K, time scale=50, 100, 150, 200, 250ps.

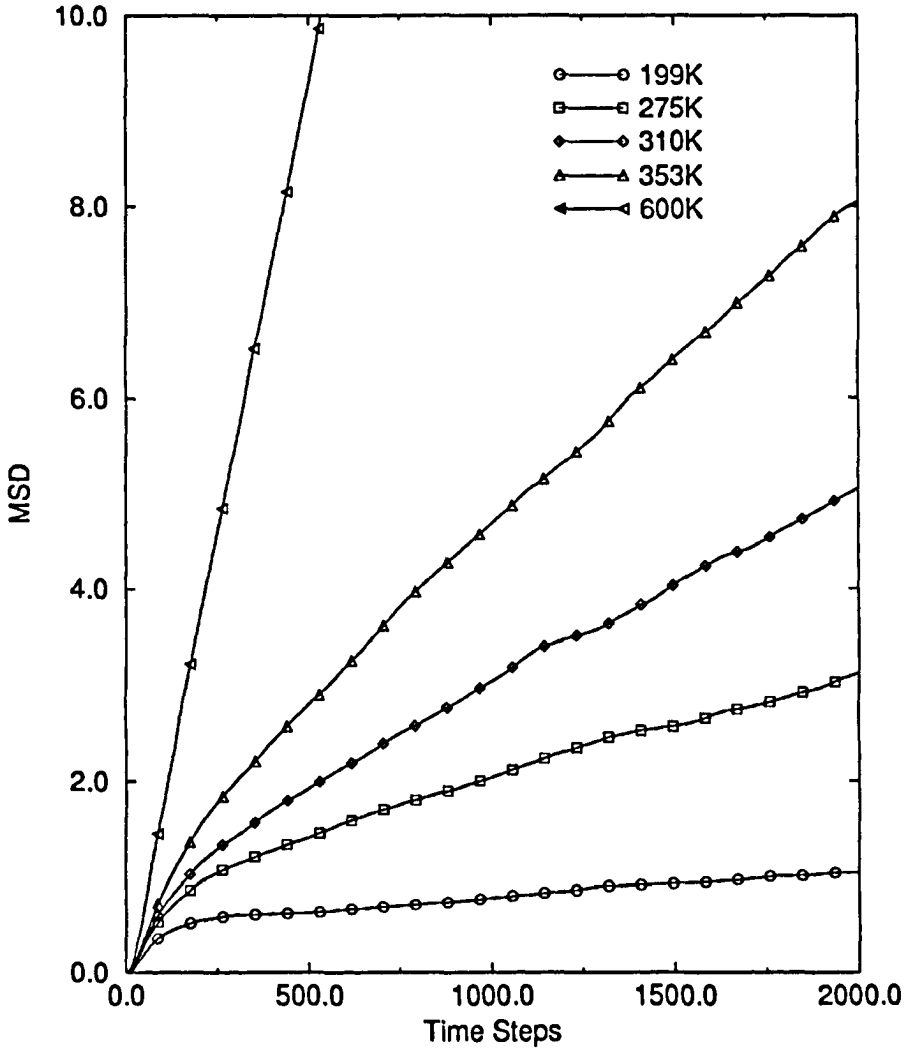

Figure 2.29: The MSD for Ag^+ ions for $(Ag_2Se)_{80}$ at different temperatures.

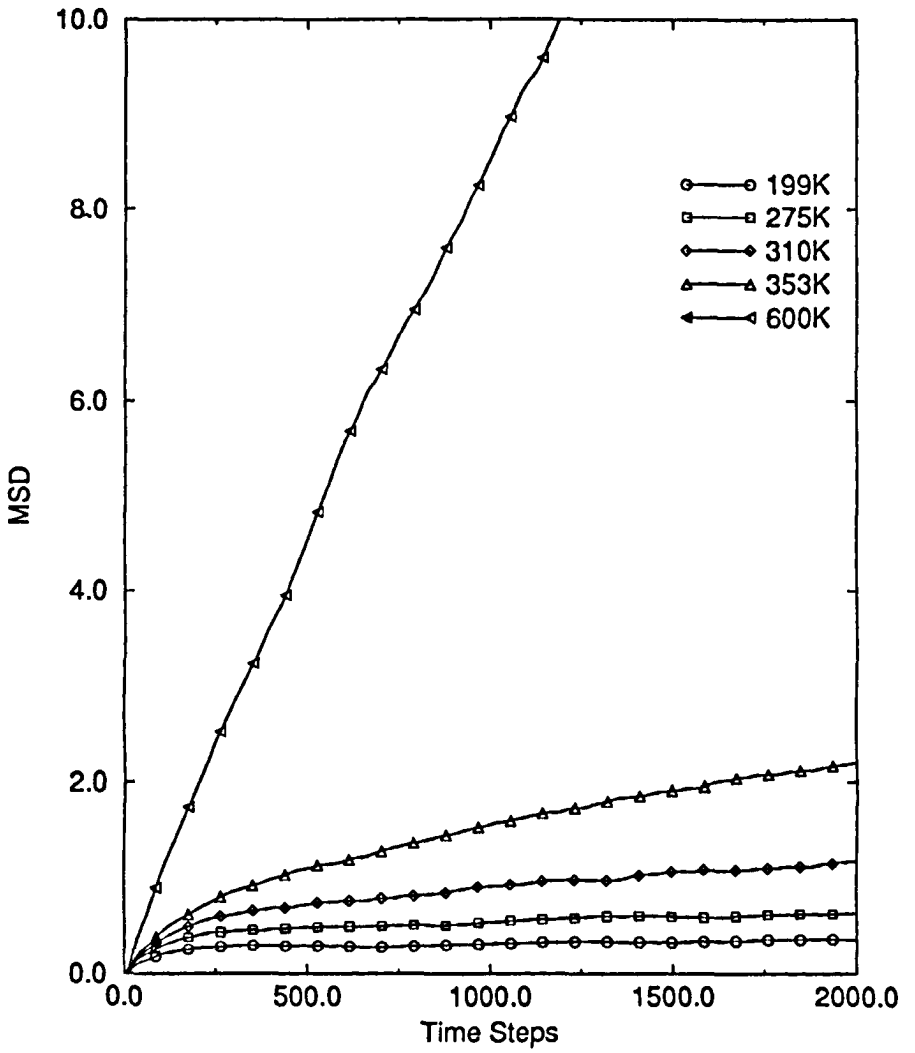

Figure 2.30: The MSD for Se^{2-} ions for $(Ag_2Se)_{80}$ at different temperatures.

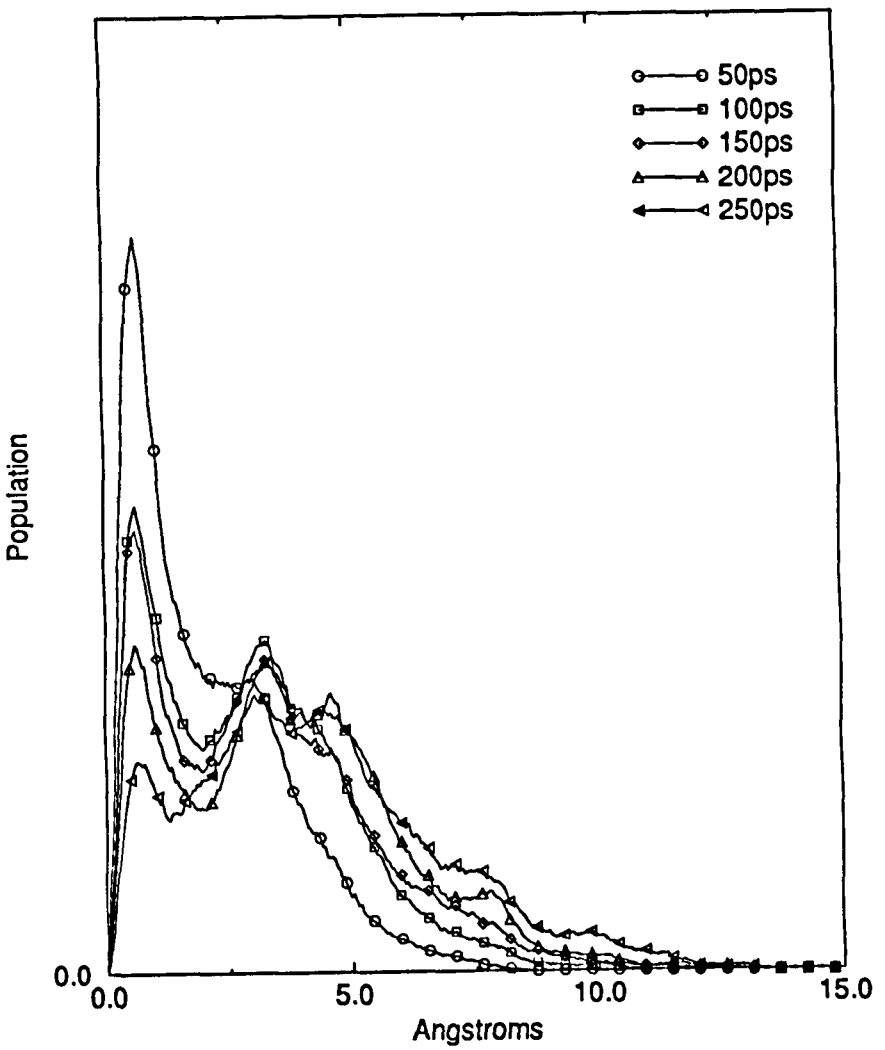

Figure 2.31: The van Hove self-correlation function for the interior Ag^+ ions for $(Ag_2Se)_{80}$ at 275K.

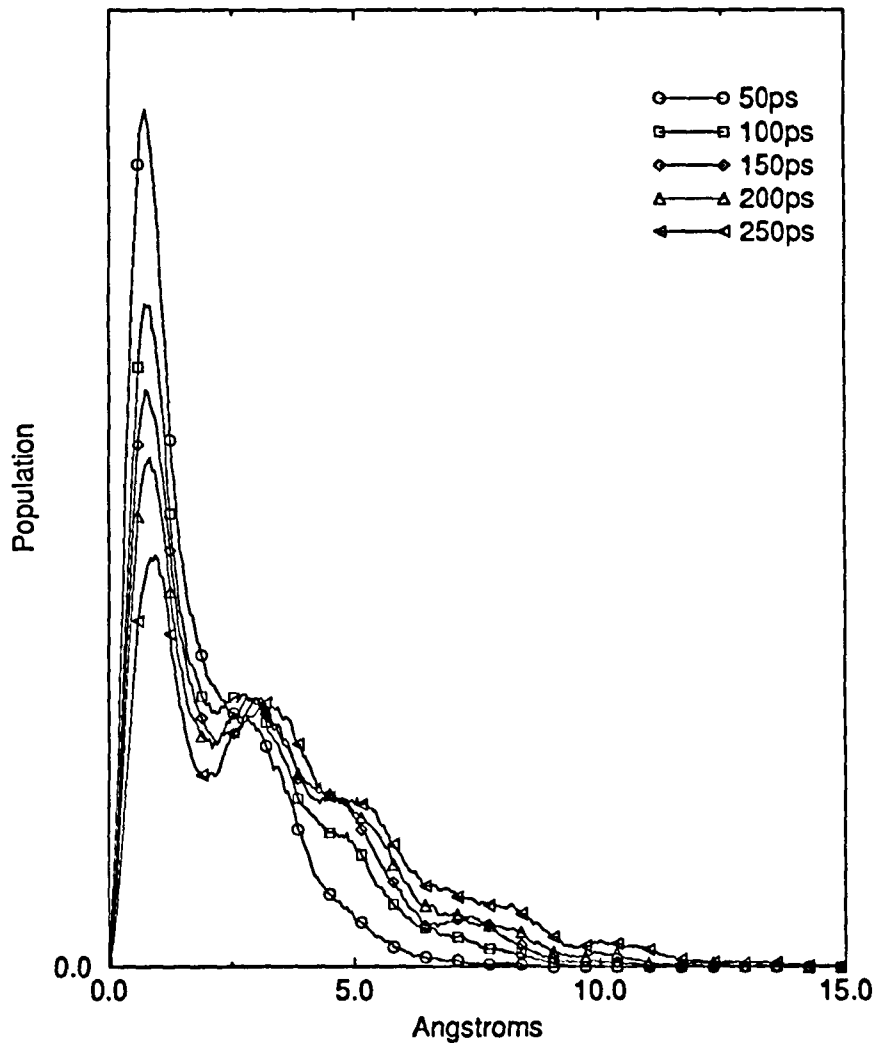

Figure 2.32: The van Hove self-correlation function for the surface Ag^+ ions for $(Ag_2Se)_{80}$ at 275K.

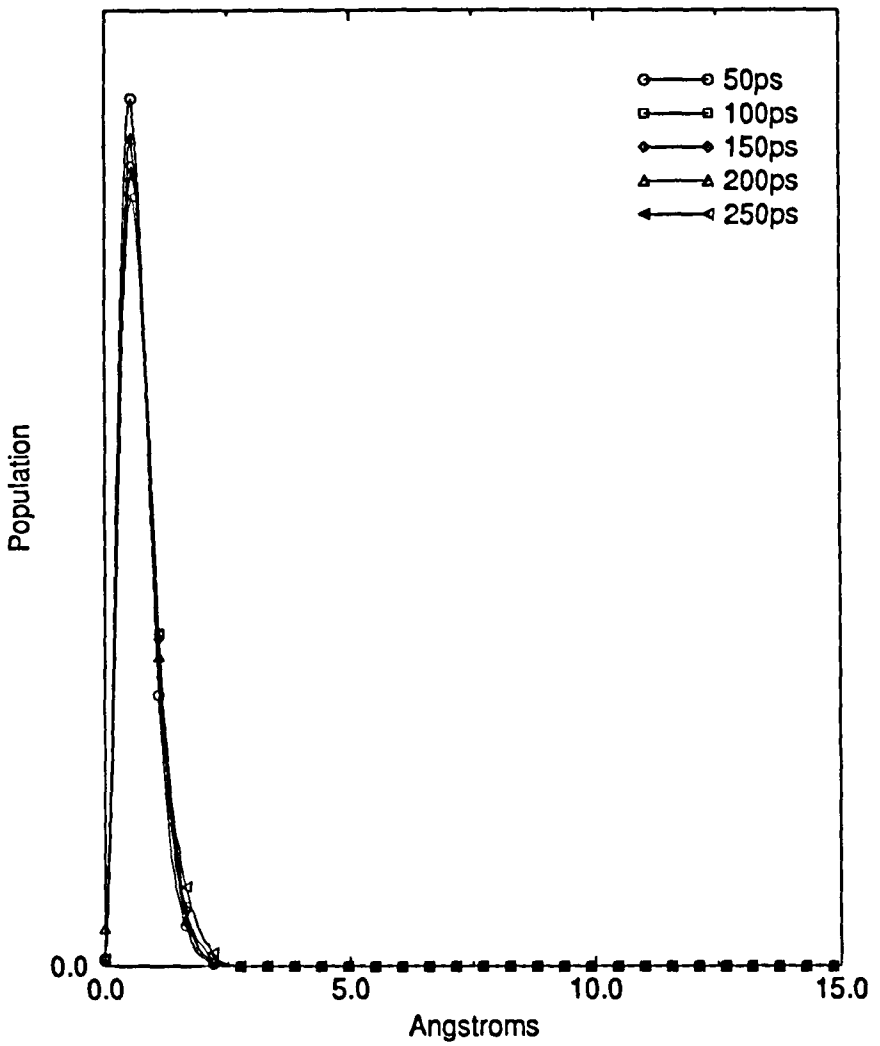

Figure 2.33: The van Hove self-correlation function for the interior Se^{2-} ions for $(Ag_2Se)_{80}$ at 275K.

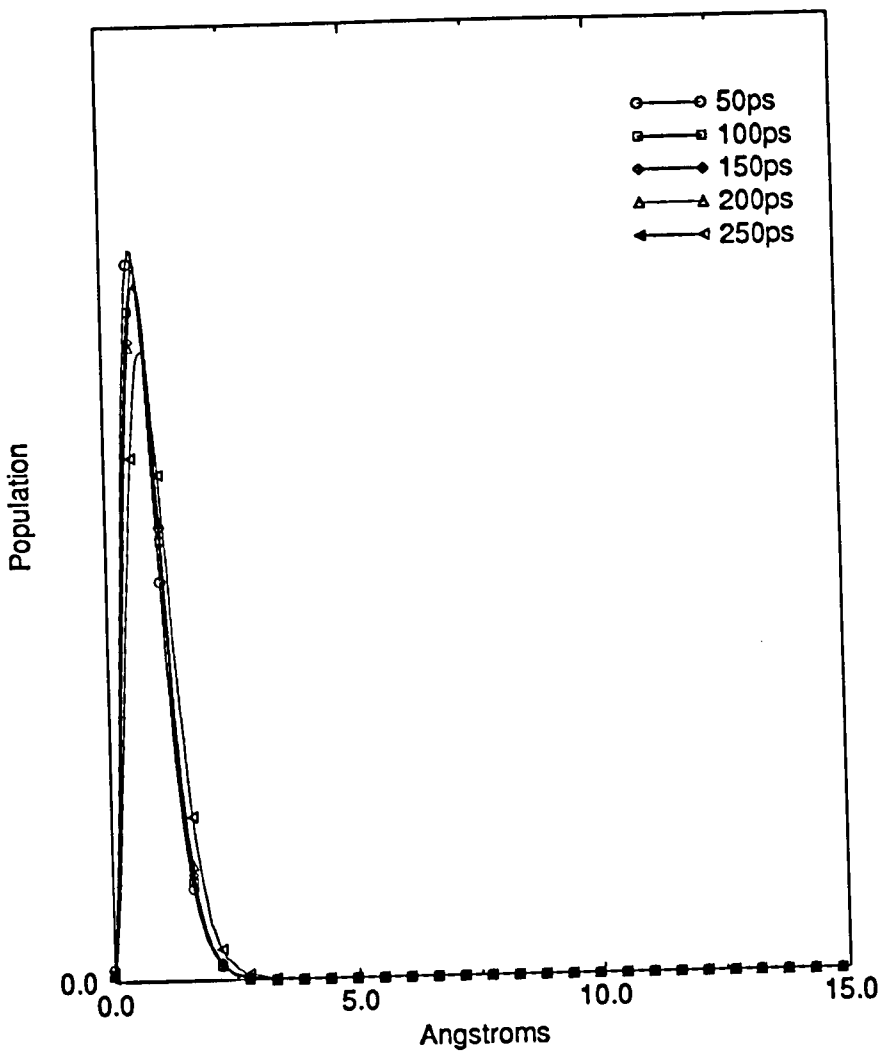

Figure 2.34: The van Hove self-correlation function for the surface Se^{2-} ions for $(Ag_2Se)_{80}$ at 275K.

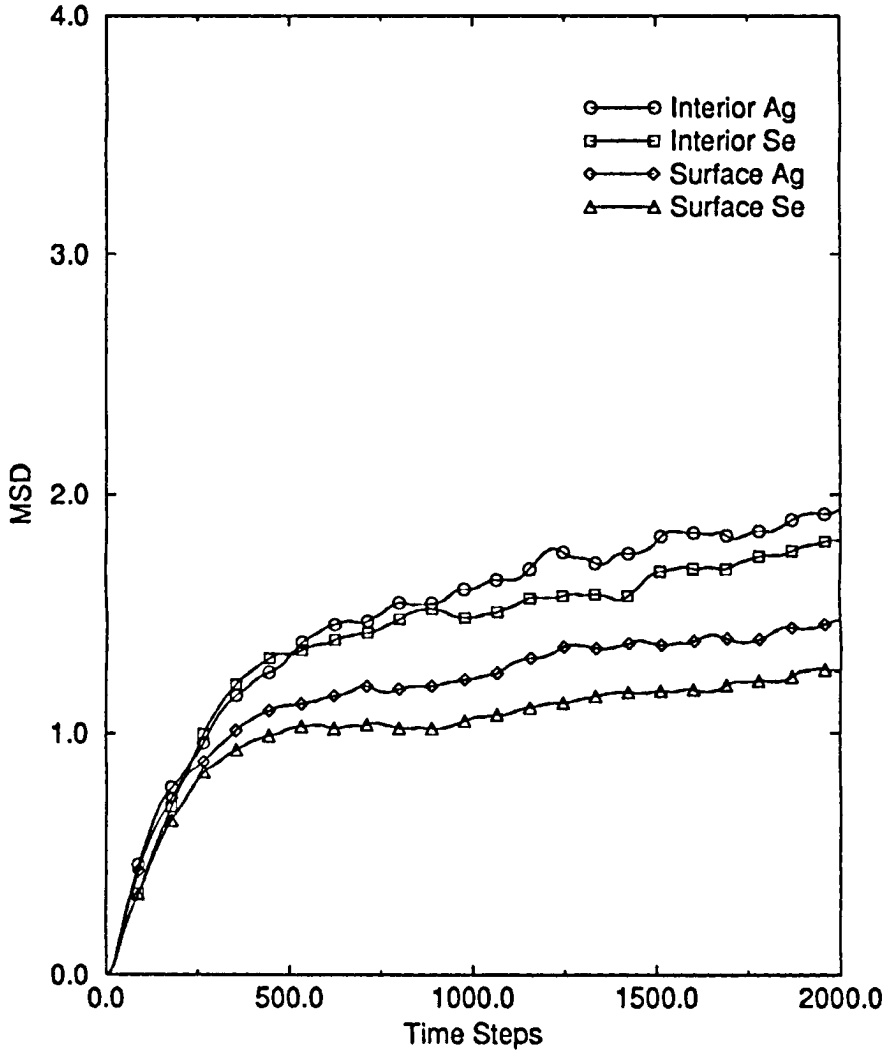

Figure 2.35: The MSD for $(AgI)_{60}$ at 244K.

Chapter 3

Origin Of Tilt Behavior In Monolayers

3.1 Introduction

Different kinds of monolayers at interfaces have been the subject of intensive research for over twenty years.[14,59] They are distinguished by their means of preparation and the types of interfaces that are formed. First, the Langmuir films are formed by spreading amphiphile molecules on a water/air or water/oil interface. If the monolayer is then transferred to a solid substrate, it is called a Langmuir-Blodgett (LB) film. Another related layered structure, termed a lipid bilayer, exists in biological membranes.[59–61] More recently, people have discovered that many molecules can spontaneously adsorb on metal surfaces and form stable and well-organized monolayers.[34,32,33,35] They are called self-assembled monolayers (SAMs). So far, it's the most effective method to generate stable and well-ordered monolayers on surfaces.

The Langmuir films, especially LB films, have been found to have widespread applications. Examples include gas and chemical sensors, paint, lubricants, microelectronic devices, *etc.* Many experimental researches[62,63] and theoretical studies[64–67] have been directed toward understanding their molecular packing and phase transitions.

Among the theoretical methods applied, molecular dynamics and Monte Carlo methods have been used to study the structure and thermodyam-

ics of Langmuir and L-B films at the molecular level. In particular, Rice and his coworkers have conducted a series of theoretical studies on liquid supported monolayers by using the Monte Carlo method and molecular dynamics.[68-74] Results have reproduced phase transition temperatures and phase structures successfully.

Cai and Rice utilized density functional theory to examine the finite temperature tilting transition behavior of the systems of rigid chain Langmuir monolayers.[65,66] By calculating the free energy difference, they found that a tilted state of the monolayer is stable only if the ratio of the chain-surface to chain-chain interaction exceeds a critical value. When the area per chain and temperature are the same, a monolayer with chains tilting toward their nearest neighbors has a larger tilt angle and lower free energy than a monolayer with chains tilting toward their next-nearest neighbors. But it is still not clear what are the underlying molecular level driving forces for the orientation behavior in monolayers at the surface.

Binder and his coworkers generated the ground-state phase diagram for rigid rods grafted on a lattice.[75] They found that for high surface density, the rods were oriented perpendicularly to the surface; for a somewhat less dense case, a sixfold degenerate uniform-tilt state occurred with all rods tilted towards one of their next-nearest neighbors; for low surface density,

the rods were tilted nonuniformly and formed a "striped" structure. The results from Monte Carlo simulation showed a first order transition between a uniformly tilted state to a disordered state, while the mean field theory predicted a second order transition.

Unlike Langmuir and LB films, molecular chains in SAMs are chemically bonded to the metal surface via a thiol group by losing a hydrogen atom. It is well known that alkane thiol chains (H-S-$(CH_2)_nCH_3$; n = 1-21) can self assemble on metal surfaces (Au, Ag, Cu, Pt). Especially on the Au(111) surface, it forms a densely packed and stable monolayer on the surface with average tilt angle from 20° to 30°, depending on experimental conditions and the length of the alkane chains.[34,32,33,35] Extensive experimental effort has been conducted related to understanding self assembled monolayers at the molecular level. Many theoretical studies have also been performed on SAMs.[76-82] Molecular dynamics (MD) simulations of C_n alkane thiols on gold have successfully reproduced structural and dynamical properties.

Recently, Miller and coworkers[36] attached thiophenol-terminated oligoimide molecules of the type HSPh-A-B-A-B-A-B-A-B, where Ph=phenyl, A= naphthalene-1,4,5,8-tetracarboxylic dianhydride, and B=3,3'-dimethoxy benzidine, via self-assembly into a dense monolayer on the Au(111) surface.

IR spectroscopy and electrochemical data showed that oligoimide molecules self assembled into a dense monolayer on the gold surface. The molecules were tilted around 60° from the surface normal and the surface density was 175 $Å^2$/molecule.

We chose to study oligoimide chains on the gold surface. We are interested in the driving forces for observed ordering of monolayers on solid surfaces. In order to answer questions like: what factors affect the packing ordering on the surface? how does surface density affect molecular packing? and how important is the surface potential?, we preformed Monte Carlo simulations of self assembled model rigid oligomers at metal surfaces. Because it is very difficult to model a complex system like the oligoimides, we first simplified the model as rigid rods. Since this thiophenol-terminated oligoimide molecule is semi-rigid along the long molecular axis, it is possible to model this system with rigid rods. It is also related to liquid crystals at interfaces. With different interaction parameters ϵ, we could also model the A-B-A-B... oligoimide with alternating segments. In later calculations, we performed detailed molecular dynamics simulations of a similar system, 4-MPP (4-mercapto-phenyl-phthalimide). Results of that work showed good agreement with IR and SERS experments. (see Appendix B)

3.2 Monte Carlo Method

The Monte Carlo method was used in this study to explore the microscopic ordering in rigid rod monolayers. The unphysical moves that can be generated by the MC method makes it is possible to study processes that occur on time scales that are too long to be accessed easily in real-time simulations like molecular dynamics.[82] So the MC method can be more efficient than MD simulation in studying phase transitions. The canonical ensemble with constant temperature and constant volume (NVT) was used in the simulation. The ensemble was obtained by generating a trajectory in phase space. The Metropolis method was used to sample the configuration space by generating a Markov chain of states.

Molecules on the surface were considered as rigid chains. Each chain consisted of 15 effective monomers connected along a single vector. Each segment interacted with other segments through a Lennard-Jones 12-6 potential.

$$E_{ij}(r) = 4\epsilon_{ij}\left[\left(\frac{\sigma_{ij}}{r}\right)^{12} - \left(\frac{\sigma_{ij}}{r}\right)^{6}\right]. \tag{3.1}$$

The values of the intermolecular Lennard-Jones potential parameters σ_{ii} and ϵ_{ii} were taken in scaled units (with factors for lengths and energies).

The following combination rules were used to obtain the cross-parameters σ_{ij} and ϵ_{ij}.

$$\sigma_{ij} = \sqrt{\sigma_{ii} \cdot \sigma_{jj}}, \tag{3.2}$$

$$\epsilon_{ij} = \sqrt{\epsilon_{ii} \cdot \epsilon_{jj}}. \tag{3.3}$$

An integrated 9-3 surface potential was used to represent the chain segment-surface interactions,

$$V(z) = 20\epsilon_s \left[\left(\frac{\sigma_s}{z} \right)^9 - \left(\frac{\sigma_s}{z} \right)^3 \right], \tag{3.4}$$

where z is the distance of the particle from the surface.

Simulations were carried out with rigid rods with head groups bonded to a triangular lattice surface at scaled temperatures correspinding to room temperature and higher temperatures. The system consisted of 64 chains. A unit vector is defined along the chain direction. A rectangular cell was used to employ periodic boundary conditions in two dimensions (xy plane). The cutoff distance for L-J interactions was double the lattice constant, which includes both nearest neighbor and next nearest neighbor interactions. Initial chains were placed on a perfect triangular lattice. The lattice

constant A was varied to change the density from near close packed to less dense values. All lengths were in units of σ. The rod length was rescaled to l=L/σ, and the lattice parameter to a=A/σ. (Figure 3.1)

After starting the system in an upright configuration, the rigid chains were moved by randomly choosing a new trial orientation. The molecule being chosen to be moved and attempted were chosen in sequential order. The new trial orientation of a chain was generated by a rejection technique. It constrained the cosine of the angle between the old and new unit vectors, *i.e.* the dot product, to greater than (1.0 – *dotmin*). (dotmin is the minimum allowed dot product.) (see Allen and Tildesley[83]) If the change in the angle exceeded a maximum angle (which is an adjustable parameter, the accpetance rate is set to be 30%), the move was automatically rejected; if not, the move was accepted or rejected based on the Metroplis algorithm. If accepted, that chain will adopt the new orientation. Otherwise, that chain will stay in the old orientation.

θ is the angle between the vector of the surface normal and the unit vector of each rod. ϕ is the polar angle of each rod. (i.e. the direction of the chain tilt)

The order parameter is defined as:

$$S_i = \frac{1}{2}\left\langle 3\cos^2\theta_i - 1 \right\rangle, \tag{3.5}$$

where θ is the tilt angle from the surface normal.

The orientational order parameter, M, is defined as:

$$M = \frac{1}{N^2}\left\langle \sum_i \sum_j \cos(2\theta_{ij}) \right\rangle, \theta_{ij} = \cos^{-1}(\mathbf{u}_i \cdot \mathbf{u}_j). \tag{3.6}$$

If M is equal to 1, all chains have exactly the same orientation. On the other hand, if M is zero, the chains are completely randomly oriented.

The radial distribution function is defined as:

$$g(r) = \frac{V}{N^2}\left\langle \sum_i \sum_{j \neq i} \delta(r - r_{ij}) \right\rangle, \tag{3.7}$$

where V is the volume and N is the number of particles in the system. This function gives the probability of finding a pair of particles a distance r apart.

3.3 Results

The chains try to minimize the total free energy of the system. The free energy includes an internal energy term and an entropy term.

$$A = E - TS, \tag{3.8}$$

where A is the Helmholtz free energy, E is the internal energy, S is the entropy and T is the temperature.

First, we calculated the potential energy as a function of tilt angle. At zero temperature, there is no entropy factor in the free energy.

Potential curves for different ratios of the chain-surface to chain-chain interactions were generated with a/σ=0.95, 1.0, 1.05, 1.15, 1.414, 2.37. ϵ_{ext} is the strength of the surface potential and ϵ is the well depth of the Lennard-Jones potential between each effective segment. Results showed that when ϵ_{ext}/ϵ increased from 0.0 to 1.0, the tilt angle corresponding to the minimum in energy stayed almost the same, while the minimum in energy of the system became lower. A monolayer with chains tilting toward their next nearest neighbor had a larger tilt angle and lower potential energy than a monolayer with chains tilting toward their nearest neighbors. (Figure 3.2) As the density decreased, the minimum tilt angle became

larger and the potential well became deeper. When ϵ_{ext}/ϵ became very large, like 1000, the minimum tilt angle became larger due to huge surface attractions.

The zero Kelvin potential energy curves showed that the next-nearest neighbor (nnn) tilt is the most stable state for all densities that we tested. The minimum energy tilt angle was found to vary considerably with chain density.

Monte Carlo simulations were performed on a model with rigid rods bonded to a solid surface at T>0. The rods were represented by effective segments. The effective segments in different chains interacted through a Lennard-Jones potential. The 9-3 integrated surface potential was used to represent the inteaction between the effective segments and surface. Two angular degrees of freedom were allowed for the orientations of the chain.

We first investigated a system with relatively high surface density. The relative density was equal to 75% of a close packed system. In order to study the surface effect, we varied the ratio of ϵ between the chain-surface and chain-chain interactions. For ϵ_{ext}/ϵ=1.0, the chains tilted toward their next nearest neighbor after 12,000 steps. Figures 3.3 and 3.4 show the tilt angle distrubution and the direction of the tilt. The average tilt angle is θ=33°. When ϵ_{ext}/ϵ=0.5, chains showed a collective tilt toward their nn

after many steps, then slowly shifted to nnn. At 400K, the shift was faster than at 300K. The average tilt angle was equal to 29° while the chains tilted towards nn and equal to 33° after the shift. (Figure 3.5) When we chose ϵ_{ext}/ϵ=0.0 (i.e. without surface potential) it took more steps for the chains to reach their equilibrium state and exhibit collective tilt. Eventually, the chains tilted toward nnn. The tilt angle was equal to 33°. (Figure 3.6) The orientational order parameters were over 0.9998, indicating all the chains are almost pointing toward the same direction. We also tested binary-oligomers and the results were the same as homo-oligomers at high density.

We decreased the relative surface density to 50% of close packing by increasing the lattice constant. For all cases, the tilt angle has a relatively broad distribution as displayed in Figure 3.7. But the chains had a tendency of tilting toward one direction. The average tilt angle is around 30°. The radial distribution function is liquid like. And the orientational order parameter is around 0.9.

In Miller's experiment, it was determined that the surface density was 175 Å^2/molecule for oligoimide molecules self assembled on the Au(111) surface.[36] That translates to about 18% of a close packed system. So we decreased the lattice constant and prepared a system at relative density

equal to 18% of close packing. Like other densities, ϵ_{ext}/ϵ=0.0, 0.5 and 1.0 were studied. Starting from staight up, the chains did not show collective tilt, but clustered into locally dense regions for all ϵ_{ext}/ϵ ratios. Figures 3.8, 3.9 show the the distributions of tilt angle and the direction of the tilting. The g(r) displayed a liquid like distribution. And the low orientational order parameter (0.5) means the chains are randomly tilting.

Starting from configurations where all chains tilt toward nnn or nn, results showed that monolayers starting from a nnn tilt (order parameter S=0.99) is much more stable than monolayers starting from nn tilt (S=0.81)

Because the chains bonded to the surface may be flexible, we added a flexible spacer in the rigid chain where connected two rigid rod segments. The first case we tested is with the shorter portion of the chains connected to the surface. At 75% closed-pack, the two sections of chains pointed toward different directions first. (see Figures 3.10, 3.11) Interestinly, upon further equilibration, the short sections shifted their tilting directions to the same direction as the long sections (nnn). (see Figures 3.12, 3.13) Then we tried the longer portion of the chains connected to the surface. Both sections of the chains tilted toward their nnn with the same direction. See Figures 3.14, 3.15.

Over the years, there have been many works investigating hard sphere cylinders at high packing densities.[84,85] However, not many people have used the MC method to study hard sphere chains grafted on a solid surface. With less degrees of freedom, what is the thermodynamic behavior of the grafted chains? We removed the potential energies between each segment on the chain and the surface potential. Chains were able to move randomly as long as no overlap occurred. This is thus a realistic model of true hard sphere cylinders on the surface. The direction of the tilt constantly shifts with the chains at 75% closed-packing. The orientational order parameters are very high (over 0.995). That suggests that the hard sphere chains move in a very correlated fashion, although they do not exhibit a constant uniform tilt. Somoza and Desai[86] used a mean-field model to study tilt order and predicted the steric interactions between rigid rods particles are not enough to induce tilt order at low densities. Furthuer numerical studies should be carried out to test the predictions of the mean field theory.

3.4 Discussion

The zero Kelvin energy curves showed that the next-nearest neighbor (nnn) tilt is the most stable state for all densities. The minimum energy tilt angle was found to vary considerably with chain density. When constrained

on the surface, the chains tilt collectively. For the 0.75 relative density case, the tilt appears to be driven primarily by energetic effects at room temperature; the tilt angle at 0 K agrees with the finite temperature result within 2°. Our result is contrary to the result from density functional theory conducted by Cai and Rice,[69] which showed that a monolayer with chains tilting toward their nearest neighbors has a larger tilt angle and lower free energy than a monolayer with chains tilting toward their next-nearest neighbors.

MC simulation results suggest that both high density homo-oligomers and binary-oligomers tilt collectivly toward nnn. These results agree with other models by Binder and coworkers[75] and Scheringer, *et al.*[64] Lower density systems do not exhibit a collective tilt but cluster into locally dense regions. For the 0.5 relative density case, chains tilt nonuniformly toward the same direction at room temperature; the tilts have a wide distribution. Results for chains with one flexible segment show that at high density, two sections of a chain may point towards different directions.

While these calculations are for idealized rigid rod chains, they provide guidelines for what can be expected for more realistic molecular models of rigid oligomers on solid surfaces. They also provide insights into the applicability of analytical theories for tethered rods at solid surfaces.

3.5 Figures

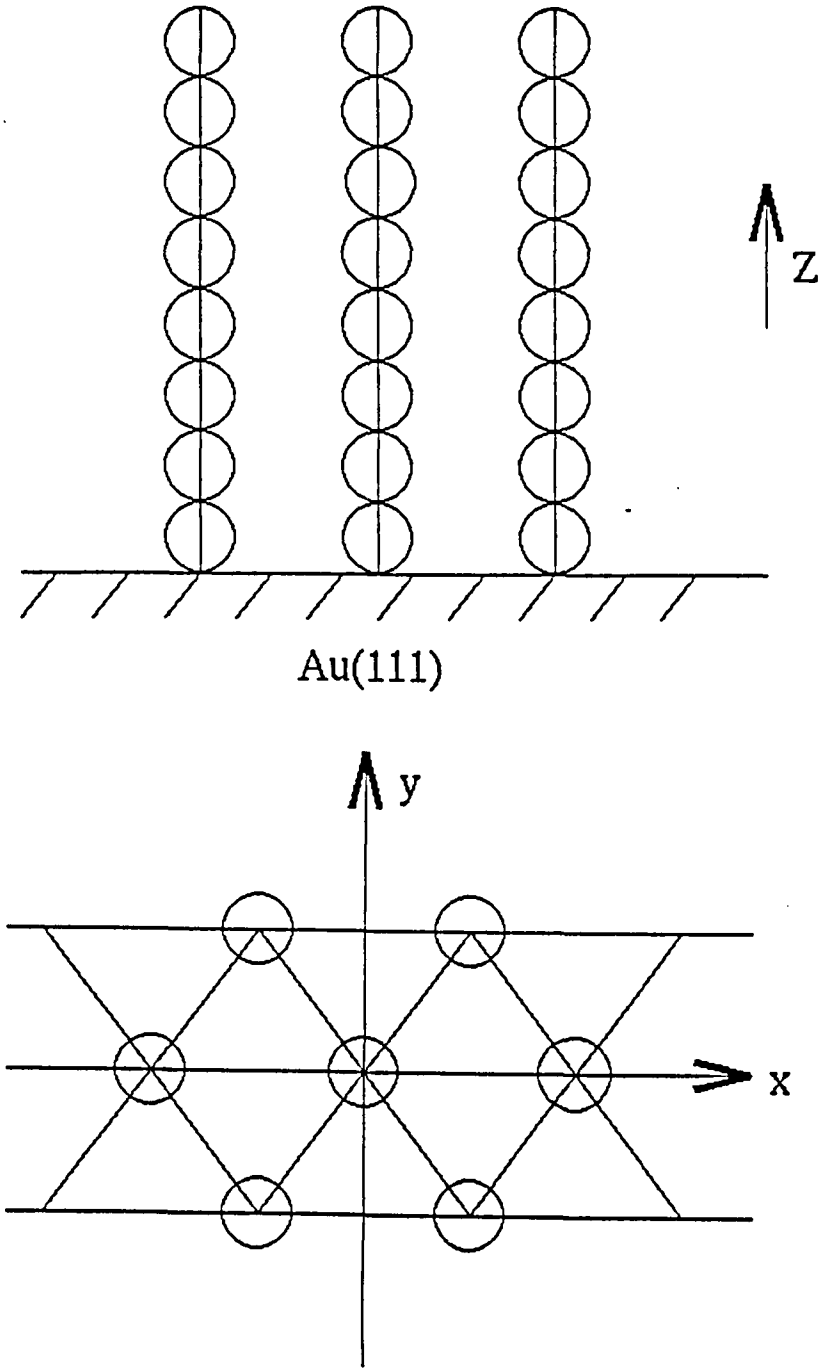

Figure 3.1: Monte Carlo method.

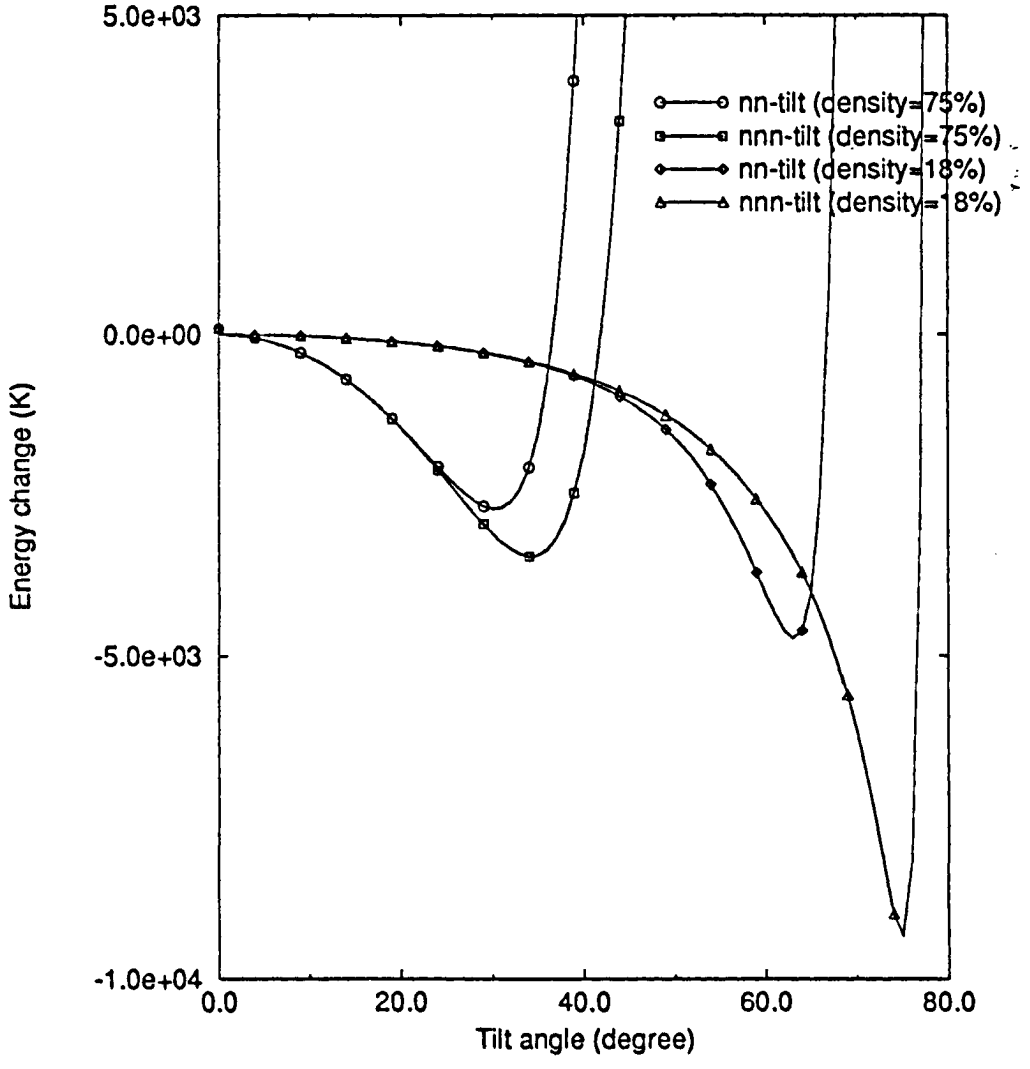

Figure 3.2: Potential Curve.

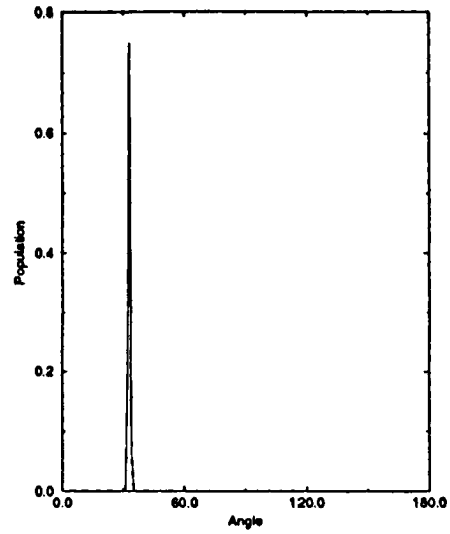

Figure 3.3: Tilt angle distribution at 75% closed packing, ϵ_{ext}/ϵ=1.0.

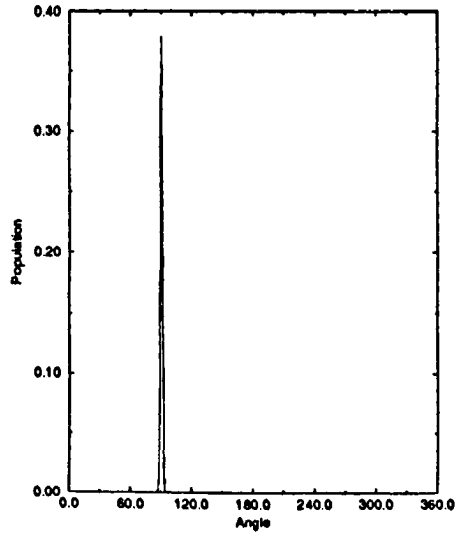

Figure 3.4: Directions of tilt at 75% closed packing, ϵ_{ext}/ϵ=1.0.

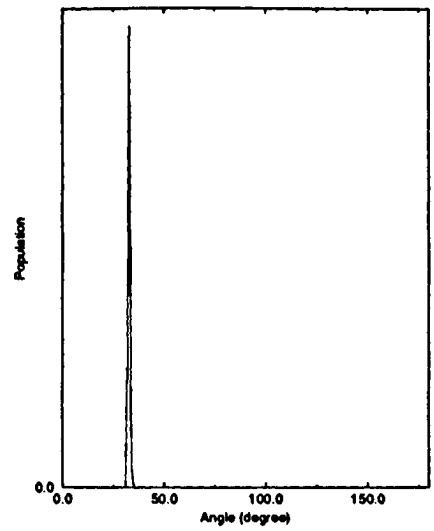

Figure 3.5: Tilt angle distribution at 75% closed packing, ϵ_{ext}/ϵ=0.5.

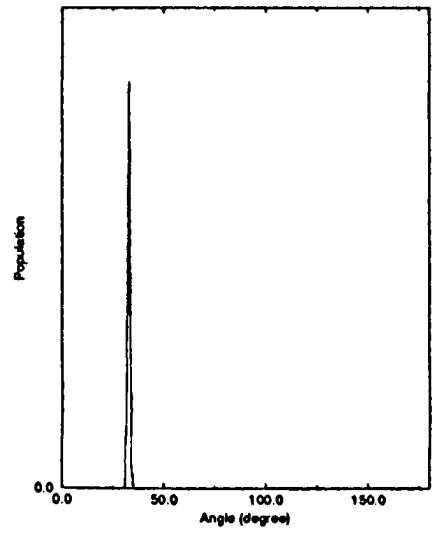

Figure 3.6: Tilt angle distribution at 75% closed packing, ϵ_{ext}/ϵ=0.0.

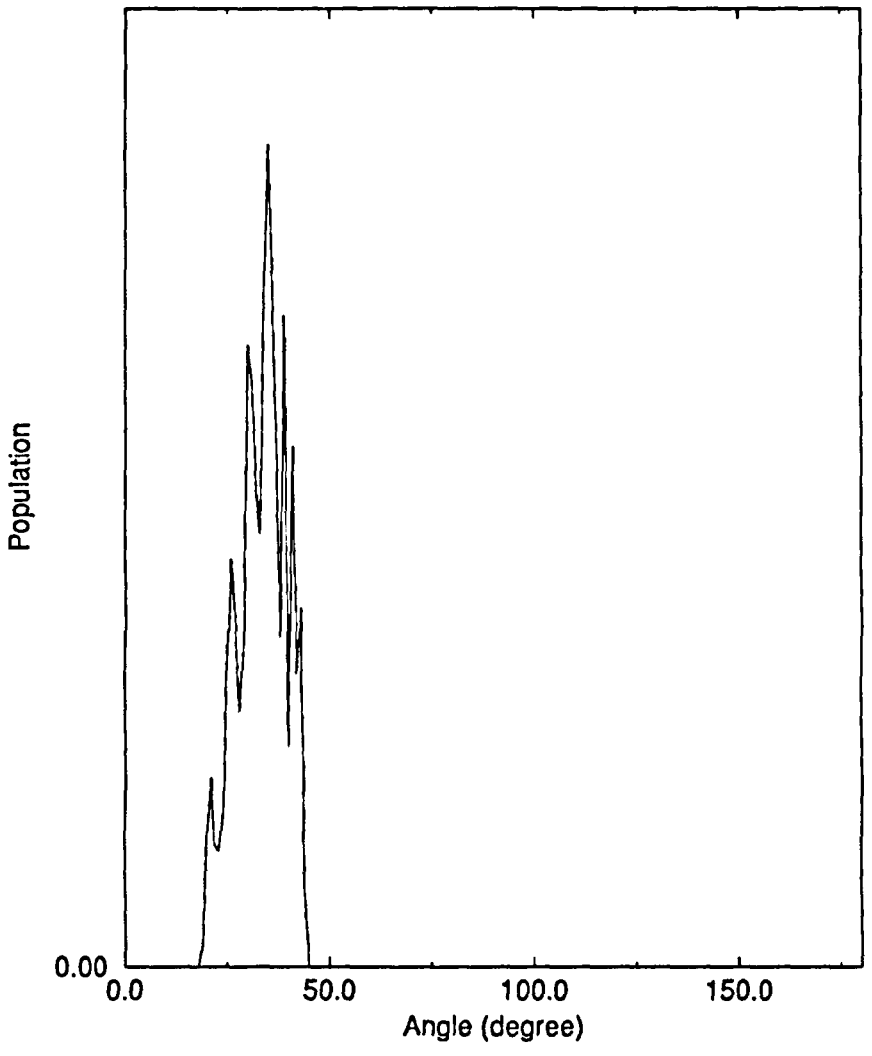

Figure 3.7: Tilt angle distribution at 50% closed packing, ϵ_{ext}/ϵ=1.0.

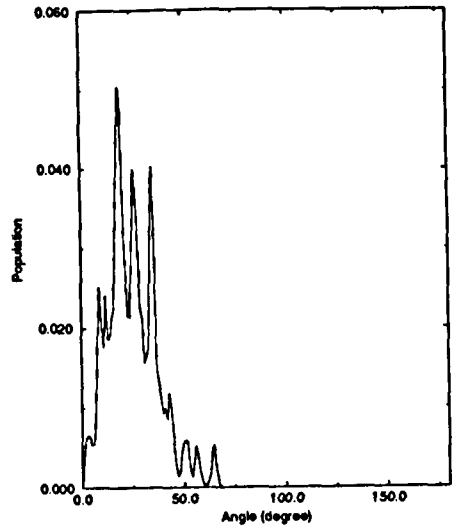

Figure 3.8: Tilt angle distribution at 18% closed packing, ϵ_{ext}/ϵ=1.0.

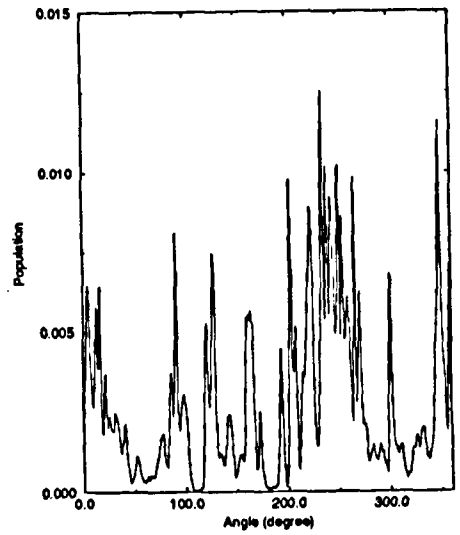

Figure 3.9: Directions of tilt angle at 18% closed packing, ϵ_{ext}/ϵ=1.0.

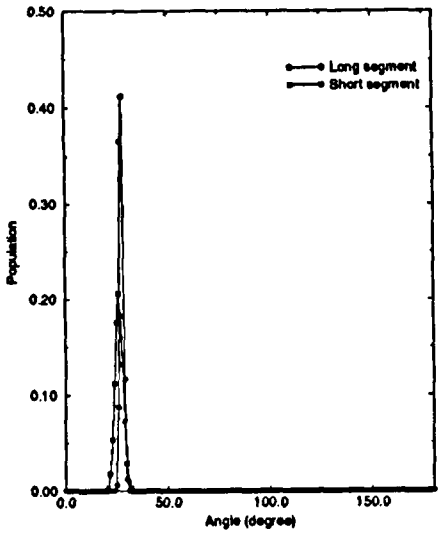

Figure 3.10: Tilt angle distribution at 75% closed packing with shorter portion of the chains bonded to the surface, ϵ_{ext}/ϵ=1.0. Initial equilibrium stage.

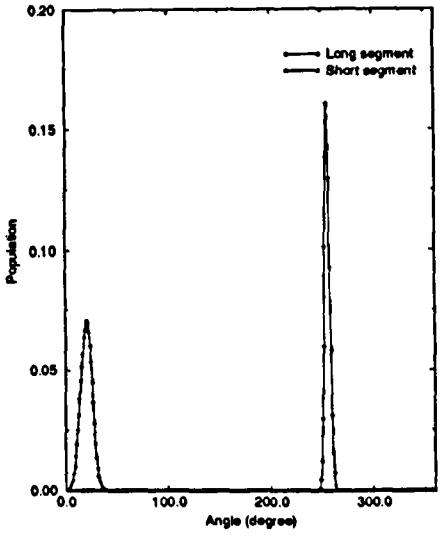

Figure 3.11: Directions of tilt angle at 75% closed packing with shorter portion of the chains bonded to the surface, ϵ_{ext}/ϵ=1.0. Initial equilibrium stage.

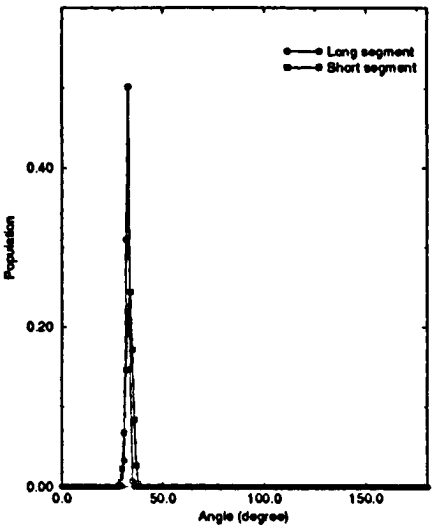

Figure 3.12: Tilt angle distribution at 75% closed packing with shorter portion of the chains bonded to the surface, ϵ_{ext}/ϵ=1.0. Final equilibrium stage.

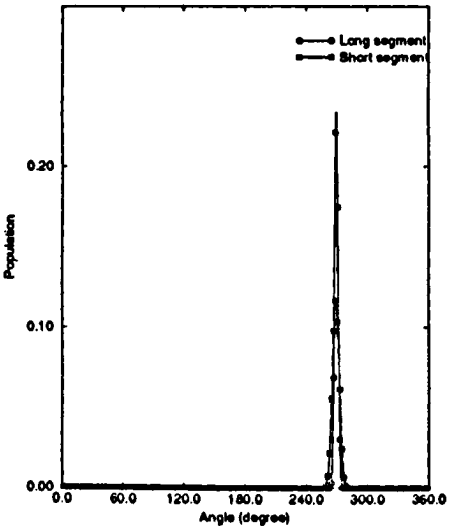

Figure 3.13: Directions of tilt angle at 75% closed packing with shorter portion of the chains bonded to the surface, ϵ_{ext}/ϵ=1.0. Final equilibrium stage.

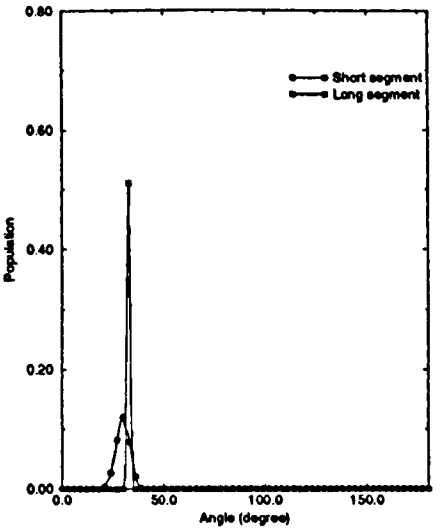

Figure 3.14: Tilt angle distribution at 75% closed packing with longer portion of the chains bonded to the surface, ϵ_{ext}/ϵ=1.0.

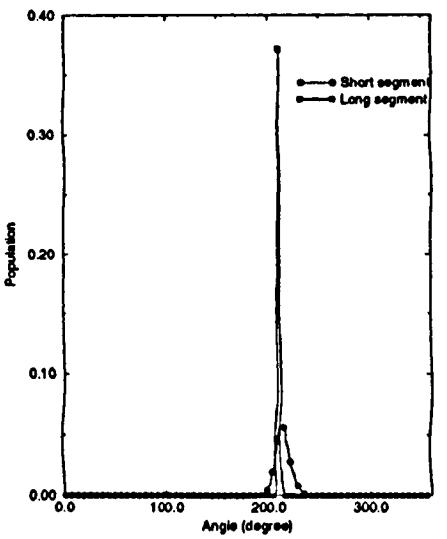

Figure 3.15: Directions of tilt angle at 75% closed packing with longer portion of the chains bonded to the surface, ϵ_{ext}/ϵ=1.0.

Chapter 4

Potts Model

4.1 Introduction

It was discussed in Chapter 3 that molecular chains can self assemble onto metal surfaces. (SAMs) Because of their wide range of applications, many experimental and theoretical studies have been conducted. But so far, most theoretical calculations have included continuous orientations of the chains. This limits the calculations to the atomic scale due to the expensive computing time of including all the intermolecular interactions. However, experiments have revealed that well defined ordered domains exist over length scales on the order of 50Å.[87,88] In order to study the nature of long range ordering, domain growth, correlation length, and phase transitions like gas to liquid and expanded liquid to condensed liquid, we have to develop new methods that require less computational time, but include larger systems. One method to save the computation time is, instead of continuous orientations, using discrete models which allow much larger calculations. The Potts model is a multistate Ising-like model that is a good candidate to model phase behavior in SAMs with high efficiency.

4.2 Method

The method we used here is based on a Potts model.[89] It is developed from the Ising model which has only two degenerate spin states. However, the Potts model allows multiple discrete states in simulations. Recently, a fast serial algorithm for the Potts model has been developed by Hassold and Holm.[90] Results showed it is much more efficient than the conventional algorithm.

We started the system with a simple square lattice model. The next step will expand to a hexagonal lattice with six tilt directions in order to mimic the Au(111) surface. The system consisted of 10,000 rodlike chains grafted on a square lattice surface. The chains had to choose discretized values of their rotational directions. In our initial studies, five orientations were allowed for each rod: one in the upright direction and four modeling tilts in directions separated by 90°.

The rods interacted only between nearest neighbors. The potential energy of the system was calculated by the Potts Hamiltonian:

$$H = \begin{cases} 0.0 & \text{when both rods tilt parallel on the surface.} \\ 0.8kT & \text{when both rods are straight up.} \\ \infty & \text{when rods are overlapping.} \\ 2.0kT & \text{else} \end{cases} \tag{4.1}$$

When the both rods tilt on the surface with the same direction, the potential energy is the lowest and it is the most favored state. When the rods tilt towards each other, the potential is infinity. It is the most unfavored state. If the two rods both are straight up without tilting, the potential energy is 0.8kT. For the other cases, the potential is assigned as 2.0kT. Figure 4.1 presents those cases.

Each Monte Carlo attempt is according to the Metropolis method as discussed in Chapter 3.

Two dimensional periodic boundary conditions were included in the calculation.

4.3 Preliminary Results

Random initial orientations were assigned to each rod. Figure 4.2 shows the initial configuration of rods on a 100 × 100 square lattice. It displayed

a very disordered system. Each of the directions of orientation are evenly distributed among the rods. After 300000 Monte Carlo steps for each rod, the final structure is presented in Figure 4.3. Large scales of domains and stripes were observed. The sizes of the domain are roughly 50Å × 50Å. As the Monte Carlo step progressed, only the chains on the edge of each domain changed their tilting directions and the chains inside the domain remained in the same tilting direction.

These promising preliminary results have inspired us to pursue a deeper investigation. If possible, this work will continue with trying to improve the efficiency of the calculation at the critical point where the equilibration time becomes very large. In order to overcome the critical slowing down, the multi-grid method will be added to perform collective and nonlocal moves.[91,92]

4.4 Figures

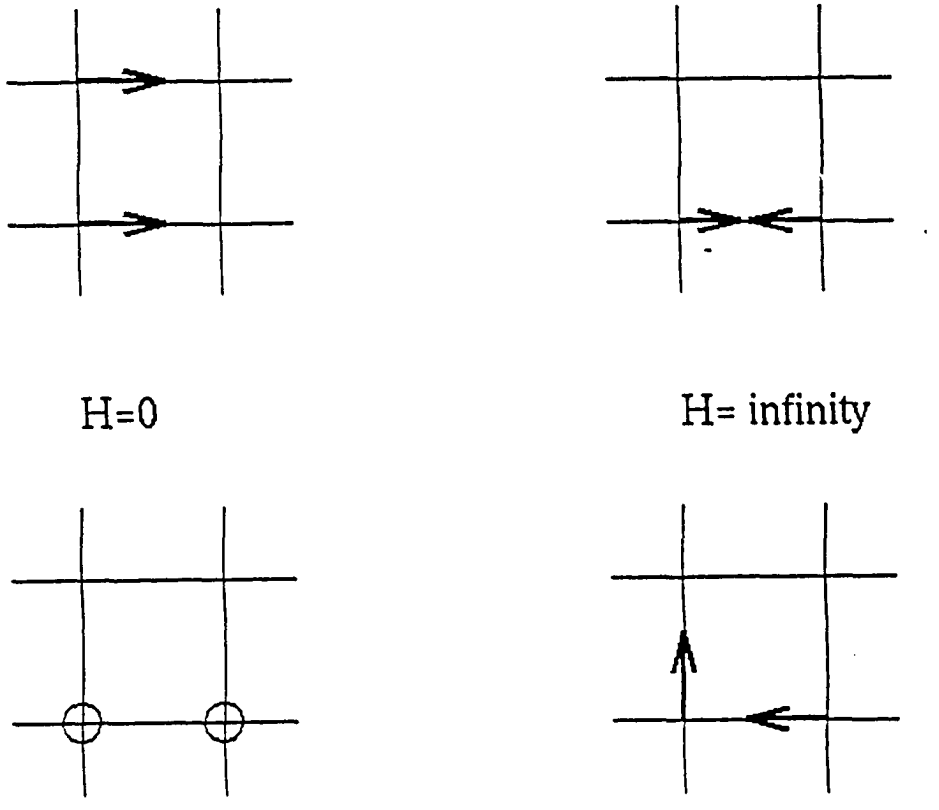

Figure 4.1: The Potts Hamiltonian.

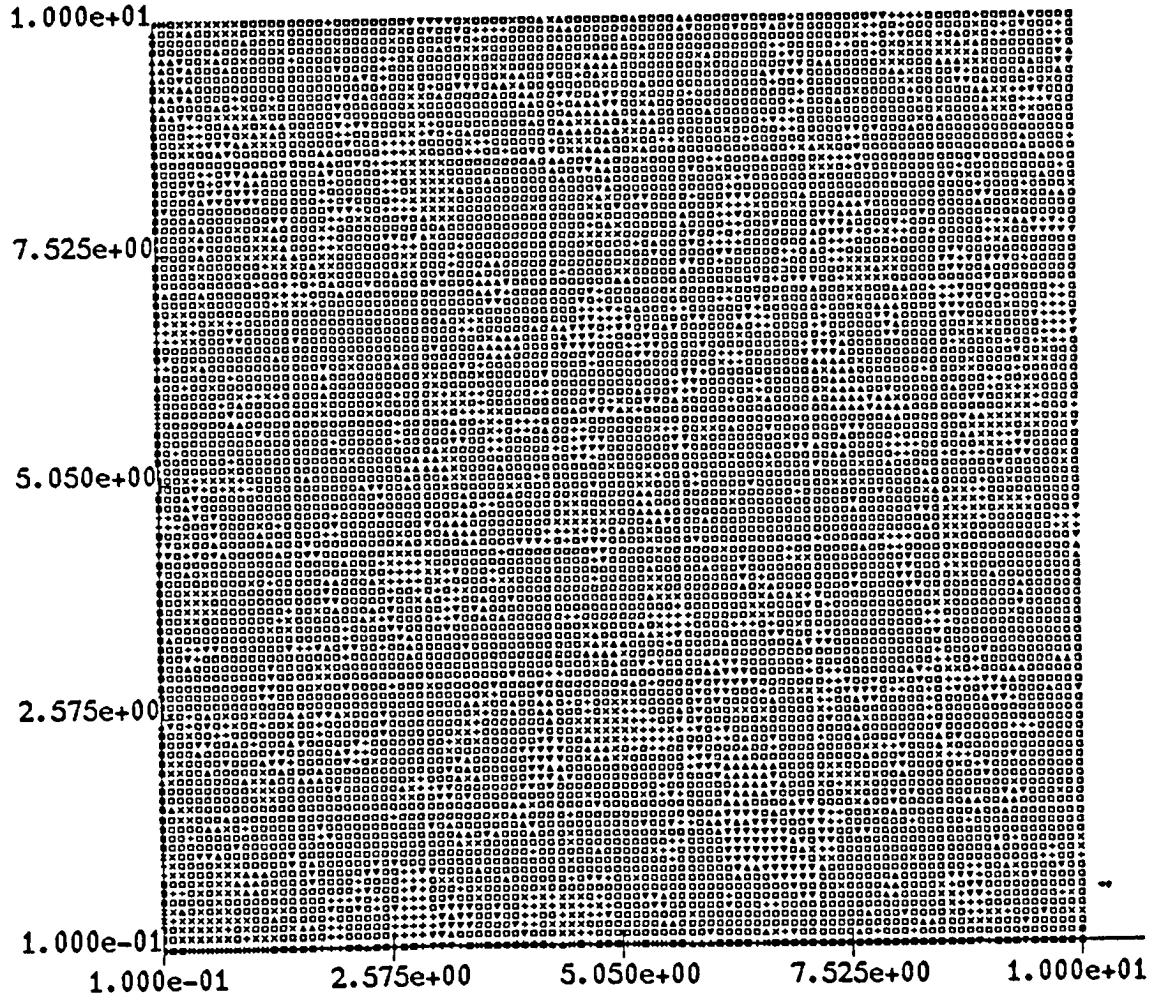

Figure 4.2: Initial Configuration.

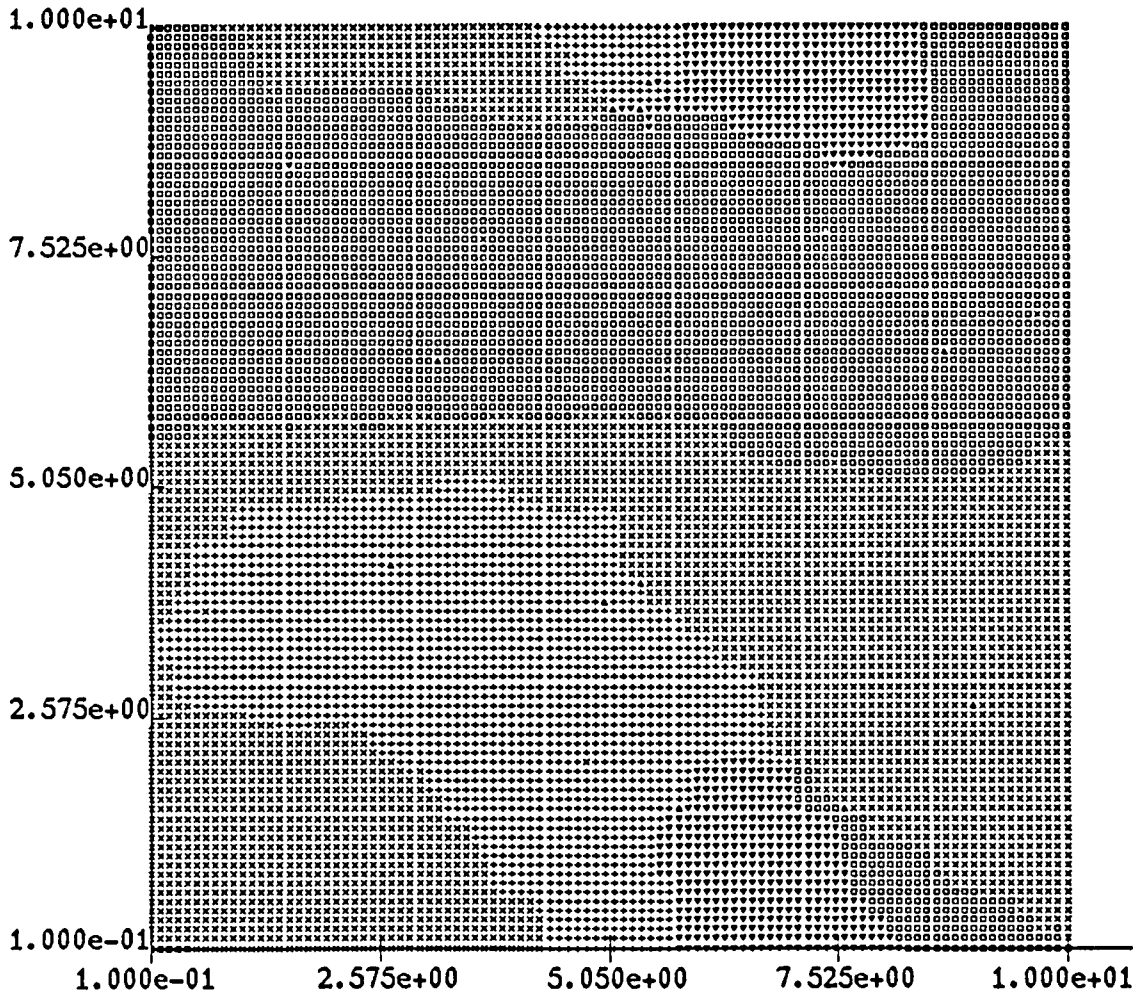

Figure 4.3: Final Configuration.

Chapter 5

Molecular Dynamics Simulations of Molecular Structure of Monolayers From Thiol-Terminated Polyimide Model Compounds on Gold

5.1 Introduction

Complex organic sulfur species chemically attached to metal surfaces during self assembly processes present significant challenges to both experiment[93,33,94-96,87,97,88,98-100,34,101,102] and theory.[103,81,82,74,76-78] There exists a complicated interplay between kinetics and equilibrium in the self assembly process, and competitions between several forces (covalent sulfur-metal bond, intrachain, interchain, and chain-surface) ultimately determine the orientations near the surface. These orientations are expected to have important consequences on the properties of the interphase.

Recently, extensive effort has been directed at understanding self assembled monolayers (SAMs) at the molecular level. Besides their intrinsic interest as models of self assembly and complex systems, these species have an impact on several areas of surface science, such as microelectrodes, lubricants,[6] and as a first binding step in adhesion processes.[7] The most attention so far has been given to alkane thiols (H-S-$(CH_2)_n CH_3$; n = 1-21) on gold substrates. Experimenters have examined the molecular level ordering of these molecules in terms of percentages of gauche defects,[101] tilt angles,[93,88,99] wetting phenomena,[99-101] surface topology,[87] directions of tilt,[88,99] and larger scale domain structure.[87,88,99,104] Some of the first theoretical studies were molecular dynamics (MD) simulations of C_n alkane

thiols on gold.[77] Two modes of attachment of the sulfur to the metal were modeled to probe the consequences on the ordering of the chains; one mode corresponded to free motion of the sulfur-first methylene bond and the other restricted this bond to lie largely parallel to the surface. The average tilt angles differed by 8° for the two models. The orientations near the surface were substantially different since the more restricted second model led to a large number of gauche defects there which 'relaxed' intermolecular overlaps. Later efforts were directed at understanding temperature[78] and density effects,[74,76] and exploration of larger scale structure (local ordering in systems with many more chains).[80] It is known from experiment[87,88] that the alkanes exhibit short range ordering, but well defined ordered domains at the chain tails occur only over length scales on the order of 50 Å.

More recently, Miller and coworkers[36] have synthesized relatively long thiophenol-terminated oligoimide species which self assemble on gold, and have characterized the monolayers by IR spectroscopy and electrochemical methods. Results from the electrochemical and IR data showed that oligoimides of the type HSPh-A-B-A-B-A-B-A-B, where Ph=phenyl, A=naphthalene-1,4,5,8-tetracarboxylic dianhydride, and B=3,3'-dimethoxy benzidine, self-assemble into a dense monolayer on the gold surface. The average tilt angle of the molecules was measured to be roughly 60° from the surface normal.

The surface density was 175 $Å^2$/molecule. A molecular structure of the monolayer was proposed according to the surface density and the tilt angle.

The previous paper presented extensive experimental data on the chemisorption and orientations of SAMs of 4-MPP (4-mercapto-phenyl-phthalimide) on gold surfaces (see Figure 5.1). This molecule is more chemically complex than the alkane species, and is a model of an adhesion promoter for the binding of polyimides to metals. The present paper presents detailed MD simulations of alkane thiols (C_{20}) and 4-MPP on a model gold surface in order to examine at the molecular level the orientations at the surface. Two models were adopted for the sulfur-metal bond, taken from the *ab initio* quantum calculations of Sellers, *et al.*[105]; the first modeled the Au-S-C bond with sp hybridization, the second with sp^3 hybridization. The two models yielded widely different orientation behavior for the near rigid 4-MPP molecules at the surface. For the sp hybridization model of 4-MPP, we obtained good agreement with experiment for the average molecular tilt angle (the sp^3 model resulted in a substantially larger tilt angle). In addition, we examined animations of movements of chains and other quantities not accessible to experiment, such as distributions of angular orientations, to gain further insights into the interphase structure and dynamics at room

temperature.

In Section II, we give the methodology of the MD simulations. Section III will discuss the simulation details. We present the results of the simulations and related discussion in Section IV, and summarize our findings in Section V.

5.2 Model

As mentioned above, there have been a large number of calculations performed on alkane monolayers on surfaces by using Molecular Dynamics (MD) and Monte Carlo (MC) methods.[81,82,74,76–78,80] The majority of these calculations have used the united atom method which considers each CH_3 or CH_2 group as one isotropic unit. These units interact with other united atoms as one group. A recent study by Hautman, *et al.*[79] compared average tilt angles for the united atom and all atom models of alkane SAMs. They computed an overall tilt of 28° for the united atom case and obtained a tilt angle of 13° at 350 K for the all atom model. Besides affecting the tilt angle, the inclusion of the all atom description alters the local orienatational properties of the chains. In the present paper, all simulations were carried out with an all atom description. We believe this is necessary to obtain an accurate model of the chemically complex 4-MPP species for

comparison with experiment. In this research, we are interested in direct comparison with the RAIR experiments of paper I measuring molecular orientation properties of oligoimides at metal surfaces. The Discover program is a commercially available software package (Biosym Technologies, San Diego, CA) that performs molecular mechanics and dynamics, and can yield a detailed molecular level description.

The calculation of the potential energy and intermolecular forces for a given configuration of atoms is the fundamental step for a molecular simulation. Discover currently supports three kinds of force fields: CVFF, AMBER, and CFF91. Discover version 2.9.5 was used here. The Consistent Valence Force Field was selected for this study (CVFF version 2.0; for complete details of the intra- and intermolecular potentials, please see the relevant Discover manuals[106]); this forcefield has been used successfully to model a wide range of chemical and biophysical systems.[107] The potential energy forms used in CVFF include quadratic bond-stretching, quadratic angle-bending, one-term torsion, 12-6 nonbonded (van der Waals), and out of plane bending potentials, and Coulombic terms for partial charges.

Although many experiments and calculations have been done on monolayers on metal surfaces, there is still no complete understanding of the chemisorption process on the Au(111) surface. For example, to which

site of the Au(111) lattice is the sulfur atom bonded? To answer those fundamental questions, Sellers, *et al.*[105] performed *ab initio* geometry optimization of HS and CH_3S on cluster models of Au(111) by using the RECP Hartree-Fock + electron correlation with second-order perturbation theory (MBPT2).

They found that there are (at least) two stable chemisorption modes for thiolates on Au(111) surfaces which are very close in energy (0.41 kcal/mol). The first (slightly less stable) mode has the sulfur chemisorbed at the hollow site of the Au(111) surface with the surface-S-C bond angle at 180° (sp hybridization). For the other mode, the sulfur is bonded again to the hollow position, but the bond angle is 104° (sp^3 hybridization). The force constant for the Au-S-C quadratic bond-angle potential is much larger (about 16 times) for the sp^3 mode than for the sp mode. However, both modes are expected to be readily accessible at room temperature due to their small energy difference and a small intervening barrier (less than 3 kcal/mol). These factors call into question harmonic modeling of the angular potential for the two modes. Near room temperature, it is quite likely that both modes (and a range of anharmonic states in between) are accessible. The potential surface for the transitions is certainly complicated and multidimensional. Depending on the molecular environment, either mode

could predominate, and frequent transitions could occur between the two at room temperature. For example, the total energy carried by the sp angular mode is roughly 5 kcal/mol or only 8kT at room temperature when it is bent at 104°, the sp^3 equilibrium angle. Hence, the thermal fluctuations and competing interactions (chain-chain, etc.) can in principle lead to populations of large angular movements in the sp mode; the sp^3 mode is substantially more restricted. These differing degrees of motion are apparent in animations of the SAMs. The different bonding modes lead to substantially different tilt angles for the rigid 4-MPP molecules. The sp^3 mode results in a substantial and unphysical forced overlap of the 4-MPP chains. For the alkanes, both modes may contribute to the overall SAM structure, as suggested previously.[105]

The molecule of interest for this research is 4-mercapto-phenyl-phthalimide (4-MPP) (Figure 5.1). It consists of one imide group connected to a para-substituted benzene ring. The molecule is relatively rigid along the long molecular axis. By using Surface-Enhanced Raman Scattering (SERS) and Reflection-Adsorption Infrared Spectroscopy (RAIR), it was found that stable and densely-packed monolayers can be obtained from the adsorption of 4-MPP solution onto a gold substrate (see paper I). RAIR results showed that 4-MPP was adsorbed onto gold through the sulfur atom with

a tilt angle of 21° from the surface normal and with no preferred rotational angle of the imide group about the molecular axis. Questions that we consider include the correlation of the simulated results with experimental measurements, ordering of the monolayer, tilt angles, and rotational behavior of the rigid rings. This information is important in interpreting the experimental measurements.

To address these questions, we adopted the two models proposed by Sellers, *et al.*[105] to describe the chemisorbed sulfur-metal interaction on the Au(111) surface. The experimental Au surface was prepared by evaporation of Au onto a glass slide; such a surface is believed to be rough, but largely Au(111).[87,108] Several force constant parameters for interactions required in this study were not available in CVFF, such as the Au-S bond-stretching potential and the Au-S-C angle-bending potential. Also, there is no 9-3 integrated surface potential term to represent the interaction between the molecule and the Au(111) surface. In order to apply the CVFF forcefield to this study, an additional set of parameters had to be added to generate a modified forcefield.

Tables 5.1 and 5.2 contain equilibrium bond distances, bond angles, and the force constants that were added to the CVFF forcefield for both models of the sulfur binding. Potential energy surfaces for the sp and

sp^3 angle bending potentials are presented in Figure 5.2 to illustrate the large differences in bending force constants and similar relative minimum energies.

The nonbonded interactions between Au and other atoms were represented by a 12-6 van der Waals potential:

$$E_{ij} = \frac{A_{ij}}{r_{ij}^{12}} - \frac{B_{ij}}{r_{ij}^{6}}, \tag{5.1}$$

where A_{ij} and B_{ij} are intermolecular Lennard-Jones parameters. The values of A and B for Au that were used in this model were 1.663×10^5 kcal mol^{-1} $Å^{12}$ and 421.3 kcal mol^{-1} $Å^6$. These parameters, along with the CVFF parameters for Carbon, result in a well depth for the C-Au pair interaction of 100K. If one converts the dispersion portion of the potential into the integrated $1/z^3$ form used by Hautman and Klein,[77] and includes the contributions from one C and two H atoms of a methylene group, a dispersion coefficient roughly 15% less than that determined by Hautman and Klein (based on data for Kr on Ag) is obtained for a methylene group/Au surface overall interaction. In other work, we have carried out extensive Monte Carlo simulations of monolayers of model rigid rods, and have found that only orders of magnitude changes in the surface potential can appreciably alter the average tilt angle;[109] furthermore, several recent

theoretical models of tilt transitions have neglected the van der Waals portion of the chain-surface potential altogether.[105,75,64] Therefore, we believe this relatively small discrepancy will not strongly influence the tilt behavior, which appears to be dominated more by the chain-chain interactions and the specific form of the chemical bond to the surface.

The parameters for Lennard-Jones interactions involving the added species were calculated from combination rules in the CVFF forcefield of the form:

$$A_{ij} = \sqrt{A_{ii}A_{jj}}. \tag{5.2}$$

All remaining interactions were generated by the CVFF forcefield.

We have omitted the quadratic bending potential for the Au-S bond from Sellers, *et al.*[105] since this effect has been included implicitly in our model due to the interactions of the sulfur atom with the surrounding Au atoms; the sulfur is tied to the surface on top of the Au_1 atom, and interacts with Lennard-Jones potentials with the surrounding Au atoms. The bending potential given in Ref. 27 is very strong, so that the Au-S bond is highly constrained in the vertical position. We computed potential energy profiles for motion of the sulfur atom in our model and found correspondingly stiff potentials for rotation of the Au-S bond. Hence, this difference

should not affect the simulation results.

5.3 Simulation details

Since gold substrates prepared by thermal evaporation are predominantly the (111) crystal surface,[87,108] we chose the Au(111) lattice as our model surface. The model was built by bonding each molecule to a specific hollow site on the Au(111) lattice. The particular site to which each molecule was bonded depended on the surface density and surface arrangement.

Six layers of Au atoms were used to achieve over 75% of the 9-3 surface potential. Au atoms were arranged in a hexagonal lattice along the XY plane with a nearest-neighbor distance of 2.88 Å. All coordinates of Au were held fixed in space during the simulation. The interactions between each Au atom and atoms of each molecule inside a specified cutoff range were included in the calculations, but interactions between the fixed Au atoms were eliminated.

In order to overcome edge effects, rectangular unit cell periodic boundary conditions (minimum image model) were used with a long third-dimension (z direction) to ensure effective two-dimensional periodicity. The cutoff for all non-bonded interactions was half of the shortest box length. This distance was taken as 14Å in our calculations, except for one simulation of a

larger system containing 64 4-MPP chains, where a 9Å cutoff was used.

The individual chains were constructed using the Insight II program, and then were quenched with a steepest descents algorithm to minimize their individual structures. The initial conditions for each full chain system were subsequently generated with the chains attached at one end via the Au-S bond and standing straight up. Then, the system was quenched further for a short time to relax the Au-S bond. The dynamics simulations were run at constant temperature with a time step of 1 fsec for 4-MPP and 2 fsec for the C_{20} alkane chains. The initial structure was allowed to equilibrate for 50 to 100 ps; then, the dynamics was run over a time interval of at least 40 ps (the range of simulation times was 40-80 ps). These times have been found sufficient to yield converged tilt angles for multiple chain monolayer films.[110] The system total potential energy was monitored, and after the equilibration time was observed to fluctuate randomly about an average value without drift. In addition, Bishop and Clarke[110] found that a system as small as 16 alkane monolayer chains can yield average tilt angles within 1.0° of size-converged values for the surface densities simulated here (representative of a high density SAM system). Fully converged results were obtained for all densities they examined with 64 chains. For our alkane studies, 48 chains were used; for the 4-MPP simulations, we

employed 36 chains for the high density system; one simulation was carried out with 64 chains, and average tilt angles within one degree of the smaller system were observed. Particle positions were saved every 100 or 200 steps and data was averaged. To ensure that the chains could sample large regions of configuration space before settling into local minima, each system was first heated to 1000K. A trajectory of 40 ps duration was run at the (unphysically) elevated temperature. Then the system was annealed at an inverse cooling rate of 30 steps / K to room temperature, prior to equilibration and data collection.

The equations of motion were solved using the Verlet Leapfrog propagation algorithm. The canonical ensemble with constant temperature, constant volume conditions (NVT) was used to mimic experimental conditions. The ensemble was obtained by controlling the temperature through direct velocity scaling during the equilibration and by Berendsen's method of temperature-bath coupling during the data collection stage. A Nosé-Hoover thermostat was used to maintain constant temperature.

An important input for the simulation is the density of the monolayer adsorbed on the surface. For the alkane simulations, the inverse bonding density was 21.6 $Å^2$/chain, consistent with a $(\sqrt{3} \times \sqrt{3})$R30° commensurate adlayer. The surface density of adsorbed 4-MPP on Au(111) was deter-

mined experimentally by Double Potential Step Chronocoulometry (paper I). Results showed the surface coverage was between 32 and 38 $Å^2$/chain, depending on the duration of the self assembly process; maximum densities were obtained with exposure times of several hours. These densities are similar to those observed for flourinated alkane chains, where a (2×2) commensurate adlayer was observed in atomic force microscopic measurements.[96] The 4-MPP chains can be expected to have a net (anisotropic) chain surface area closer to the fluorinated alkanes than the hydrogenated case above. Such a structure yields an inverse surface density of 28.8 $Å^2$/chain. While no experimental evidence exists that the 4-MPP surface is commensurate, we assumed a commensurate form for the high density case. A range of densities which spanned the experimentally measured range was used in the simulations. The lower surface densities were obtained by the removal of six, eight, and twelve chains followed by movement of chain heads to generate a nearly uniform (incommensurate) distribution on the surface. These cases correspond to inverse bonding densities of 34.7, 37.2, and 43.4 $Å^2$/chain. The two measured surface densities in paper I were 32 and 38 $Å^2$/chain, but there is likely a several $Å^2$/chain uncertainty in the measurements. Therefore a slightly greater density range was chosen for the present simulations.

The definitions of the tilt angle and rotational angles of 4-MPP adsorbed on the gold surface are described as follows. Because 4-MPP is a semi-rigid molecule and has a linear structure, its tilt angle was calculated by coordinates of the nitrogen atoms which were assumed in the molecular axis. The tilt angle of the S-N vector from the surface normal was then considered to be the tilt angle of the molecule (see Figure 5.1). In order to calculate the rotational angles of the two ring portions of the molecule, a reference plane was defined as that formed by three atoms: the gold immediately below the sulfur (Au_1), the second gold directly below the first(Au_2), and the first carbon atom(C_1) of the chain (the YZ plane in Figure 5.1). The locations of Au_1 and Au_2 ensured that the reference plane was always perpendicular to the gold surface and the C_1 location ensured that the reference plane was pointing toward the long molecular axis. The 1st rotational angle(ϕ_1) refers to the angle between the imide group and the reference plane. If the imide group is parallel to the gold surface, ϕ_1 is equal to 90°. The 2nd rotational angle(ϕ_2) is the angle between the benzene ring attached to the sulfur and the reference plane. The relative angle between the imide group and the benzene ring is the 3rd rotational angle($\phi_3 = \phi_1 - \phi_2$).

Since RAIR experiments can measure just the average orientations of

molecules adsorbed on the surface, computer simulation can supplement this information by generating full probability distributions. For example, the experiments measured the average rotational angle for the imide ring in the high density 4-MPP SAM as 42°, close to a uniformly averaged value of 45°. This suggests it is possible there was no preferred orientation. Also, RAIR experiments were unable to determine the rotational angle of para-substituted benzene rings due to the very weak intensity of bands assigned to those rings. Results are presented below concerning both of these rotation angles. The distributions of tilt angles and all three rotational angles were obtained by binning angles obtained from the dynamics.

5.4 Results

We first present results of MD simulations of the C_{20} alkane SAMs in order to provide a comparison with previously studied systems. Following the annealing cycles discussed above, simulations were run for both the sp and sp^3 bonding models. For the sp case at room temperature, the chains existed in a nearly all-trans configuration, and the final average tilt angle was 12°. This is in relatively close agreement with the value of 13° computed by Hautman, *et al.*[79] for a C_{16} system at 350 K and with a similar bonding model. The nearly vertical chains appeared to fluctuate between tilting

towards nearest and next nearest neighbors throughout the course of the simulation. During the course of the equilibration run for the sp^3 alkane model, the chains underwent a collective motion from a largely nearest neighbor tilt with an angle of roughly 15° to a next nearest neighbor tilt. The transition was accompanied by a substantial drop in total potential energy. The system remained in this state during the entire room temperature production run for the sp^3 model, and the potential energy fluctuated only a small amount around its mean value. The average tilt angle for this system was 26°, and the chains tilted in a predominantly all-trans configuration, including near the surface. This value for the tilt angle agrees well with experimental results measured via IR spectroscopy[93] and X-Ray scattering.[88] The X-ray results also imply a tilt direction 8° from the next nearest neighbor direction. This model corresponds more closely with the model II of Hautmann and Klein.[77] However, they observed a predominance of gauche bonds near the surface in their united atom simulations of that model. Sellers, *et al.*[105] presented a molecular mechanics study of the minimimum energy (all-trans) structure for the sp and sp^3 bonding models (a single chain in periodic boundary conditions) and found a tilt angle of roughly 30° for the fully minimized structure in both models. They argued that, due to similar energetics for the two models, there likely is a coexis-

tence of the two forms on a surface for longer chain alkanes. Therefore, we cannot distinguish unambiguously between the two bonding models for the alkane SAMs. However, it does appear that of the two bonding models, the sp^3 type leads to better agreement with available experimental data. We do believe, based on our high temperature annealing procedure and the agreement with the simulations of Hautman, *et al.*[77] for the sp-type all-atom model, that the results represent equilibrated systems and that the two bonding models can lead to different tilt behaviors at room temperature. In addition, there likely can occur transitions between the two idealized bonding models at room temperature in the alkane systems, as argued above. We judge that the CVFF forcefield with the added surface bonding models of Sellers, *et al.*,[105] yields a reliable description of the interface.

Simulations of the 4-MPP rigid SAMs were then performed. The first set of simulations pertained to the sp^3 model in a (2×2) commensurate layer at a bonding density of 28.8 $Å^2$/chain. The highly constrained sp^3 mode led to a very large and unphysical overlap of the chains (Figure 5.3). To test whether the initial conditions for the simulation might have affected the results, we first simulated the system at 1000K with a Au-S-C bending force constant of zero. Then, the force constant was gradually

incremented up to the realisitc sp^3 value over a time period of 130 ps, still at 1000K. Subsequently, the system was cooled in an annealing cycle to room temperature. Again, a large and unphysical overlap occurred accompanied by a very high total potential energy. The average computed tilt angle at room temperature was 42°, which differs substantially from the measured experimental value of 21°. We conclude that the constrained sp^3 mode does not yield a realistic description of the surface bond for rigid chains, at least at densities where they interact appreciably with each other. Therefore, the remainder of the 4-MPP simulations were carried out using the sp bonding mode.

Each of the four bonding density systems of 4-MPP (sp type) was carried through an annealing cycle as for the systems discussed above. Equilibration and production runs were then conducted at room temperature. We first present results for the high density bonding case which should correspond closely to the experimental system exposed to the self assembling solution over a long period of time (12 hrs.). Figure 5.4 displays the distribution of chain tilt angles averaged over the entire simulation. At 1000K the chains exhibit a uniform distribution of tilt angles, and an animation of the chains shows that they undergo large thermal fluctuations and rotate freely at this very high temperature designed to ensure a full sampling of

configuration space. When the system is cooled to room temperature, the distribution of tilts changes to a bimodal form. The largest peak is centered around 20°, with a substantial peak for larger angles up to about 40°. The average tilt is 23°, very close to the experimentally measured result for the long exposure SAM. Visual inspection of the chains reveals a disordered system with no clear long range order(Figure 5.5). Yet animations show that, while there exist substantial thermal fluctuations at room temperature, the overall rotational motions of the ring structures are hindered due to interchain interactions. One simulation was performed on a 64 chain system to test the effect of system size. An average tilt of 21° was computed, close to that for 36 chains. In addition, the three average rotational angles were within 2° of the 36 chain system, and the thermal motions were restricted by neighboring chains. Therefore, we concluded that 36 chains were sufficient to capture the essential features of this interphase.

The experiments in the preceding paper measured the average orientational angle ϕ_1 in addition to the tilt angle. The measured value for long solution exposure times was 42°; we obtained a mean value of 39°. The distribution of this angle is presented in Figure 5.6, along with those for ϕ_2 and ϕ_3. The distribution of ϕ_1 is quite broad, consistent with an average angle around 45° for a uniform distribution. The other two angles also

exhibit broad distributions. This indicates that, even though the overall rotational motions of the rings are restricted to some extent by neighboring chains, the thermal fluctuations in the orientational angles at room temperature are relatively large within the local region accessible to each chain.

Next, simulations were conducted for three lower densities to determine the effect of bonding density on tilt and orientation behavior. The computed data for the average tilt and orientational angles are presented in Table 5.3.

The tilt angle increases with decreasing density, in agreement with the experimental data from the shorter time exposure 4-MPP SAM in the previous paper (31° measured tilt for a shorter exposure time, 30 min., which resulted in lower surface density). Similar to the higher density case considered above, these chain systems also display a substantial degree of disorder, but cluster into local dense regions(Figure 5.7). The distributions of tilt angles and orientational angles for the 37.2 $Å^2$/chain system are presented in Figs. 5.8 and 5.9. The distribution of tilt angles again displays a bimodal form, but the peak at larger angles (centered around 35°) has shifted somewhat to larger angles and has increased in magnitude, presumably due to the availability of larger free volume per chain. The dis-

tributions of the three orientational angles are again broad. The computed average ϕ_1 is 30°, which differs from the experimental value of 52°. This may result from limitations in the forcefield for the intramolecular degrees of freedom.[111]

5.5 Conclusions

We have presented extensive molecular dynamics simulations of organic SAMs of C_{20} alkanes and 4-MPP oligoimides on the Au(111) surface. Two bonding models of the sulfur to gold were employed based on *ab initio* quantum calculations in the literature.[105] The first corresponds to sp hybridized bonding with a relatively loose force constant for bending of the Au-S-C angle and an equilibrium angle of 180°; the second bond has sp^3 hybridization with a stiff bending force constant and equilibrium angle of 104°. The sp^3 mode leads to a S-C bond oriented largely parallel to the gold surface. This structure has been proposed based on IR measurements on alkane monolayers.[93] The alkane studies were carried out to test the model by comparison with previous simulations and experiment. The systems were heated to high temperature to overcome possible local equilibration problems, and were then annealed to room temperature. Equilibration runs followed by 40-80 ps simulations were then performed. These simula-

tion times have previously been found long enough to yield converged tilt properties in alkane monolayers.[110] For the sp model, we observed a predominantly all-trans collection of chains and obtained good agreement for the average tilt angle with the similar all-atom model of Hautman, *et al.*[79] (12-13°). The sp^3 model simulation yielded a nearly all-trans monolayer with next nearest neighbor tilt angle of 26°, in relatively good agreement with both IR spectroscopic[93] and X-ray scattering experiments.[88] The energetics of the two bonding modes is very close, so it is likely a coexistence of forms can exist on a given surface (with thermally accessible transitions between), and we cannot unambiguously distinguish between the two models for the alkanes.

Then simulations were carried out of SAMs of the oligoimide 4-MPP in order to examine the system studied experimentally in the previous paper. These systems were carried through annealing cycles as for the alkanes, followed by equilibration and data collection. Four densities were examined which span the experimental range. The highest density was placed on a (2×2) lattice commensurate with the Au(111) surface. The lower densities were obtained by removal of chains and subsequent movement of the remaining chains to create a relatively uniform (incommensurate) monolayer. We found that the sp^3 model led to a highly strained monolayer

with substantial overlap of the rigid chains and very large total potential energy. The computed average tilt angle was 42°, much larger than the experimental value of 21°. The sp bonding model resulted in tilt angles which agreed much better with experiment. We thus conclude that, for the rigid chain dense monolayers, the sp bonding mode gives a more realistic description. A broad distribution of the orientational angle, ϕ_1, also was consistent with the experimental finding of no preferred angle. The overall appearance of the 4-MPP system was of a dense but disordered monolayer. The distribution of tilt angles displayed a bimodal form. The chains exhibited substantial thermal fluctuations at room temperature, but were hindered in their overall rotational motion due to interactions with neighboring chains. Well defined monolayers of thioaromatic species (p-terphenylmercaptan, TPM) have been observed recently, and a model was proposed of a $(\sqrt{3} \times \sqrt{3})$R30° structure the inverse density of which is 21.6 Å^2/chain and corresponds to a well ordered and packed monolayer.[112] The 4-MPP chains are of larger van der Waals volume and are less isotropic in structure, so the densities measured in the previous paper and the range examined in the present study appear to be reasonable. The relatively good agreement of our simulations of the 4-MPP chains with experiment lends further support that these SAMs exist in a dense state on the gold surface

and tilt only slightly from the normal due to substantial interactions with neighboring chains. Future research will focus on longer chain oligoimides and on the effects of differing functionalities and varying rigidities of the chains.

5.6 Tables

Quadratic Bond: E=$k_2 \times (R - R_o)^2$			
i	j	R_o (Å)	k_2 (kcal/mol-Å^2)
sp			
Au	S	4.255	100.0332
S	C	1.826	431.7978
sp^3			
Au	S	2.390	96.003
S	C	1.902	434.6765

Table 5.1: Values of the parameters for the quadratic bond distance potentials add to the CVFF forcefield for both models of the sulfur binding

Quadratic Angle: E=$k_2 \times (\theta - \theta_o)^2$				
i	j	k	θ_o (degree)	k_2 (kcal/mol-rad^2)
sp				
Au	S	C	180	2.87865
sp^3				
Au	S	C	104	46.3463

Table 5.2: Values of the parameters for the quadratic bond angle potentials add to the CVFF forcefield for both models of the sulfur binding

Density(Å^2/chain)	θ(degree)	ϕ_1(degree)	ϕ_2(degree)	ϕ_3(degree)
28.8	23	37	31	21
34.7	27	31	28	20
37.2	27	30	26	22
43.4	33	32	28	22

Table 5.3: Computed values of average tilt and rotational angles (sp mode) for the 4-MPP systems at four densities.

5.7 Figures

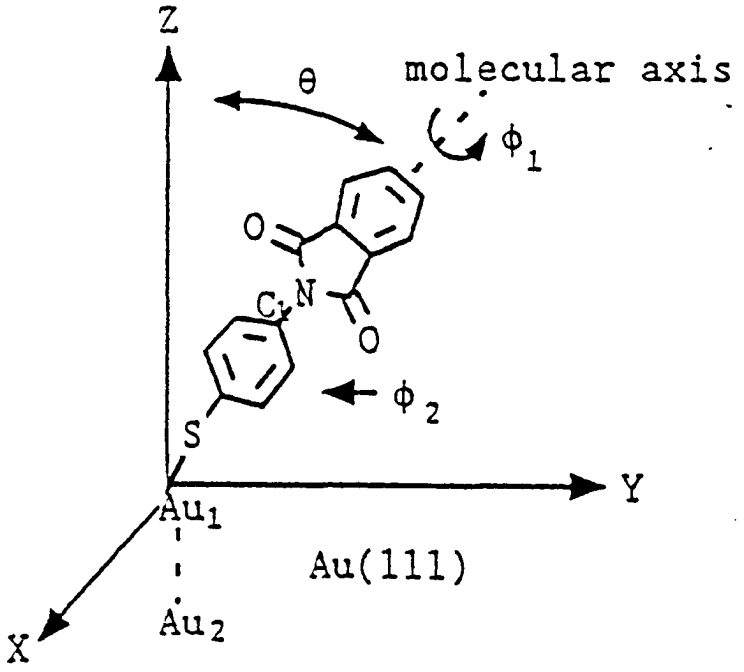

Figure 5.1: The definition of the tilt angle θ and rotational angles ϕ_1, ϕ_2, ϕ_3 of 4-MPP adsorbed on the gold surface. The first rotational angle ϕ_1 refers to the angle between the imide group and the reference plane, defined by Au_1-Au_2-C_1. The 2nd rotational angle (ϕ_2) is the angle between the benzene ring attached to the sulfur and the reference plane. The relative angle between the imide group and the benzene ring is the 3rd rotational angle($\phi_3 = \phi_1 - \phi_2$).

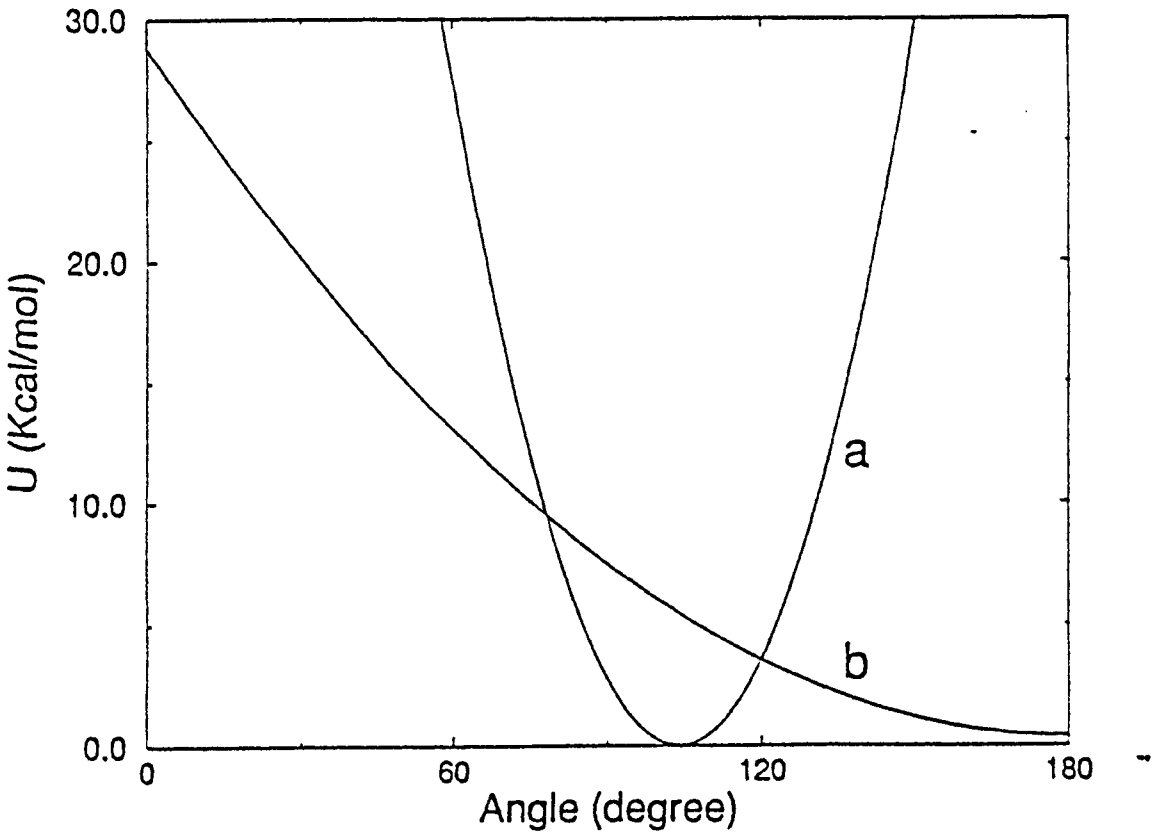

Figure 5.2: The Au-S-C quadratic bond-angle potential for (a) the sp^3 mode and (b) the sp mode. A small intervening barrier is found between the two bonding modes.

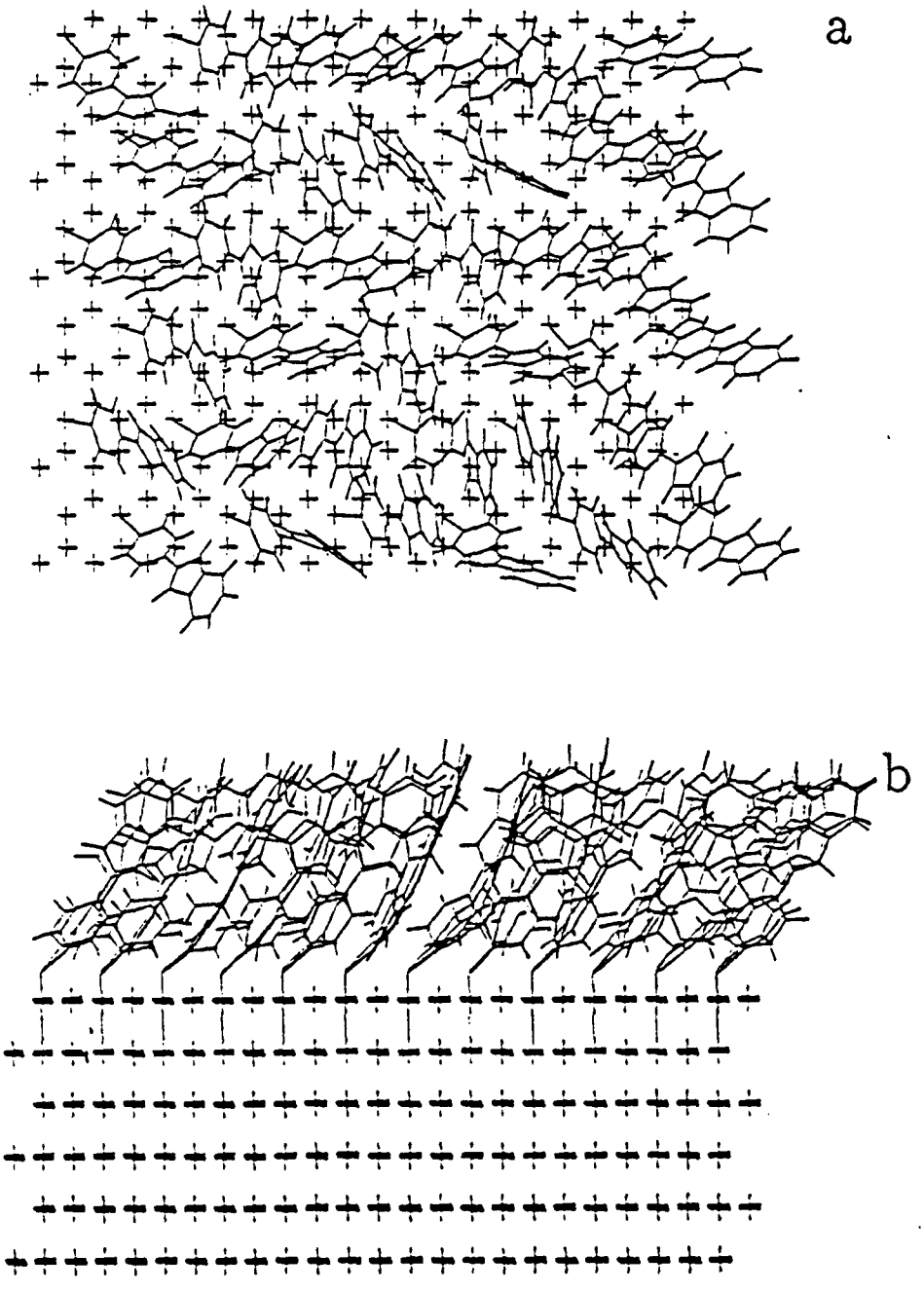

Figure 5.3: Snapshot of 4-MPP molecules on Au(111) surface with sp^3 bonding mode at inverse surface density of 28.8 $\AA^2$/chain, with topview(a) and sideview(b).

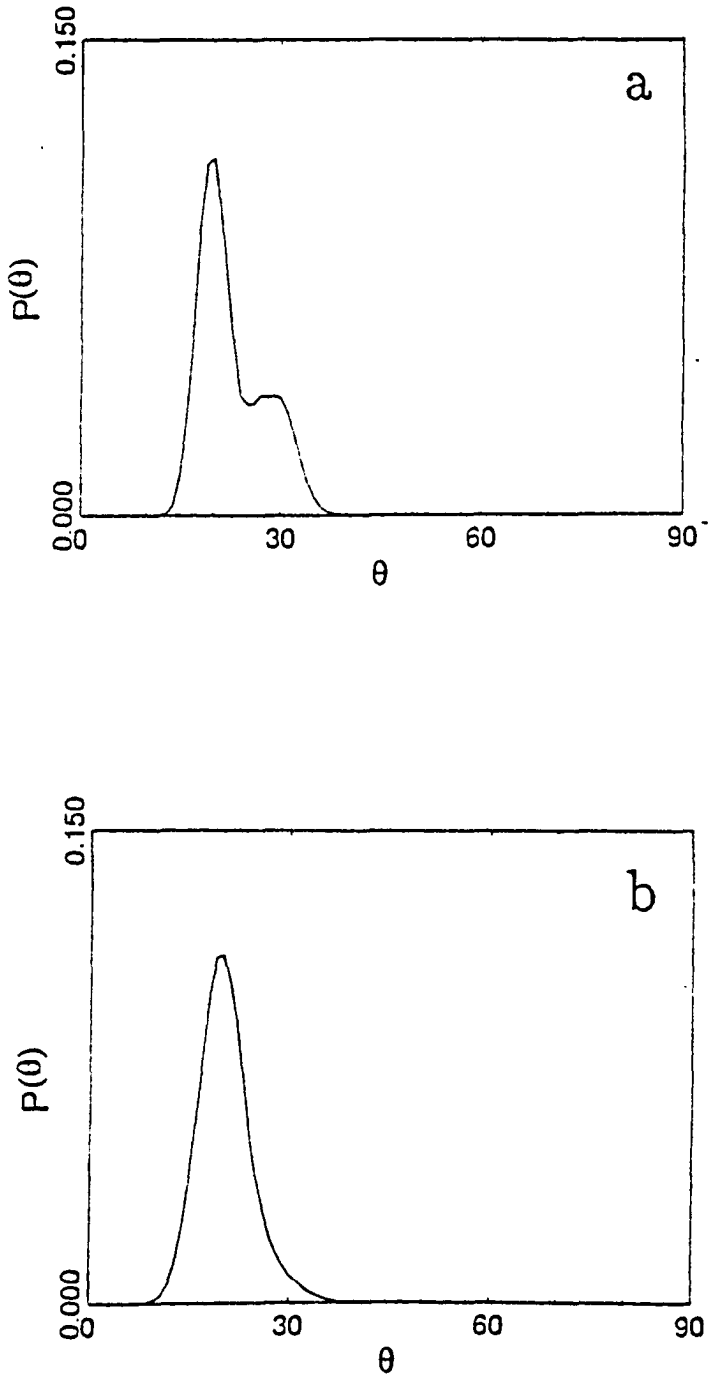

Figure 5.4: The distributions of the tilt angles of 4-MPP adsorbed on Au(111) lattice at 300K(a) and 1000K(b). The surface density equal to 28.8 $Å^2$/chain.

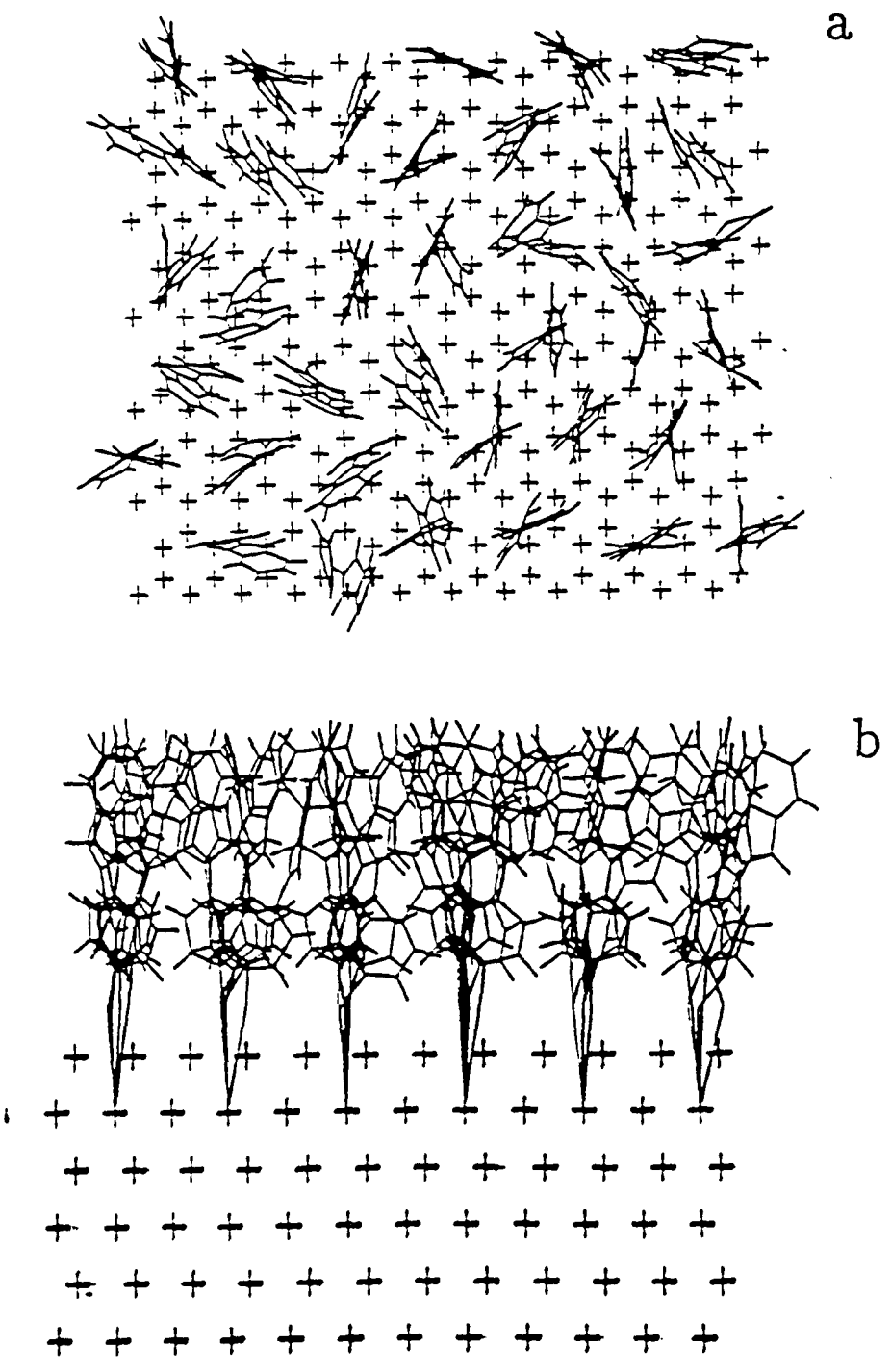

Figure 5.5: Snapshot of 4-MPP molecules on Au(111) surface with sp bonding mode at inverse surface density of 28.8 $\AA^2$/chain, with topview(a) and sideview(b).

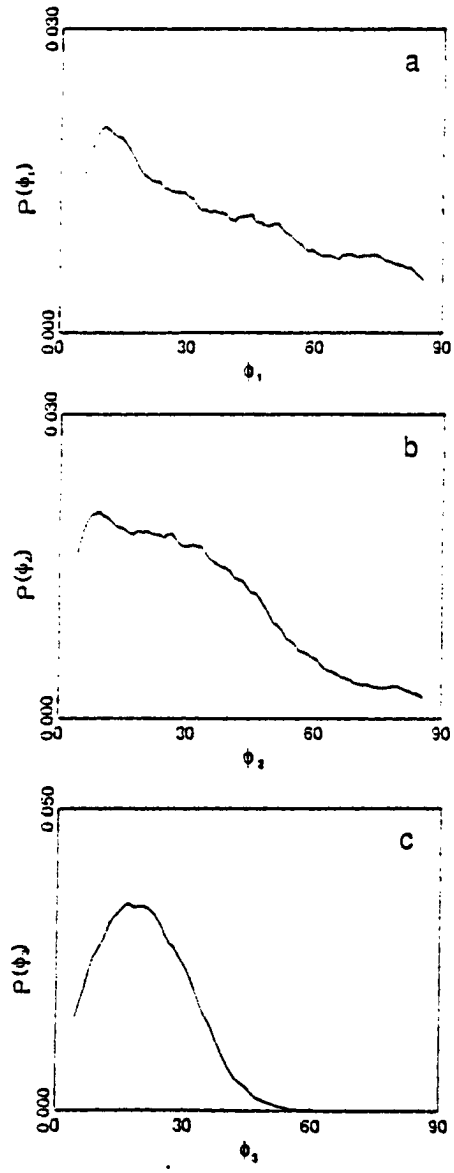

Figure 5.6: The distribution of the rotational angles ϕ_1(a), ϕ_2(b), ϕ_3(c) of 4-MPP at the gold surface. The surface density is equal to 28.8 $\AA^2$/chain.

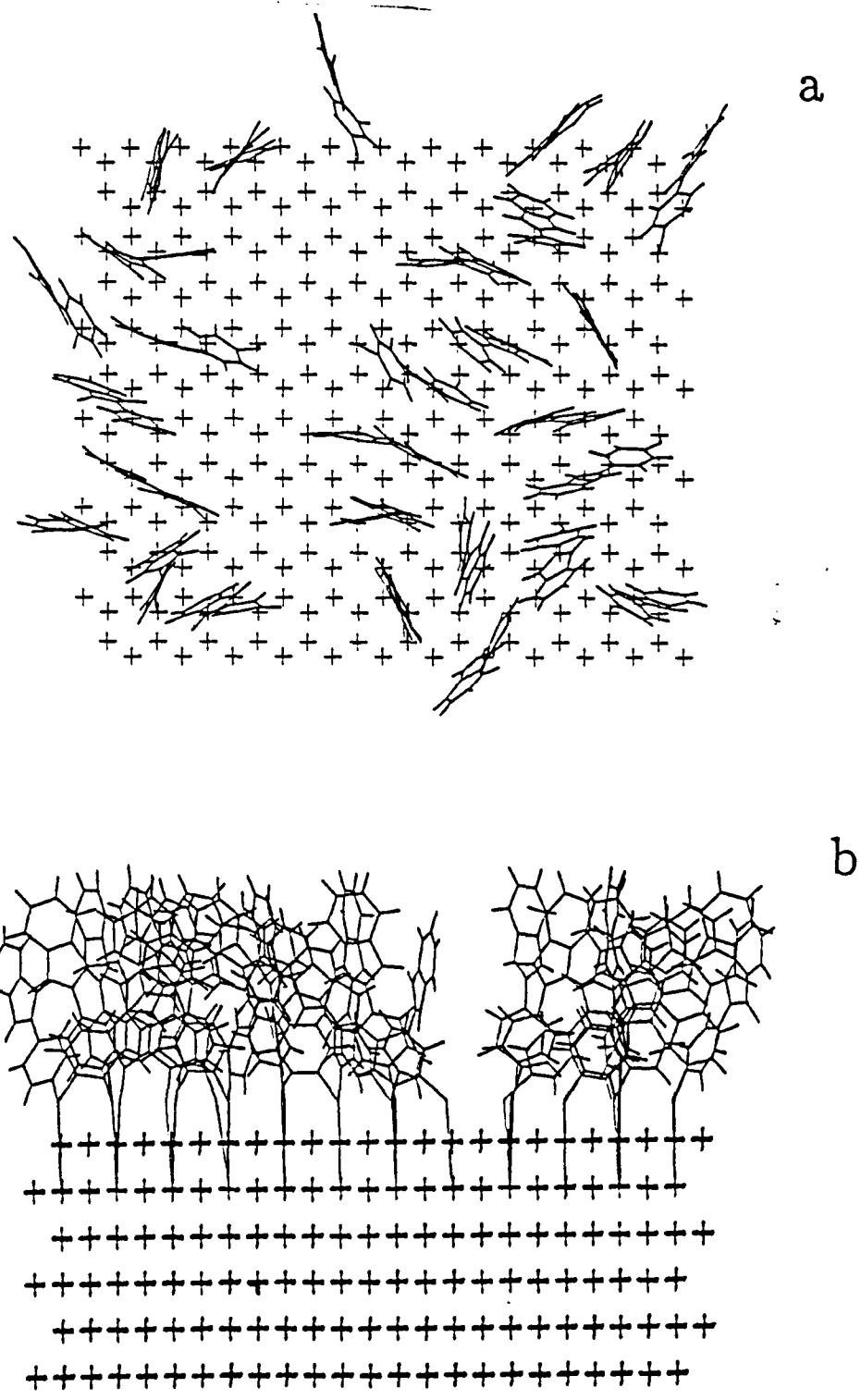

Figure 5.7: Snapshot of 4-MPP molecules on Au(111) lattice with sp bonding mode at inverse surface density of 37.2 $\AA^2$/chain, with topview(a) and sideview(b).

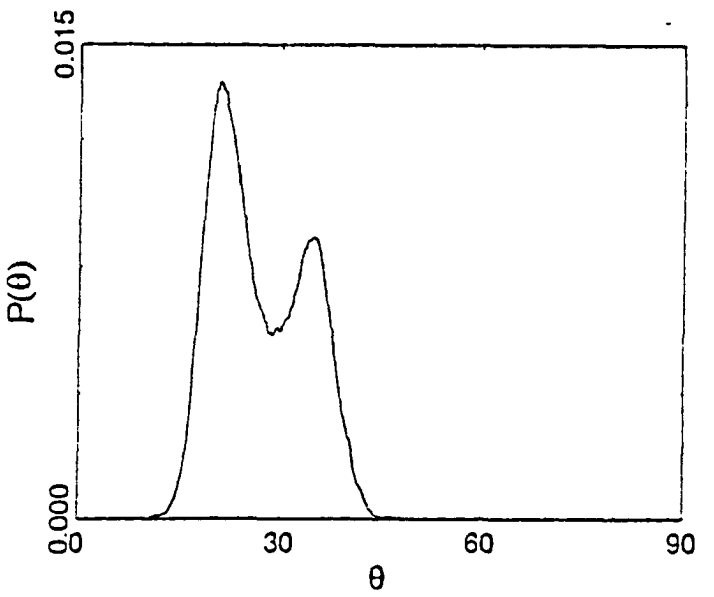

Figure 5.8: The distribution of the tilt angles of 4-MPP adsorbed on Au(111) lattice. The surface density is equal to 37.2 $\AA^2$/chain.

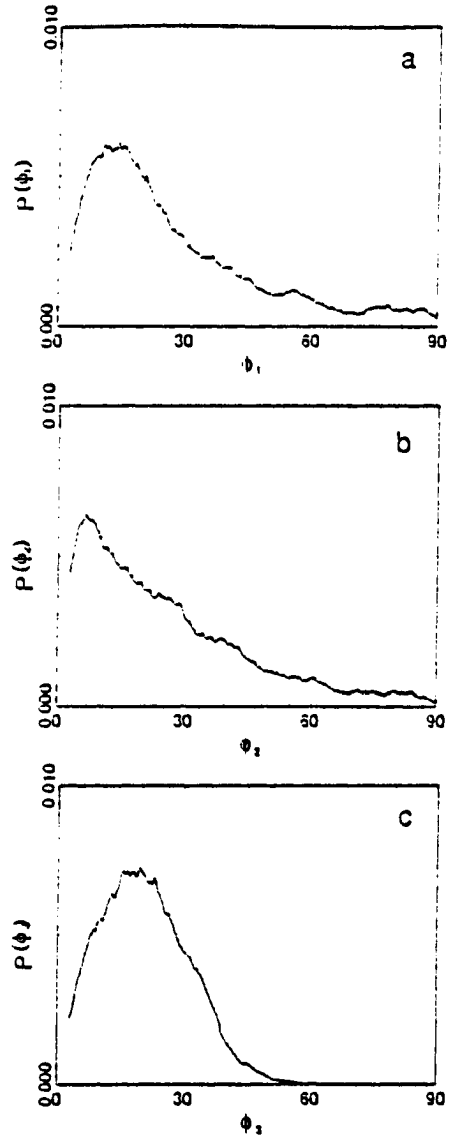

Figure 5.9: The distributions of the rotational angles ϕ_1(a), ϕ_2(b), ϕ_3(c) of 4-MPP at the gold surface. The surface density equal to 37.2 $\AA^2$/chain.

Chapter 6

Summary

In summary, we presented theoretical research on properties and mechanisms of electrode materials, including the superionic clusters and molecular monolayer modified metal electrodes.

For the first part of my research, molecular dynamics simulations were performed on $(Ag_2Se)_n$ ionic clusters to investigate microscopic mechanisms for the onset of diffusion. The Ag_2Se crystal is a superionic conductor in the bulk. Both structural properties and dynamical correlations were calculated. For small clusters, $(Ag_2Se)_n$ (n=1-5) , the normal mode analysis agreed with the power spectra very well at low temperatures. However, no significant superionic behavior was observed in small clusters.

The $(Ag_2Se)_{41}$ cluster presented superionic behavior which was similar to that observed in the bulk. Below 200K, the cluster was in the solid state. Both the Ag and Se ions displayed only thermal vibrations about their lattice sites. Above 200K, the mean-square displacement for the Ag ions increased with temperature dramatically, while the Se ions remained on their sites. On the time scales from 50ps to 250ps, the van Hove self-correlation function showed that there was a jumping mechanism when silver ions diffused at 251K. But on time scales from 5ps to 25ps, no jumping mechanism was observed. The results also showed that the $(Ag_2Se)_{80}$ cluster displayed more distinguished bulk-like superionic bebavior than the

$(Ag_2Se)_{41}$ cluster. This size dependent property agrees with previous studies on alkali halide clusters.

To compare the properies of $(Ag_2Se)_n$ with other ionic clusters, MD calculations were also performed on $(AgI)_{60}$ and $(NaCl)_{108}$. AgI is the most well known superionic conductor. However, no superionic behavior was displayed in the $(AgI)_{60}$ cluster. As the temperature increased, the diffusion constants for the Ag^+ and the I^- ions increased comparably. No distinguished phase where the I^- ions stayed in the solid state and the Ag^+ ions displayed liquid like behavior was observed.

The second part of my thesis involved studying structural and dynamical properties of self assembled monolayers on metal surfaces. We started by discussing the driving forces which lead to ordering behavior at the solid-liquid interfaces. Monte Carlo simulations on the origins of tilt behavior in self assembled model rigid oligomers were presented. The zero Kelvin potential energy curves showed that the next-nearest neighbor (nnn) tilt is the most energetically stable state for all densities that we tested. The minimum energy tilt angle was found to vary considerably with chain density. Several surface densities were investigated with Monte Carlo simulations. For a system with a density of 75% of the close packed system, results showed the next-nearest neighbor (nnn) tilt with a tilt angle of 33°.

The same results were obtained for different ratios of ϵ_{ext}/ϵ from 0.0 to 1.0. The orientational order parameter remained above 0.99 during all the simulations. When the relative surface density decreased to 50% of a close packed system, the tilt angles exhibited a relatively broad distribution. As the relative surface density decreased to 18% of a] close packed system, which is close to that measured by Miller and coworkers[36] in experiments for oligoimide molecules on the gold surface, the chains showed very broad distributions in both the tilt angles and the directions of tilt. And the chains did not show collective tilt, but clustered into locally dense regions.

Some preliminary results from a Potts model calculations were also presented. The work here is the first step to begin to examine domain structure and phase transitions in the monolayer-solid interpahses.

Finally, we performed extensive molecular dynamics simlulations of organic thiol monolayers self assembled on gold surface. The molecule that we were interested in for this research was 4-mercapto-phenyl-phthalimide (4-MPP). The structure and dynamics of the interphase were simulated at several surface densities. Interaction parameters obtained from quantum mechanical calculations included two bonding geometries, one with the sulfur atom sp hybridized and one with sp^3 hybridization. The calculated tilt angle for a high density monolayer was 23° for the sp hybridized

case, in good agreement with the experiments presented in Appendix B. It was also found that the tilt angle increased with decreasing surface density. The distribution of rotation angles of the imide ring was very broad.

In conclusion, we have studied the structural and dynamical properties of some important electrode materials and found very interesting results. These results that we revealed could be useful in directing the discovery of new electrode materials and modification of the properties of given materials.

Appendix A

Computer Simulation of Chain Molecule-Inorganic Interphases: Chromatographic Stationary Phases and Rigid Rod Self-Assembled Monolayers

COMPUTER SIMULATION OF CHAIN MOLECULE-INORGANIC INTERPHASES: CHROMATOGRAPHIC STATIONARY PHASES AND RIGID ROD SELF-ASSEMBLED MONOLAYERS

S. J. KLATTE, Z. ZHANG, AND T. L. BECK
Department of Chemistry, University of Cincinnati, Cincinnati, OH 45221-0172

ABSTRACT

Molecular dynamics simulations of alkane chains chemically tethered to silica surfaces are presented. The system was modeled after the stationary phases of chromatographic columns. The interphase properties were computed as functions of chain length, surface bonding density, and temperature. At densities appropriate for chromatography, the chains undergo a gradual transition with increasing temperature from a glassy state to a liquid-like state. The simulations are consistent with extensive experimental data including neutron scattering, NMR, IR, and EPR methods. The implications for chromatographic retention are discussed. In a second series of studies, we explored driving forces for observed ordering on the solid surface in terms of the various components of the chain-chain and chain-surface forces. Interfacial z profiles are sensitive functions of each of the forces. Finally, we present preliminary Monte Carlo results on origins of tilt behavior in self assembled monolayers of rigid chain species on metal surfaces.

INTRODUCTION

The statistical mechanics of chain molecules, as opposed to simple atomic liquids, presents many fundamental problems. The connectivity of the chains introduces constraints on both equilibrium and dynamical quantities which lead to the necessity of inclusion of increased length and time scales for an accurate description. In the past twenty years, our understanding of the structure and dynamics of bulk chain liquids ranging from short alkanes to lengthy polymers has increased rapidly due to close collaboration between experiment, theory, and computer simulation. More recently, researchers have begun to focus on chain molecules at interfaces[1]. While these problems provide additional challenging theoretical issues, they are also of clear practical importance. A short list of relevant topics of active research are Langmuir-Blodgett (LB) films, Self Asssembled Monolayers (SAMs), model membranes, polymer brushes, thin tribological films, and adhesive systems. This paper summarizes recent theoretical computer simulation studies in our group of two model interphase systems: chromatographic stationary phases and orientational behavior of rigid rod oligomers self assembled on metal surfaces.

Reversed Phase Liquid Chromatography (RPLC) is the most widely used method for separation of chemicals in solution[2,3]. The typical RPLC column consists of a porous silica network to which a stationary phase of alkane molecules has been chemically attached at one end via a silanization reaction. The maximum bonding density corresponds to roughly 40 $Å^2$/chain, which is one half the close packed densities obtained with SAMs on gold. A polar solution (typically water / methanol or water / acetonitrile) containing the chemical species of interest is then passed through the column under pressure. Differential free energies of transfer of solutes from the polar mobile phase to the hydrophobic stationary phase lead to separation. In fact, the solute chemical potential change upon transfer is measurable given the volumes of the stationary and mobile phases. In addition, dynamical processes in solution and at the interphase lead to important considerations of peak resolution. While a great deal of experimental data has accumulated concerning the structure and dynamics of the stationary phase, and solvent (hydrophobic effects), density, and temperature effects (phase transitions)[4-6], a complete theoretical understanding of the underlying molecular level driving forces for retention is lacking. Recently, analytical theoretical approaches have been developed employing mean-field lattice based statistical mechanics, which have had success in emphasizing the important role of the stationary phase in retention[2,7,8]. Our approach is to examine the interphase via a combination of Molecular Dynamics (MD) simulation and statistical mechanical theory. In this way, we can gain a clearer insight into basic molecular processes (equilibrium and dynamical) which occur at the chromatographic interphase.

In a second series of studies, we have begun to explore orientational behavior in monolayers at metal surfaces. It is well known that alkane thiols self assemble on metals to form high density monolayers. Recently, Miller and coworkers[9] found that more complex rigid-rod oligomers (oligoimides) also self assemble on a metal surface and are surprisingly stable to

Mat. Res. Soc. Symp. Proc. Vol. 304. © 1993 Materials Research Society

electrochemical processes in the interphase. These materials may have important applications for microelectronic devices and for adhesive systems, and are closely related to liquid crystalline phases near surfaces. By grazing angle IR, the authors determined an average tilt angle of roughly 60°, contrasting to tilts of 20-30° for the dense alkane monolayers. The oligoimides self assemble at lower relative densities than the alkanes, presumably due in part to their rigid nature and greater length (76Å). The orientational behavior may be controllable by variation of chemical components along the chains, and thus be important in developing useful monolayer properties. We utilize Monte Carlo simulations of model rigid rod oligomers at a solid surface in order to probe orientational behavior of the monolayers.

METHODS

The basic methodology of computer simulation of liquids via MD and MC methods is extensively reviewed in Refs. 10 and 11. We employed MD methods for the simulation of the RPLC stationary phase. Three chain lengths were considered, N = 8, 12, and 18. The choice of interatomic potentials followed previous workers who have modeled liquid alkanes, LB films, and SAMs[12,13]. We treated each CH_2 subunit as a united atom. This approximation is not valid for high density chains (where specific chain geometric effects are important for packing considerations) but is appropriate for the lower densities (and disordered nature) of the RPLC system. United atom segments interacted with Lennard-Jones potentials if on different chains or separated by four or more bonds along a given chain. Each chain included torsional and angle bending potentials. The chains were placed randomly on the surface by a sequential addition process with excluded volume interactions to mimic the inherent disorder of the silica surface. Periodic boundary conditions were adopted in two dimensions. Each united atom segment also experienced a 3-9 surface potential. Initial simulations modeled a flat surface. Later work utilized an oscillating surface potential to further mimic the roughness of the silica surface. The z range of the oscillations was taken as 4 Å, while the xy wavelength was 6 Å. These limits were chosen to provide roughness on atomic-level scale; silica is believed to exhibit roughness down to molecular scales. The chains were started in an all-trans configuration at high temperature (500K where substantial chain tail mobility occurs) and gradually cooled down to a low temperature state. Further details of our simulation approach are presented in Refs. 14 and 15. Various equilibrium and dynamical quantities were computed (see below) along extensive constant energy simulations to probe the physical state of the chains at several densities and temperatures. The simulations were conducted in the absence of solvent; future work will include the water / cosolvent mobile phase.

Finite temperature MC simulations of rigid chain species bonded at one end to a flat surface were performed. Each chain consisted of N segments connected along a single vector. The chains were placed on the surface in a triangular array. The interchain spacing a_0 was varied so as to change the density from near close packed to less dense values. The rigid chains were moved by randomly choosing an angle obtained by uniform sampling on the surface of a sphere. A new chain director was then constructed by changing the chain angle. If the change in angle exceeded a critical value the move was automatically rejected; if not, the move was accepted or rejected based on the Metropolis algorithm. The critical angle was chosen so as to give an acceptance probability of 50%. The potential interactions were all Lennard-Jones 6-12 potentials for interactions of the segments, and a 3-9 surface potential as for the alkane chains above. Periodic boundary conditions were employed in two dimensions. The work presented below concerns simulations of A-A-A... oligomers. The oligoimides of Ref. [9] are A-B-A-B-.... sequences, which are the subject of ongoing simulations. Our model correctly portrays simple interactions of monomer units along rigid rod oligomers; of course it does not include rotational freedom of molecular units along the rigid rod, which may have important packing implications in the oligoimide system. Future simulations will include geometric modifications (sequences of disks, one flexible segment, etc.) to assess their role in interfacial orientational ordering. Complete inclusion of all atoms in a molecular modeling scheme for a reasonably sized system of oligoimides would prove very costly at this time. We have begun some all-atom molecular modeling studies to explore local geometric effects on binding energies of 2, 3, ... chains.

RESULTS AND DISCUSSION

RPLC Stationary Phases

Our first set of simulations examined the temperature dependent properties of a C_4 stationary phase at 41.5 Å^2 / chain [14]. The chains undergo a slow transition from a low temperature glassy state to a high temperature liquid-like state between 200 - 300 K. The z density profile, p(z), displays several disordered peaks at low temperature, which contrasts with high density SAMs[13], where segment-by-segment oscillatory profiles are observed. The z profile softens with increasing temperature, and shifts some density to larger z values. The population of gauche conformations increases from 20% at low temperature to 30% above 300K. There exists a gradient in the structure of the glassy or liquid state with increasing z away from the surface, as evidenced by radial distribution functions computed for a sequence of layers. A more distinct indication of melting behavior comes from dynamical quantities, namely the mean square displacements of the chain segments and power spectra (closely related to phonon densities of state) of the Velocity Autocorrlation Function (VAF). Short time diffusion constants (there can be no diffusion over long time scales since the chains are tethered) increase from zero at 200 K to liquid-like values above 300 K. The spectra exhibit a softening of distinct modes and onset of nonzero zero frequency components (proportional to diffusion constants) with increasing temperature. Dynamical gradients exist with increasing z; the tail segments exhibit more mobility than segments in the middle of the chain. The simulations are consistent with available experimental data on phase transitions in bonded alkane phases. No sequence of rotator transitions was observed, as for high density SAMs[16], since the silica surface is inherently disordered and the densities are less than those where collective tilt angles can be observed.

In progress, we are carrying out a series of simulations of C_{12} and C_{18} systems at several densities and temperatures. In this communication, we present initial results on C_{18} systems. The z density profiles at two densities are presented in Fig. 1. An interesting layering is apparent for the C_{18} system. At 41.5 Å^2 / chain, there are three segment layers and at a lower density, 65 Å^2 / chain, two layers. Similar ordering was observed previously in SAM monolayers by Klein and coworkers[17]. The separation between layers is roughly 4 Å, which corresponds to the minimum of the intersegment Lennard-Jones potential. The layering appears similar to profiles observed in wetting phenomena of simple gases[18,19] and alkanes on a solid surface[20], and it differs from the segment-by-segment layers for high density chains. In effect, the chains have enough accessible free volume to allow (disordered) packing of chain segments in a fashion which does not clearly reflect the connectivity of the chains.

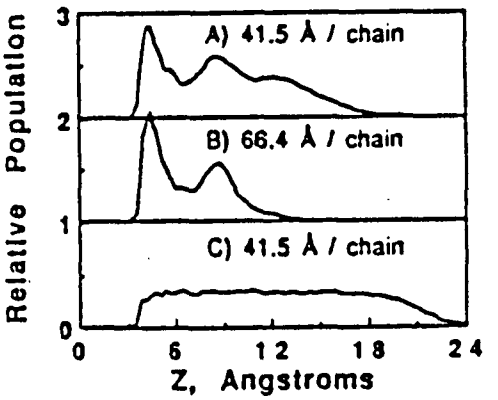

Figure 1. Room temperature density profiles as a function of z for a) high density C_{18} system b) low density C_{18} system c) WCA purely repulsive C_{18} chains at high density.

In order to assess the role of the various force components in inducing this interfacial ordering, we have performed simulations with combinations of the full chain potentials and WCA (Weeks-Chandler-Andersen) repulsive potentials. The WCA potential is a truncated version (at the minimum) of the 6-12 Lennard-Jones potential, and hence is purely repulsive. It provides the starting point for mean field perturbation treatments of liquids. In this sense it mimics near hard sphere interactions. The WCA potential simulations are directly analogous to simulations of grafted polymer brushes in good solvent by Murat and Grest[21], except our relative chain densities are higher by a factor of two than the highest densities examined by them. The z profile for the complete WCA model is presented in Fig. 1c. In addition, we find that *each* force component (chain-chain and chain-surface) is required to produce the layering. Hence, these results indicate the importance of inclusion of *all* attractive and repulsive forces in modeling subtle ordering effects which may occur at the molecular interphase. We have also introduced an undulatory surface potential to mimic further the disorder of the silica surface. We find that if the amplitude of the undulations is on the order of 4 Å and the wavelength 8 Å, the layering is destroyed; the chains cannot organize into clear layers as on a flat surface.

C_{18} simulations have also been conducted at several temperatures, and we observe similar melting behavior to the C_8 system. The melting transition begins at slightly higher temperatures, and appears to set in more abruptly than for the C_8 chains. Again, structural and dynamical gradients are apparent with increasing z, with the chain tails exhibiting the largest degree of fluid-like behavior at room temperature.

The "phase" of the stationary phase, solid or liquid, is crucial in determining the nature of retention in chromatography. If the bonded chains are in a disordered solid phase, a solute will likely only adsorb at the interface and not penetrate since the chains are in a condensed state and little volume is available for passage through cavities in the matrix. If the stationary phase is liquid-like (as it appears to be in our simulations at room temperature), the fluctuating environment at the interface allows the solute to effectively transfer into the phase. In addition, if the stationary phase density is too high, little accessible space is available for solute penetration. The extent to which the solute penetrates is an open question. Our results which indicate structural and dynamical gradients with increasing z suggest that a solute experiences differing local interactions as it passes further into the stationary phase. Clearly, the distribution of free volume and the dynamics of its motion in the interfacial region is an important determinant of solute motion there. Recent results of Pratt and Pohorille[22] suggest that the free volume distribution is a very important determinant of solubility behavior in molecular liquids, and they have shown that analysis of cavity distributions in water vs. alkane fluids lends clear insight into origins of hydrophobic effects on solvation.

Orientational Behavior of Rigid Rod SAMs

Motivated by the recent experimental results of Miller and coworkers [9], we have begun Monte Carlo simulations of orientational behavior in SAMs of complex molecular rigid rod chains at metal surfaces. The purpose is to understand the origins of tilt behavior and to predict effects of segment chemical variations and geometries on the observed ordering. In this way, better strategies for design of useful monolayer properties may be devised. Closely related studies include the MC simulations of Binder and coworkers[23] and the density functional theory of Cai and Rice[24] for tilt transitions in rigid rod monolayers.

MC simulations of 72 15-segment A-A-A... chains at several densities were performed at room temperature. The model system Lennard-Jones potential parameters were: σ_{AA}= 2 Å, σ_{AS}= 2 Å, ϵ_{AA}= 51.2 K, ϵ_{AS}= 60 K. In Fig. 2, a snapshot of the final configuration after a 12,000 step run at relative density 0.75 is presented. Starting from an all-upright configuration, the chains have assumed a collective tilt angle of 31°. The chains tilt toward the next nearest neighbor, in agreement with the results of Binder and coworkers. The distributions of tilt angles (θ) and xy plane rotational angle (ϕ) were computed (not presented here) and have quite narrow distributions about 31° and 30° respectively. An orientational order parameter was also computed[25] which indicates a strong collective tilt for this density, as is apparent from Fig. 2.

We also computed zero Kelvin energetic contributions to the tilt by starting the system at an upright configuration and moving the chains collectively towards either nearest(nn) or next nearest neighbors(nnn). The nnn tilt is the most stable for all densities examined, and the minimum energy tilt angle is found to vary considerably with chain density. The effect of

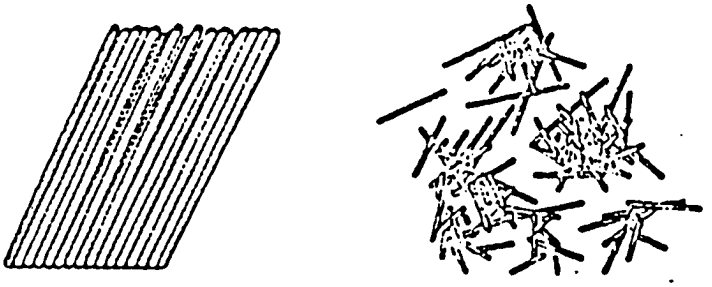

Figure 2. Snaphots of rigid rod conformations at end of two MC simulations at high relative density (0.75, left) and low density (0.18, right). The first is a side view and the second a top view.

entropic contributions to the free energy is an interesting question, but for the 0.75 relative density case, the tilt appears to be driven primarily by energetic effects at room temperature; the tilt angle at 0 K agrees with the finite temperature result to within 2°.

In a second study, we examined a much lower relative density system (0.18), which is a density closer to that of the oligoimide SAMs (It is difficult to determine precisely the close packed density of the oligoimides due to their molecular complexity. The area per chain for the SAM in Ref. 9 is 175 Å^2. We estimated the closest approach distance to be roughly 6Å). The chains were again started in an all vertical configuration. The potential well depths were taken as 150 K for this case. Instead of developing a collective tilt, the chains clustered into locally dense regions (Fig. 2); entropic contributions are more substantial at this density. This simulation is only a highly idealized model, but it suggests that a clear collective tilt for the lower density systems is likely difficult to attain unless specific chain-chain interactions drive such a tilt in an organized way. Future work will explore this issue.

CONCLUSIONS

We have presented MD and MC simulations of model interphase systems. MD simulation and statistical mechanical theory was utilized to examine the structure and dynamics of bonded alkane layers of relevance to chromatographic stationary phases. Temperature, density, and chain length effects on the physical properties of the interphase system have been explored. The stationary phases undergo a gradual transition with increasing temperature from a disorderd solid state to a liquid-like state in the temperature range 200 - 300 K. Interfacial ordering is observed for the C_{18} chains where a layering is apparent in the z direction. Each component of chain-chain and chain-surface interactions is important in inducing the ordering. Work is in progress to include solvent contributions and to study the equilibrium and dynamical aspects of solute motion near a realistic RPLC interphase.

MC simulations of origins of collective tilt behavior in rigid chain monolayers were presented which suggest that high density homo-oligomers tilt collectively toward next nearest neighbors. Energetic contributions appear to drive the transition at room temperature. Substantially lower density systems do not exhibit a collective tilt but cluster into locally dense regions.

ACKNOWLEDGMENTS

We acknowledge a grant from the Donors of the Petroleum Research Fund of the American Chemical Society for partial support of this work. We thank the Ohio Supercomputer Center for a grant of time on the OSC Cray-YMP, where some of these calculations were performed. Profs. John Dorsey and F. J. Boerio are also thanked for many informative discussions.

REFERENCES

[1]*Physics of Polymer Surfaces* , ed. I. C. Sanchez (Butterworth-Heinemann, Boston, 1992).
[2]J. G. Dorsey and K. A. Dill, Chem. Rev. 89, 331 (1989).
[3]L. C. Sander and S. A. Wise, CRC Crit. Rev. Anal. Chem. 18, 299, (1987).
[4]K. B. Sentell and J. G. Dorsey, Anal. Chem. 61, 930 (1989).
[5]L. A. Cole and J. G. Dorsey, Anal. Chem. 64, 1317 (1992).
[6]L. A. Cole, J. G. Dorsey, and K. A. Dill, Anal. Chem. 64, 1324 (1992).
[7]M. R. Bohmer, L. K. Koopal, and R. J. Tijssen, J. Phys. Chem. 95, 6285 (1991).
[8]C. Yan and D. E. Martire, J. Phys. Chem. 96, 7510 (1992).
[9]W. S. V. Kwan, L. Atanasoska, and L. L. Miller, Langmuir 7, 1419 (1991).
[10]M. P. Allen and D. J. Tildesley, *Computer Simulation of Liquids* (Oxford, Oxford, 1987)
[11]*Computer Simulation of Polymers*, ed. R. J. Roe (Prentice-Hall, New Jersey, 1991).
[12]J. Harris and S. A. Rice, J. Chem. Phys. 89, 5898 (1988).
[13]J. Hautman and M. L. Klein, J. Chem. Phys. 91, 4994 (1989).
[14]S. J. Klatte and T. L. Beck, J. Phys. Chem. (in press).
[15]J. F. Wheeler, T. L. Beck, S. J. Klatte, L. A. Cole, and J. G. Dorsey, J. Chromatogr. (in press).
[16]J. Hautman and M. L. Klein, J. Chem. Phys. 93, 7483 (1990).
[17]J. P. Bareman, G. Cardini, and M. L. Klein, Phys. Rev. Lett. 60, 2152 (1988).
[18]D. E. Sullivan and M. M. Telo de Gama, in *Fluid Interfacial Phenomena*, ed. C. A. Croxton (Wiley, New York, 1986).
[19]J.-P. Hansen and I. R. McDonald, *Theory of Simple Liquids* (Academic, New York, 1986).
[20]T. K. Xia, M. W. Ouyang, M. W. Ribarsky, and U. Landman, Phys. Rev. Lett. 69, 1967 (1992).
[21]M. Murat and G. S. Grest, in *Computer Simulation of Polymers*, ed. Roe, R. J. (Prentice Hall, New Jersey, 1991).
[22]L. R. Pratt and A. Pohorille, Proc: Natl. Acad. Sci. 89, 2995 (1992).
[23]M. Scheringer, R. Hilfer, and K. Binder, J. Chem. Phys. 96, 2269 (1992).
[24]Z. Cai and S. A. Rice, J. Chem. Phys. 96, 6229 (1992).
[25]M. C. Duro, J. A. Martin-Pereda, and L. M. Sese, Phys. Rev. A 37, 284 (1988), Eqn. 3.

Appendix B

Molecular structure of monolayers from thiol-terminated polyimide model compounds on gold. Part I: A spectroscopic investigation

Molecular Structure of Monolayers From Thiol-Terminated Polyimide Model Compounds on Gold. Part I : A Spectroscopic Investigation.

by:

J. T. Young and F. J. Boerio
Department of Materials Science and Engineering
University of Cincinnati
Cincinnati, Ohio 45221-0012

and

Z. Zhang and T. L. Beck
Department of Chemistry
University of Cincinnati
Cincinnati, Ohio 45221-0172

June 30, 1995

ABSTRACT

The molecular orientation and/or packing for monolayers formed by adsorption of 4-mercapto-phenyl-phthalimide (4-MPP), a thiol-terminated polyimide model compound, onto gold substrates, was determined using surface-enhanced Raman scattering (SERS), reflection-absorption infrared spectroscopy (RAIR), X-ray photoelectron spectroscopy (XPS), ellipsometry, and electrochemistry. SERS, RAIR, and XPS showed that 4-MPP molecules were chemisorbed onto the gold surface through the thiol groups to form an oriented monolayer. For adsorption times less than about two hours, the ellipsometric thickness of the films increased as a function of time but for longer times the ellipsometric thickness reached a limiting value of about 11.5 Å. For adsorption times greater than about two hours, the surface density was about 5.2×10^{-10} mole/cm^2, corresponding to a molecular area of 32 Å^2/molecule. Considering the size of the 4-MPP molecule compared to that of an alkylthiol molecule, it was concluded that the adsorbed molecules were highly packed on the gold surface. The orientation of adsorbed 4-MPP molecules was determined quantitatively using infrared spectroscopy. It was found that the molecules were oriented with a vertical configuration in which the molecular axes tilted away from the surface normal by about 21°. There was no preferred rotation angle for the imide ring in 4-MPP. The thickness and orientation determined by infrared spectroscopy were in excellent agreement with results obtained from molecular dynamics which are presented in the following paper.

I. INTRODUCTION

As part of our research concerned with the preparation, characterization, and adhesion of polyimide films on metals, we are interested in the modification of metal substrates with self-assembled monolayers of organothiol compounds and using these monolayers as adhesion promoters for polyimide-to-metal bonding. The idea is to link polymer and metal chemically via the thiol groups. Because of the high affinity of thiols for metals such as gold, silver, and copper, monolayers can easily be prepared by immersing metal substrates into dilute solutions of organothiol compounds. Organofunctional groups in these monolayers can further react with polyamic acids, ultimately forming chemical bridges between the polyimide and the metal and leading to improved adhesion.[1]

Self-assembled monolayers of alkylthiol compounds have been extensively investigated. Sandroff et al used surface-enhanced Raman scattering (SERS) to characterize the conformation of hexadecanethiol adsorbed onto silver substrates.[2] They found that adsorption involved dissociation of the thiol groups and that the hydrocarbon tail had a mostly trans conformation with gauche bonds near the end of the trans sequence. Porter et al used ellipsometry, reflection-absorption infrared spectroscopy, and electrochemistry to characterize the structure of n-alkylthiols on gold.[3] Long-chain thiols formed densely packed, crystalline-like assemblies with fully extended chains tilted about 20-30° from the vertical. As the chain length decreased, the packing density and surface coverage also decreased. Bain et al investigated the adsorption of organic thiols having the structure $X-(CH_2)_n-SH$ onto gold and found that ordered, oriented monolayers were formed in which the X-functional groups were exposed at the air/monolayer interface.[4] Alves and Porter investigated adsorption of the perfluorinated alkyl compound $CF_3(CF_2)_7(CH_2)_2SH$ onto Au(111) using AFM, electrochemistry, and RAIR.[5] They found that the tilt angle was 20° from the surface normal and that the molecular area was about 29.1 $Å^2$/molecule compared to about 19.8 $Å^2$/molecule for n-alkanethiols. The greater molecular area for the perfluorinated compound was attributed to the larger van der Waals diameter of the fluorocarbon tail (5.6 Å) compared to the hydrocarbon tail (4.2 Å).

Aromatic thiols have also been investigated. Stern et al investigated adsorption of thiophenol and several related thiols onto Pt(111) electrodes using EELS, Auger spectroscopy, and cyclic voltammetry.[6] They found that thiophenol was adsorbed through the sulfur atoms by dissociation of the thiol group and that the phenyl groups had a vertical orientation in which the benzene rings were perpendicular to the surface. Gui et al investigated adsorption of thiophenol and related compounds onto Pt(111) and Ag(111).[7] Thiophenol layers adsorbed onto Ag had long range order whereas those on Pt did not. The packing density on Ag was 0.544 nmol/cm^2, which was about 19% less than the theoretical maximum (0.67 nmol/cm^2) based on molecular models. Carron and Hurley used surface-enhanced Raman scattering (SERS) to determine the orientation of thiophenol in self-assembled monolayers on silver and gold.[8] They found that thiophenol molecules were adsorbed through the sulfur atoms with a vertical orientation in which the angle between the C_2 axis and the *surface* was 81.3° for silver and 77.0° for gold. Bryant et al[9] obtained normal Raman spectra of thiophenol at mechanically polished, polycrystalline Pt surfaces and observed several bands whose relative intensity changed when the substrate was changed to gold or silver, apparently because of orientation effects. Sabatani et al[10] investigated the adsorption of several aromatic thiols onto gold. p-Biphenyl mercaptan and p-terphenyl mercaptan formed monolayers with reproducible contact angles and ellipsometric thicknesses on Au(111). The molecular axes were oriented almost perpendicular to the surface.

Little information concerning the use of sulfur-containing compounds as coupling agents for polyimides on metals has been reported. Grunze used second harmonic generation to characterize interfaces between polyamic acids derived from pyromellitic dianhydride (PMDA) and 4,4'-diaminophenyldisulfide and metal substrates such as gold and silver.[11] A chemical interaction was observed between the sulfide groups in the polymer chains and the metal substrates. Kwan, Atanasoska and Miller used X-ray photoelectron spectroscopy (XPS), infrared spectroscopy, and electrochemical methods to study thiophenol-terminated oligoimide monolayers covalently attached to gold.[12] Oligoimides with different chain length were derived from naphthalene-1,4,5,8-tetracarboxylic dianhydride and 3,3'-dimethoxybenzidine. It was

found that oligoimide molecules were chemisorbed onto the gold surface through the thiol groups to form an oriented monolayer. Molecules in the monolayer were tilted away from the surface normal by an angle of about 60°. The molecular area was about 175 $Å^2$/molecule.

In the work of Grunze and that of Kwan, the sulfur-containing groups were incorporated into the polymers or oligomers prior to the deposition of films onto the metal substrates. Another approach for introducing sulfur-containing species into the polymer/metal interface is to pretreat the metal substrates with an organosulfur compound and then deposit the polymer films onto the modified metal surfaces. Recently, we have used surface-enhanced Raman scattering (SERS) along with reflection-absorption infrared spectroscopy (RAIR) to characterize interphases between polyimide model compounds and organosulfur derivatized metal substrates.[13,14] These model systems were formed by depositing phthalic anhydride (PA) onto a gold substrate pretreated with 4-aminophenyl-disulfide (APDS) (PA/APDS/Au system) or onto a silver substrate pretreated with meta-aminothiophenol (m-ATP) (PA/m-ATP/Ag system), followed by chemical curing in a mixture of acetic anhydride and either pyridine or triethylamine. It was found that APDS and m-ATP were adsorbed dissociatively through the sulfide and thiol groups, respectively. When PA was deposited onto organosulfur-treated metal substrates, anhydride groups of PA reacted with amino groups of APDS or m-ATP to form amic acids. Chemical curing of these amic acid films produced isoimide and imide species.

Subsequently, we used SERS, RAIR, and XPS to determine the molecular structure of interphases formed by curing the polyamic acid (PAA) from PMDA and oxydianiline (ODA) against silver substrates pretreated with m-ATP (PAA/m-ATP/Ag system).[15] It was found again that m-ATP was chemisorbed onto silver substrates via the thiol groups. When thin films of the PAA were deposited onto the silver substrates modified with m-ATP, an interphase that was only a few angstroms in thickness was formed in which acid groups of the PAA and amino groups of the m-ATP combined to form ammonium carboxylate species. The bulk of the PAA films was easily cured to the polyimide by immersion in mixtures of acetic anhydride and pyridine or triethylamine. However, the ammonium carboxylate species suppressed curing in the interphase.

In addition to the chemical structure of imide films described above, the orientation of molecules adsorbed onto metal substrates has also been an important structural parameter in these studies. Previously, we have used infrared spectroscopy to determine quantitatively the tilt and rotation angles of APDS and m-ATP molecules adsorbed onto metal substrates.[13,14] However, the orientation of molecules in subsequent imide and isoimide layers was not determined due to the lack of relevant transmission infrared spectra. In order to determine the orientation of molecules in these imide films and to gain insights into the structures and properties of sulfur-containing imide films on metals, a thiol-terminated polyimide model compound, 4-mercapto-phenyl-phthalimide (4-MPP) (see Figure 1), was synthesized and its monolayer structure was investigated.

The purpose of this paper is to describe results we have obtained using SERS, RAIR, XPS, ellipsometry, and electrochemistry to determine the molecular orientation and/or packing for 4-MPP monolayers deposited onto gold substrates. Results obtained indicated that 4-MPP was chemisorbed onto the gold surface through the thiol groups to form a densely-packed monolayer. The molecules were oriented with a nearly vertical configuration in which the average tilt angle with respect to the surface normal was about 21° and the rotational angle for the imide ring was approximately 42°. The experimental results will be compared with those obtained from molecular dynamics simulations in the following paper.[16]

II. EXPERIMENTAL

Synthesis and Identification of 4-mercapto-phenyl-phthalimide (4-MPP)

4-MPP was synthesized in our laboratory. Equal molar amounts of phthalic anhydride (Aldrich Chemical Co.) and 4-aminothiophenol (Lancaster Synthesis) were dissolved in N,N-dimethylacetamide (DMAc) and mixed together. The mixture was refluxed overnight at a temperature of about 160°C under a nitrogen environment and then cooled to room temperature. The pale yellow precipitate which formed was filtered, rinsed with copious amounts of ether, and vacuum dried at 75°C for several hours to remove residual solvents.

Gold Substrates and Monolayer Formation

Gold substrates were prepared for SERS investigations as described below. Glass slides were cleaned by immersion in 0.1N aqueous NaOH for 1 hour and rinsed in 0.1N aqueous HCl for another hour. The glass slides were then rinsed ultrasonically in distilled-deionized water, blown dry with nitrogen, cleaned ultrasonically in absolute ethanol several times, and again blown dry with nitrogen.

The clean glass slides were immediately placed into a vacuum chamber which was purged with nitrogen and pumped down to 10^{-6} Torr using sorption, sublimation, and ion pumps. Gold wires wrapped around resistively heated tungsten filaments were then slowly heated to evaporate gold island films onto the glass slides at a rate of approximately 0.2 Å/s. The final thickness of the gold island films was controlled at about 65 Å using a quartz crystal oscillator thickness monitor. SERS spectra of as-deposited gold substrates were featureless.

Monolayers of 4-MPP were prepared by immersing a gold substrate into a 10^{-3} M solution of 4-MPP in chloroform for 12 hours to ensure maximum coverage. After that, the samples were rinsed thoroughly with chloroform. Similar procedures were used to prepare samples for RAIR, XPS, and ellipsometry experiments except that thick gold films were used as substrates instead of gold island films. Thick gold films (~1000 Å) were prepared by thermally evaporating gold onto clean glass slides using the procedures described above. RAIR spectra of as-prepared thick gold films were also featureless.

Thickness Measurements

The thickness of the 4-MPP monolayers on gold substrates was determined using a Rudolph Research Model 436 ellipsometer to examine the substrates before and after deposition of the monolayer. Monolayers were deposited onto thick gold films as described above. The optical constants of the substrate were determined from measurements of the ellipsometric parameters Δ and ψ before deposition of the monolayer. The thickness of the films was determined from measurements of Δ and ψ after deposition of the monolayer using the experimentally determined values for the optical constants of the substrate and an assumed value of 1.5 for the refractive index of the monolayer. McCrackin's program[17] was used to perform

all of the calculations. Each thickness value was the average of measurements taken on five different samples.

Surface Density Measurements

The surface density of 4-MPP monolayers on gold was measured using double potential step chronocoulometry. These measurements were based on the reduction of imide groups in 4-MPP. Several authors reported that imide groups can undergo electron-transfer reactions on a metal electrode at a potential of about -1.35 V to form a radical-anion.[12,18-19] Experiments were performed using a potentisotat (Bioanalytical Systems) and a three-electrode cell consisting of a polished gold disk working electrode, a platinum counter electrode, and a Ag/AgCl reference electrode. The supporting electrolyte was 0.1 M tetramethylammonium fluoroborate in dimethylformamide (DMF) or acetonitrile. Solutions were degassed with nitrogen for 15 minutes prior to the measurement. The potential was stepped from an initial value (0.0 V) where no redox reaction occurred to a final value (-1.5 V) where the reduction of imide groups occurred. The charges measured for the gold electrode before and after the monolayer adsorption were used to calculate the surface density of 4-MPP monolayers adsorbed on the gold surface. The surface density presented in this paper was an average of measurements taken on five different samples.

In order to determine the surface density or surface coverage, it was necessary to know the actual area of the gold disk electrode. The roughness factor or ratio of actual area to geometrical area for the electrode was determined as follows. Double potential step chronocoulometry was carried out for long-chain alkanethiols adsorbed onto polished gold disk electrodes to determine the number of molecules on the surface. Assuming that the molecular area was 19.8 $Å^2$/molecule as reported in the literature,[5] the roughness factor was found to be about 2.0. A similar value was found by Kwan et al.[12]

XPS Measurements

XPS spectra were obtained using a Perkin-Elmer Physical Electronics Model 5300 X-ray photoelectron spectrometer with Mg Kα radiation at a power of 300 W. The pass energy was

44.75 eV (0.5 eV step, 25-ms dwell time per step) and 17.90 eV (0.05 eV step, 50ms dwell time per step) for the survey and high-resolution spectra, respectively. During the analysis, the pressure in the test chamber was kept between 10^{-8} and 10^{-9} Torr. A take-off angle of 45° was used to obtain all of the spectra. Data acquisiton and analysis was done using an Apollo workstation and software provided by Perkin-Elmer. The XPS spectra were corrected for charging by referencing the C(1s) peak for hydrocarbons to 284.6 eV. Elemental compositions of the various surfaces were determined from the area under the individual elemental peaks using sensitivity factors provided with the software. High-resolution spectra were analyzed in order to determine the various chemical species present. The spectra were fitted using a 90%/10% Gaussian/Lorentzian peak shape.

Raman Measurements

SERS spectra were obtained using a spectrometer equipped with a Spex 1401 double monochromator, a Hamamatsu R943-02 photomultiplier, a Stanford Research Model 400 gated photon counter interfaced to a Hewlett-Packard Vectra computer, and a Lexel 3000 krypton-ion laser. The slit setting of the monochromator provided a spectral resolution of about 10 cm^{-1} for the SERS spectra. The red line of the laser (6471 Å) was incident on the sample at an angle of about 65° relative to the normal to the sample surface for SERS experiments and was s-polarized. The laser power used for SERS experiments was about 100 mW. Scattered light was collected using an f/0.95 collection lens and focused onto the entrance slits of the monochromator. Spectra were obtained using a scan speed of 23 cm^{-1} per minute. Plasma lines were removed from the spectra by placing a narrow-bandpass filter between the laser and sample. Normal Raman spectra of 4-MPP were obtained from small amounts of 4-MPP powder supported in a glass capillary tube using the instrument described above. All of the instrumental parameters were the same as used for the SERS spectra except that the slits were set for a spectral width of 5 cm^{-1}.

Infrared Measurements

RAIR spectra were obtained using a Perkin-Elmer Model 1800 Fourier-transform infrared spectrophotometer equipped with a deuterated triglycine sulfate (DTGS) detector and external reflection accessories provided by Harrick Scientific Co. Spectra were collected in the quantitative mode at a resolution of 4 cm^{-1} using one reflection at an angle of 78°. Seven hundred and fifty scans were averaged for each spectrum collected. The spectra reported here are difference spectra obtained by subtracting spectra of bare gold substrates from spectra of film-covered substrates. Transmission infrared spectra of 4-MPP were obtained using the same spectrophotometer. Samples of 4-MPP were prepared by mixing a small amount of 4-MPP powder with KBr powder and then pressing the mixture into a clear pellet under high pressure.

III. RESULTS AND DISCUSSION

Ellipsometry Measurements

The optical constants of the gold substrate at a wavelength of 5461 Å were n = 0.35 and k = 2.26. These values were very close to those given in the literature[20] for evaporated gold films at 5500 Å (n = 0.33, k = 2.32). Using these values for the optical constants of the substrate, assuming a value of 1.5 for the refractive index of the films, and making the usual assumptions regarding uniform films with parallel sides, the thickness of the layer formed by adsorption of 4-MPP onto gold for 30 minutes was about 8.0 ± 1.0 Å. This was somewhat smaller than the theoretical length of a 4-MPP molecule (12.5 Å), probably indicating that the monolayer did not reach the maximum coverage. When the adsorption time was increased to more than 2 hours, the thickness of the layer reached a constant value of about 11.5 ± 0.8 Å. Varying the refractive index of the film from 1.45 to 1.55 did not result in a significant change in the film thickness (from 12.3 to 10.7 Å). Taking into account the 20° tilt angle of the adsorbed molecules (see infrared results described below), the theoretical length became 11.8 Å which was very close to the measured thickness.

Considering the assumptions involved in interpreting ellipsometry results, some caution is in order regarding the agreement between the ellipsometric and theoretical thicknesses. What can be said is that assuming that the refractive index of the film was about 1.5 and that the film

was uniform with parallel sides, the ellipsometric thickness was consistent with the theoretical thickness if the tilt angle was about 20°.

Electrochemistry Measurements

The surface density measured for the monolayer prepared using an adsorption time of 30 minutes was about 4.3 x 10^{-10} mole/cm^2, corresponding to a molecular area of 38 Å^2/molecule. When the adsorption time was increased to 12 hours, the surface density was about 5.2 x 10^{-10} mole/cm^2 (surface area 32 Å^2/molecule). For the longer adsorption time, the surface density indicated that the monolayer was more densely packed. The molecular area of 4-MPP was much higher than that of the long oligoimide molecules (175 Å^2/molecule) investigated by Miller et al.[12] However, considering the much smaller size of 4-MPP and its vertical orientation on gold (see infrared results described below), a much smaller molecular area was expected for 4-MPP. The molecular area for 4-MPP was lower than that of alkylthiols adsorbed onto Au(111) substrates (19.8 Å^2/molecule)[5] but roughly similar to that of $CF_3(CF_2)_7(CH_2)_2SH$ (29.1 Å^2/molecule).[5] The relatively high surface density of 4-MPP implied that a well-packed monolayer was formed on the gold surface, which was in agreement with thickness measurements.

X-Ray Photoelectron Spectroscopy (XPS)

Atomic concentrations for neat 4-MPP as determined by XPS were 77.1% C, 11.8% O, 5.8% N, and 5.3% S (see Table I). These values were in good agreement with the theoretical atomic concentrations, 77.7% C, 11.1% O, 5.6% N, and 5.6% S. The observed C/N, C/S, and O/S ratios were 13.3, 14.5, 2.2, respectively and were close to the theoretical values of 13.8, 13.8, and 2.0, respectively. High-resolution C(1s) spectra of neat 4-MPP consisted of four components (see Figure 2A). The main component near 284.6 eV was assigned to C-C and C-S bonds,[21] while the component near 285.6 eV (Δ = 1.0 eV) was assigned to C-N bonds. The component shifted upward by about Δ = 3.5 eV (288.1 eV) was attributed to imide carbonyl carbons. The weak component shifted upward by about Δ = 6.0 eV (290.6 eV) was related to $\pi \rightarrow \pi^*$ transitions in the phenyl rings.[22]

High-resolution N(1s) spectra showed a single symmetric peak near 400.0 eV which was due to imide nitrogen. However, a spin-orbit doublet was observed in the high-resolution S(2p) spectra (see Figure 2B). The stronger component near 163.5 eV was due to the $S(2p_{3/2})$ in S-H groups, while the weaker component near 164.6 eV was due to $S(2p_{1/2})$. The relative intensity ratio of the two components [i.e., $S(2p_{3/2})/S(2p_{1/2})$] was about 2.

XPS spectra of a 4-MPP monolayer on gold were also obtained. The monolayer was prepared by immersing a gold film into a 1 mM 4-MPP solution in chloroform for 12 hours to ensure maximum coverage and then rinsing the film thoroughly with chloroform. The thickness and surface-density measurements had indicated that the monolayer reached the maximum coverage after a few hour adsorption.

Atomic concentrations for a 4-MPP monolayer on gold were 71.0% C, 20.0% O, 4.6% N, and 4.5% S (see Table I). The C/N, C/S, and O/S atomic ratios were about 15.3, 15.8, and 4.4, respectively. Although the C/S ratio was only slightly greater for the monolayer than for the neat compound, the O/S ratio increased significantly, from 2.2 to 4.4, indicating the orientation of the S atoms toward the substrate and the O atoms toward the surface of the 4-MPP films as expected for a vertically oriented monolayer in which the molecules were anchored to the substrate by the S atoms.

The high-resolution C(1s) spectra of a 4-MPP monolayer on gold are shown in Figure 3A. The overall line shape of the C(1s) spectrum of monolayers was very similar to that of the neat 4-MPP (see Figure 2A). Four components were observed in the C(1s) spectra of the 4-MPP monolayer. The main component near 284.6 eV was again assigned to C-C and C-S bonds. Components shifted upwards by about 1.0, 3.5, and 6.0 eV were due to C-N, C=O, and $\pi \rightarrow \pi^*$ transitions, respectively. The relative area under each individual component was close to that of the C(1s) spectra for neat 4-MPP. High-resolution N(1s) spectra of the 4-MPP monolayer again showed a single peak near 400.0 eV which was due to imide nitrogen. The C(1s) and N(1s) spectra indicated that 4-MPP monolayers had similar chemical compositions compared to neat materials.

However, the S(2p) spectra of 4-MPP monolayers (see Figure 3B) were quite different from the S(2p) spectra of neat 4-MPP (see Figure 2B). As mentioned above, the S(2p) spectra of neat 4-MPP consisted of a doublet near 163.5 and 164.6 eV which was assigned to S-H groups. This doublet shifted downward to about 162.0 and 163.2 eV in the S(2p) spectra of 4-MPP monolayers, indicating that 4-MPP was chemisorbed onto the gold surface through thiolate groups.[23,24]

Surface-Enhanced Raman Scattering (SERS)

The normal Raman spectrum obtained from neat 4-MPP is shown in Figure 4. For convenience, the observed bands and their assignments are summarized in Table II. Strong bands due to imide vibrations were observed in Figure 4. Bands near 1789 and 1771 cm^{-1} were assigned to the symmetric and asymmetric stretching mode of imide carbonyl groups, respectively, while the band near 1395 cm^{-1} was assigned to the CNC axial stretching mode. The medium intensity band near 2581 cm^{-1} in Figure 4 and the weak band near 915 cm^{-1} in Figure 4 were due to the stretching and bending modes of S-H groups, respectively. The remaining bands in the normal Raman spectra of 4-MPP were related to vibrational modes of para- and ortho-disubstituted benzene rings and were assigned using the Wilson numbering system.[25,26] For example, the strong band near 1110 cm^{-1} was assigned to the ring breathing mode ν(1) of p-disubstituted rings. Another strong band near 1604 cm^{-1} was assigned to the C-C stretching mode ν(8a) of p-disubstituted rings. Detailed assignments for the relatively weak bands are described in Table II. It should be noted that vibrational modes associated with aryl-S bonds were coupled with ring modes so that no distinct aryl-S vibrations were observed. Weak bands near 2777 and 1870 cm^{-1} in the normal Raman spectra were attributed to instrumental artifacts.

The SERS spectrum obtained from the 4-MPP monolayer is shown in Figure 5. The monolayer was prepared by immersing a gold island film into a 1 mM solution of 4-MPP in chloroform for 12 hours and then rinsing the film thoroughly with chloroform. Significant differences were observed when the SERS and normal Raman spectra were compared. The band

near 2581 cm^{-1}, which was assigned to ν(S-H), disappeared in the SERS spectra (see Figure 5), indicating that dissociation of the S-H bonds occurred upon adsorption of 4-MPP onto gold. Chemisoption of 4-MPP through the thiol group was further supported by the shift in position of substitutent-sensitive ring modes. Bands near 1604 and 1100 cm^{-1} (see Figure 4) due to the ν (8a) and ν(1) modes of p-disubstituted benzene rings remained strong in the SERS spectra (see Figure 5) and shifted downward to about 1595 and 1085 cm^{-1}. The shift in position of these bands was attributed to a change of environment for adsorbed molecules.

No bands due to S-Au bonds were observed between 150–400 cm^{-1} in the SERS spectra. However, formation of S-metal bonds between organic thiols and metals such as gold and silver has been reported by several authors using SERS.[14,15,27-29] These authors also observed the cleavage of S-H bonds and the shift of substitutent-sensitive ring vibrations such as the ring breathing mode ν(1) in their SERS spectra. XPS results described above provided direct evidence that thiolate species were formed between 4-MPP and gold.

The orientation of 4-MPP molecules adsorbed onto gold substrates can be determined qualitatively by comparing the relative intensities of several bands in the normal Raman and SERS spectra using the "surface selection rules." Moskovits developed selection rules for Raman scattering by molecules adsorbed onto metal substrates which were based strictly on electromagnetic effects.[30] According to the theory, vibrational modes belonging to the totally symmetric representation and involving atomic motions mostly perpendicular to the surface were predicted to be strongly enhanced in the surface spectra, while those belonging to non-totally symmetric representations and involving atomic motions mostly parallel to the surface were expected to be less strongly enhanced.

As mentioned above, strong bands near 1595 and 1085 cm^{-1} were attributed to the ring breathing mode ν(1) and the ring stretching mode ν(8a) of p-disubstituted benzene rings. These vibrations both belong to the totally symmetric representation and their atomic motions are mostly parallel to the long molecular axis. The strong intensity of these two bands in the SERS

spectra (see Figure 5) implied that 4-MPP was adsorbed onto the gold surface with a vertical orientation.

Additional support for a vertical orientation was provided by the weak intensity of bands due to imide moieties and o-disubstituted benzene rings. Since SERS is an interfacial effect, vibrational modes of functional groups located further away from the metal surface would appear with reduced intensity. If the 4-MPP molecule was adsorbed vertically through the thiol group, the imide groups and o-disubstituted rings were located further away from the metal surface relative to the p-disubstituted rings. Therefore, vibrational modes due to imide groups and o-disubstituted rings would decrease in intensity in the SERS spectra. This is exactly what was observed. Bands near 1789 and 1771 cm^{-1} assigned to imide groups and bands near 1619, 1226, 1084, 894, 857, 734, and 594 cm^{-1} assigned to o-disubstituted rings were all very weak in the SERS spectra. On the other hand, bands near 680 and 1020 cm^{-1}, which were assigned to vibrations of p-disubstituted rings, still had some intensity in the SERS spectra.

It should be noted that the band near 1395 cm^{-1} in the SERS spectra of 4-MPP was also expected to decrease in intensity, since this band was due to the imide CNC axial stretching mode. However, this band still exhibited relatively strong intensity in the SERS spectra. This was probably attributed to the orientation effect. The atomic motion of the CNC axial stretching mode was mostly parallel to the long molecular axis. If 4-MPP was adsorbed vertically through the sulfur atom, this band would increase in intensity. The medium intensity of the band near 1395 cm^{-1} was thus considered to be contributed from the orientation effect.

Reflection-Absorption Infrared Spectroscopy (RAIR)

The transmission infrared spectrum obtained from 4-MPP is shown in Figure 6. Observed bands and their assignments are also summarized in Table II. In the region between 600 and 2000 cm^{-1}, the spectrum was dominated by bands related to imide vibrations. Bands near 1782, 1710, 1388, 1121, and 717 cm^{-1} were assigned to the symmetric C=O stretching, asymmetric C=O stretching, CNC axial stretching, CNC transverse stretching, and CNC out-of-plane bending modes, respectively. The bands near 2572 and near 908 cm^{-1} in Figure 6 were

attributed to the S-H stretching and bending modes, respectively. Other bands related to modes of p- and o-disubstituted rings were assigned using the Wilson numbering system (see Table II).

Figure 7 shows the RAIR spectrum obtained from a 4-MPP monolayer prepared by immersing a gold substrate into a 1 mM solution in chloroform for 12 hours and then rinsing the substrate with chloroform extensively. The disappearance of the bands near 2572 and 908 cm^{-1} in the RAIR spectra again indicated that 4-MPP was chemisorbed through the sulfur atom.

It is well-known that RAIR can be used for quantitative determination of the orientation of molecules adsorbed on reflective surfaces. Bands corresponding to vibrational modes having transition moments perpendicular to the substrate appear with enhanced intensity in RAIR spectra, while those with transition moments parallel to the surface appear with reduced intensity. The band intensities are thus orientation-dependent and can give information about the tilt and rotation angles of molecules adsorbed on metal substrates. The tilt and rotation angles of 4-MPP molecules adsorbed onto the gold surface were determined using RAIR as follows.

Figure 8 defines the laboratory coordinates so that z is the direction perpendicular to the surface, while x and y represent directions in surface. The angle between the long axis of the adsorbed molecules and the z coordinate was defined as θ (i.e., tilt angle of the long molecular axis away from the surface normal). ϕ was the angle between the molecular plane and the x-z plane (i.e., rotation angle of the molecule about the long molecular axis). By calculating the intensity ratios of selected bands in RAIR and transmission infrared spectra, θ and ϕ can be obtained using equations 1 and 2.[12,31]

$$A_{//}(R)/A^{i}_{\perp}(R) = [A_{//}(T)/A^{i}_{\perp}(T)]\,[\cot^2\theta/\cos^2\phi] \quad (1)$$

$$A_{//}(R)/A^{o}_{\perp}(R) = [A_{//}(T)/A^{o}_{\perp}(T)]\,[\cot^2\theta/\sin^2\phi] \quad (2)$$

where

$A_{//}(R)$: absorbance of a band in RAIR spectra having the dipole moment parallel to the long molecular axis.

$A^{i}_{\perp}(R)$: absorbance of a band in RAIR spectra having the dipole moment perpendicular to the long molecular axis and in the molecular plane.

$A^{o}_{\perp}(R)$: absorbance of a band in RAIR spectra having the dipole moment perpendicular to the long molecular axis but out of the molecular plane.

$A_{//}(T)$: absorbance of a band in the transmission IR spectra (isotropic spectra) having the dipole moment parallel to the long molecular axis.

$A^{i}_{\perp}(T)$: absorbance of a band in transmission IR spectra (isotropic spectra) having the dipole moment perpendicular to the long molecular axis and in the molecular plane.

$A^{o}_{\perp}(T)$: absorbance of a band in transmission IR spectra (isotropic spectra) having the dipole moment perpendicular to the long molecular axis but out of the molecular plane.

In order to use equations 1 and 2 for the calculation of tilt and rotation angles, it was necessary to choose two pairs of bands such that the dipole moments of the bands in each pair are perpendicular to each other (one parallel to the molecular axis, the other perpendicular to the axis). In this study, strong bands near 1388, 1710, and 717 cm^{-1} were selected to determine the tilt and rotation angles of imide moieties in 4-MPP. The band near 1388 cm^{-1} was assigned to the imide CNC stretching mode which has the dipole moment mostly parallel to the long molecular axis whereas the band near 1710 cm^{-1} was assigned to the imide C=O asymmetric stretching mode which has the dipole moment mostly perpendicular to the long molecular axis and in the imide plane. Intensity ratios of these two bands (i.e., $A_{//}(R)/A^{i}_{\perp}(R)$ and $A_{//}(T)/A^{i}_{\perp}(T)$) were used in equation 1. The band near 717 cm^{-1} was attributed to the imide CNC out-of-plane bending mode which has the dipole moment mostly perpendicular to the long molecular axis but out of the imide plane. Intensity ratios of bands near 1388 and 717 cm^{-1} (i.e., $A_{//}(R)/A^{o}_{\perp}(R)$ and $A_{//}(T)/A^{o}_{\perp}(T)$) were used for equation 2.

A tangent-line technique was used to draw the base line for bands near 1388, 1710, and 717 cm^{-1} in both transmission IR and RAIR spectra of 4-MPP (see Figures 6 and 7). Absorbance ratios, including $A_{//}(R)/A^{i}_{\perp}(R)$, $A_{//}(T)/A^{i}_{\perp}(T)$, $A_{//}(R)/A^{o}_{\perp}(R)$, and $A_{//}(T)/A^{o}_{\perp}(T)$, were calculated to be approximately 7.92, 0.64, 20.60, and 1.33, respectively. The tilt and rotation angles were then calculated to be approximately 21^{o} and 42^{o}, respectively.

Since the 4-MPP molecule has a linear structure, the angle θ determined using the three imide bands described above can be considered as the tilt angle of the entire molecule. However, the molecule consists of an imide ring and a p-substituted benzene ring which may not be coplanar. The angle φ determined using bands characteristic of the imide group can only represent the rotational orientation of the imide group in 4-MPP. Unfortunately, we were unable to determine the rotational angle of the p-disubstituted benzene rings due to the low intensity of bands assigned to those rings. The relative rotation angle between the imide rings and the p-disubstituted benzene rings was thus unknown. However, information regarding this relative rotational angle was provided by results from computer simulation presented in the following paper.[16]

Results described above showed that 4-MPP was adsorbed onto gold through the sulfur atom with the molecular axis tilted away from the surface normal about 21° (see Figure 8). The calculated rotation angle (42°) was close to the average value (45°), probably indicating that there was no preferred rotation angle for the imide group in 4-MPP. These results were in excellent agreement with results obtained from molecular dynamics.[16]

It should be noted that the angles θ and φ determined above are for the 4-MPP monolayer prepared using a 12 hour adsorption time. The tilt and rotation angles for the 4-MPP monolayer deposited on gold using a short adsorption of 30 minutes were calculated to be approximately 31 and 52°, respectively. The smaller θ (21°) for the monolayer prepared using a long adsorption time probably implied that molecules were more densely-packed than those deposited using a short adsorption time. This caused the molecule to tilt up a little more from the metal surface. This result was consistent with those obtained from thickness and surface density measurements which showed that the monolayer reached the maximum coverage after a few hours adsorption.

It is of interest to compare the orientation of 4-MPP monolayers with those of polyimide and oligoimide films prepared using different methods such as spin-coating and Langmuir-Blodgett (LB) techniques. As mentioned above, Miller and coworkers have used infrared spectroscopy to determine the tilt angle of oligoimide films deposited onto gold using self-

assembling[12] and LB techniques.[31] These oligoimides were synthesized from naphthalene-1,4,5,8-tetracarboxylic dianhydride and 3,3'-dimethoxybenzidine with different chain lengths (ranging from about 20 to 80 Å) and end groups. In the case of self-assembled oligoimide monolayers, molecules were tilted away from the surface normal about 54-60°, depending on the molecular length. In the case of LB films, the tilt angles with respect to the surface normal were in the range of 60 to 80°, depending on the structural details of oligoimide molecules.

Previously, we have used RAIR to determine the orientation of spin-coated PMDA/ODA polyimide films on gold substrates.[32] The polyimide was oriented on the gold surface with an in-plane zigzag conformation in which the PMDA moieties were adsorbed edge-on with the carbonyl groups mostly perpendicular to the surface and the ODA moieties were mostly parallel to the surface. Very recently, we used the same infrared technique described above to determine the tilt and rotation angles of these PMDA/ODA polyimide films on gold.[33] The PMDA moieties of polyimide chains were found to tilt away from the surface normal by an angle of about 63°.

Results described above indicated that long rigid oligoimides[12,31] and PMDA/ODA polyimide[32,33] tended to lie down on the metal surface. On the other hand, the 4-MPP molecule was adsorbed vertically on the gold surface. This significant difference in orientation was probably related to the effect of molecular length. It has been proposed by Miller and coworkers that the increased van der Waals interactions between longer molecules tended to overcome the tilt imposed by the Au-S-C bond angle and thus the longer molecules lay down a little bit more.[12] We are currently extending the length of thiol-terminated polyimide model compounds and studying the effect of molecular length on the structure of monolayers. Results regarding this effect will be reported subsequently.

IV. CONCLUSIONS

The molecular structure of 4-mercapto-phenyl-phthalimide (4-MPP) monolayers deposited onto gold substrates was determined using surface-enhanced Raman scattering (SERS), reflection-absorption infrared spectroscopy (RAIR), X-ray photoelectron spectroscopy

(XPS), ellipsometry, and electrochemistry. It was concluded that 4-MPP was chemisorbed onto the gold surface via the sulfur atom, forming an oriented monolayer. Thickness and surface density measurements indicated the formation of a highly-packed monolayer. The tilt and rotation angles of adsorbed 4-MPP molecules were determined quantitatively by infrared spectroscopy. 4-MPP was adsorbed with a vertical configuration in which the molecular axis tilted away from the surface normal by about 21°. There was no preferred rotation angle for the imide plane. The orientation determined by infrared spectroscopy was in excellent agreement with results from molecular dynamics.[16]

V. ACKNOWLEDGEMENTS

This research was supported in part by a grant from the Office of Naval Research. Many helpful discussions with Prof. Harry B. Mark and Dr. Ahmed Galal are also acknowledged.

VI. REFERENCES

1. Stewart, K. R.; Whitesides, G. M.; Godfried, H. P.; Silvera, I. F. *Rev. Sci. Instrum.* 1986, *57*, 1381.
2. Sandroff, C. J.; Garoff, S.; Leung, K. P. *Chem. Phys. Lett.*, 1983, *96*, 547.
3. Porter, M. D.; Bright, T. B.; Allara, D. L.; Chidsey, C. E. D. *J. Am. Chem. Soc.* 1987, *109*, 3559.
4. Bain, C. D.; Troughton, E. B.; Tao, Y.-T.; Evall, J.; Whitesides, G. M.; Nuzzo, R. G. *J. Am. Chem. Soc.* 1989, *111*, 321.
5. Alves, C. A.; Porter, M. D. *Langmuir* 1993, *9*, 3507.
6. Stern, D. A.; Wellner, E.; Salaita, G. N.; Laguren-Davidson, L.; Lu, F.; Batina, N.; Frank, D. G.; Zapien, D. C.; Walton, N.; Hubbard, A. T. *J. Am. Chem. Soc.* 1988, *110*, 4885.
7. Gui, J. Y.; Stern, D. A.; Frank, D. G.; Lu, F.; Zapien, D. C.; Hubbard, A. T. *Langmuir* 1991, *7*, 955.
8. Carron, K. T.; Hurley, L. G. *J. Phys. Chem.* 1991, *95*, 9979.
9. Bryant, M. A.; Joa, S. L.; Pemberton, J. E. *Langmuir* 1992, *8*, 753.
10. Sabatani,E.; Cohen-Boulakia, J.; Bruening, M.; Rubinstein, I. *Langmuir* 1993, *9*, 2974.

11. Grunze, M., *Proc. 16th Annual Meeting of The Adhesion Society*, The Adhesion Society, Inc., Blacksburg, VA, 1993, p. 378.

12. Kwan, W. S. V.; Atanasoska, L.; Miller, L. L. *Langmuir* 1991, *7*, 1419.

13. Young, J. T.; Boerio, F. J.; Jackson, K. M. *J. Adhesion* 1994, *44*, 103.

14. Young, J. T.; Boerio, F. J. *J. Adhesion* 1994, *44*, 119.

15. Young, J. T.; Boerio, F. J. *J. Adhesion* 1994, *46*, 243.

16. Zhang, Z.; Beck, T. L.; Young, J. T.; Boerio, F. J. *Langmuir*, submitted for publication.

17. McCrackin, F. L. *U. S. Nat. Bur. Stand. Tech. Note 479*, U. S. Govt. Print. Off., Washington, DC, 1969.

18. Mazur, S.; Lugg, P. S.; Yarnitzky, C. *J. Electrochem. Soc.* 1987, *134*, 347.

19. Leedy, D. W.; Muck, D. L. *J. Am. Chem. Soc.* 1971, *93*, 475.

20. *American Institute of Physics Handbook*, 3rd edition, D. E. Gray, ed., McGraw-Hill, New York, NY, 1972, p. 6-138.

21. Clark, D. T.; Thomas, H. R. *J. Polym. Sci.: Polym. Chem.* 1978, *16*, 791.

22. Tsai, W. H.; Boerio, F. J.; Jackson, K. M. *Langmuir* 1992, *8*, 1443.

23. Nuzzo, R. G.; Zegarski, B. R.; Dubois, L. H. *J. Am. Chem. Soc.* 1987, *109*, 733.

24. Bain, C. D.; Biebuyck, H. A.; Whitesides, G. M. *Langmuir* 1989, *5*, 723.

25. Wilson, E. B. *Phys. Rev.* 1934, *45*, 706.

26. Varsanyi, G. *Vibrational Spectra of Benzene Derivatives*, Academic Press, New York, 1974.

27. Sandroff, C. J.; Herschbach, D. R. *J. Phys. Chem.* 1982, *86*, 3277.

28. Joo, T. H.; Yim, Y. H.; Kim, K.; Kim, M. S. *J. Phys. Chem.* 1989, *93*, 1422.

29. Yim, Y. H.; Kim, K.; Kim, M. S. *J. Phys. Chem.* 1990, *94*, 2552.

30. Moskovits, M. *J. Chem. Phys.* 1982, *77*, 4408.

31. Cammarata, V.; Atanasoska, L.; Miller, L. L.; Kolaskie, C. J.; Stallman, B. J. *Langmuir* 1992, *8*, 876.

32. Young, J. T.; Boerio, F. J. *Surf. Interf. Anal.* 1993, *20*, 341.

33. Boerio, F. J.; Zhao, W. W.; Young, J. T. *Advances in Chemistry Series*, American Chemical Society, Washington, DC, 1995, to be published.

Table I. Atomic concentrations for neat 4-mercapto-phenyl-phthalimide (4-MPP) and for a 4-MPP monolayer on gold.

	Atomic Concentration (%)						
	C	O	N	S	O/S	C/N	C/S
Theoretical values	77.7	11.1	5.6	5.6	2.0	14.0	14.0
Neat 4-MPP	77.1	11.8	5.8	5.3	2.2	13.3	14.5
4-MPP monolayer	71.0	20.0	4.6	4.5	4.4	15.3	15.8

Table II. Tentative band assignments for infrared and Raman spectra of 4-MPP.

NR (cm^{-1})	SERS (cm^{-1})	IR (cm^{-1})	RAIR (cm^{-1})	Assignments
3096 (w)				ν(20a)-para & ortho, C-X stretching
3078 (m)				ν(2)-para, C-X stretching
2581 (m)		2572 (w)		ν(S-H)
			2360, 2340	CO_2
1789 (m)		1782 (w)	1787 (w)	ν_s(C=O), imide I
1771 (m)		1710 (vs)	1715 (w)	ν_{as}(C=O), imide I
		1762 (vw)	1762 (vw)	overtone
		1738 (w)	1739 (w)	overtone
1619 (w)		1608 (vw)		ν(8b)-ortho, C-C stretching
1604 (vs)	1595 (s)	1593 (vw)	1587 (w)	ν(8a)-para, C-C stretching
1505 (w)		1494 (m)	1490 (s)	ν(19a)-para, C-C stretching
1395 (vs)	1390 (m)	1388 (s)	1387 (vs)	CNC axial stretching, imide II
1226 (w)		1219 (w)	1221 (w)	ν(7a)-ortho, C-X stretching
1182 (w)		1178 (w)	1180 (vw)	ν(9a)-para, C-H in-plane bending
1124 (w)	1122 (w)	1121 (w)	1119 (w)	CNC transverse stretching, imide III
1100 (s)	1085 (s)	1095 (w)	1087 (w)	ν(1)-para, radial skeletal vibration
1084 (w)		1080 (w)	1077 (w)	ν(13)-ortho, C-X stretching
1023 (m)	1021 (w)	1015 (w)	1014 (w)	ν(18a)-para, C-X in-plane bending
915 (w)		908 (w)		β(S-H), bending mode
894 (w)		882 (w)		ν(17b)-ortho, out-of-plane mode
857 (w)		849 (w)	849 (w)	ν(17a)-ortho, out-of-plane mode
		815 (w)		ν(17b)-para, out-of-plane mode
		794 (w)	791 (w)	ν(11)-ortho, out-of-plane mode
734 (m)				ν(1)-ortho, radial skeletal vibration
		717 (m)	715 (w)	CNC out-of-plane bending, imide IV
678 (w)	672 (w)	668 (w)		ν(12)-para, radial skeletal vibration
			666 (m)	CO_2
643 (w)		632 (w)		ν(6b)-para, radial skeletal vibration
594 (w)				ν(6a)-ortho, radial skeletal vibration

s : strong ; m : medium ; w : weak ; vs : very strong ; vw : very weak.

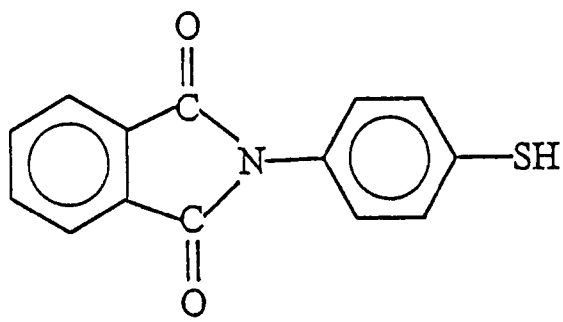

Figure 1. The molecular structure of 4-mercapto-phenyl-phthalimide (4-MPP).

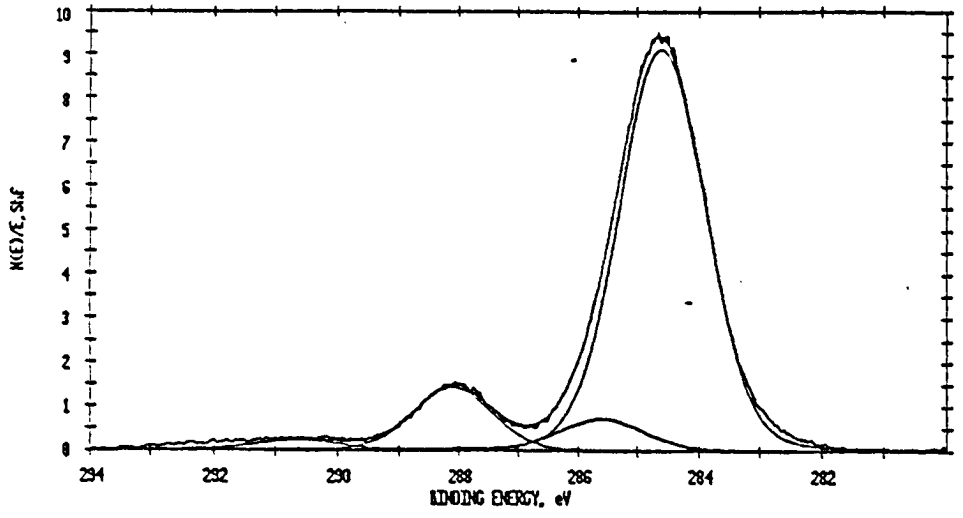

(A)

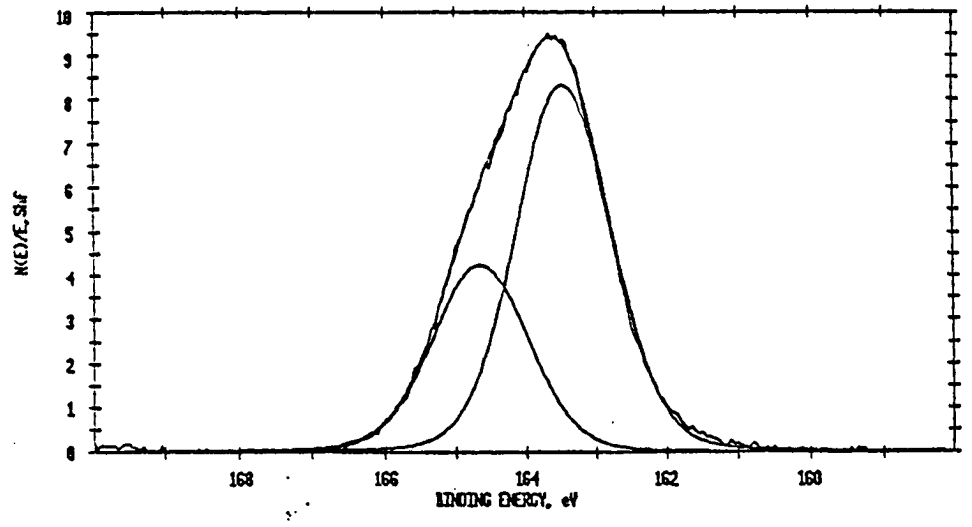

(B)

Figure 2. The XPS high-resolution (A)-C(1s) and (B)-S(2p) spectra of neat 4-MPP.

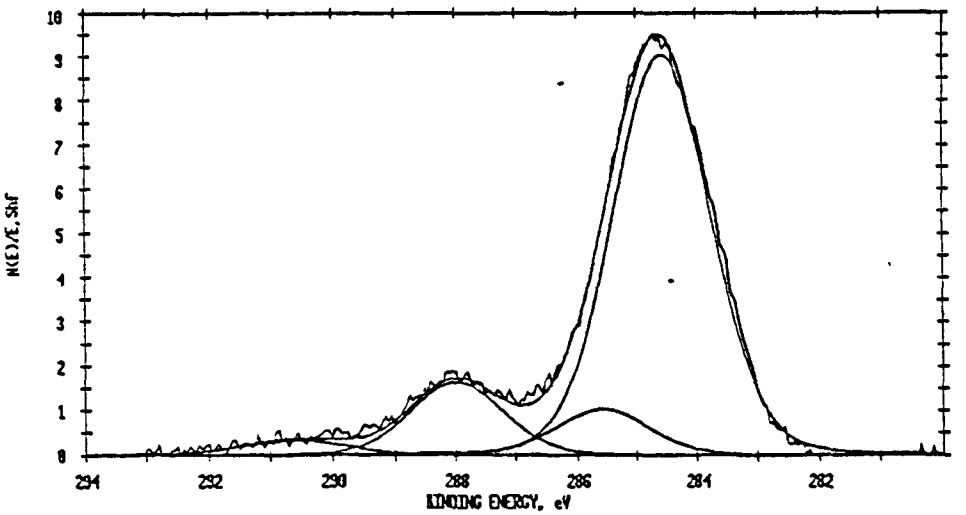

(A)

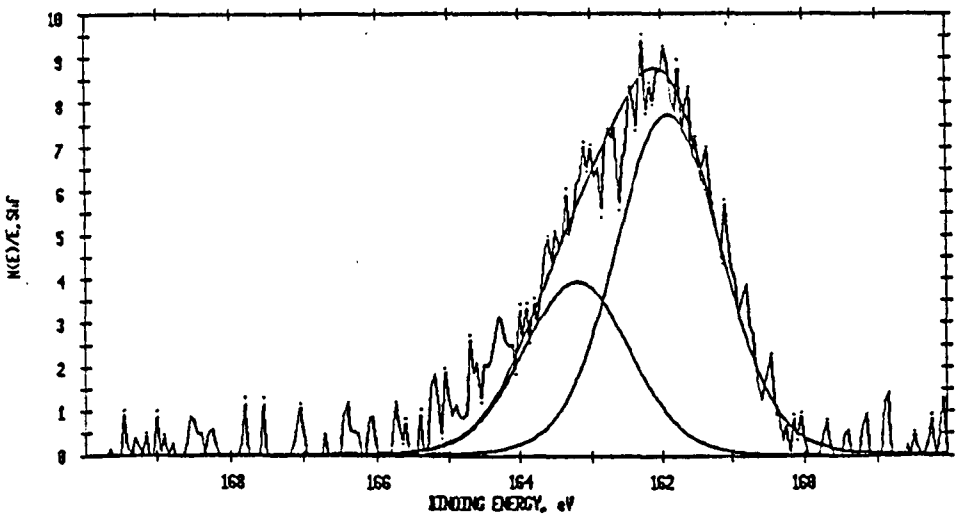

(B)

Figure 3. The XPS high-resolution (A)-C(1s) and (B)-S(2p) spectra of a 4-MPP monolayer deposited onto the gold substrate.

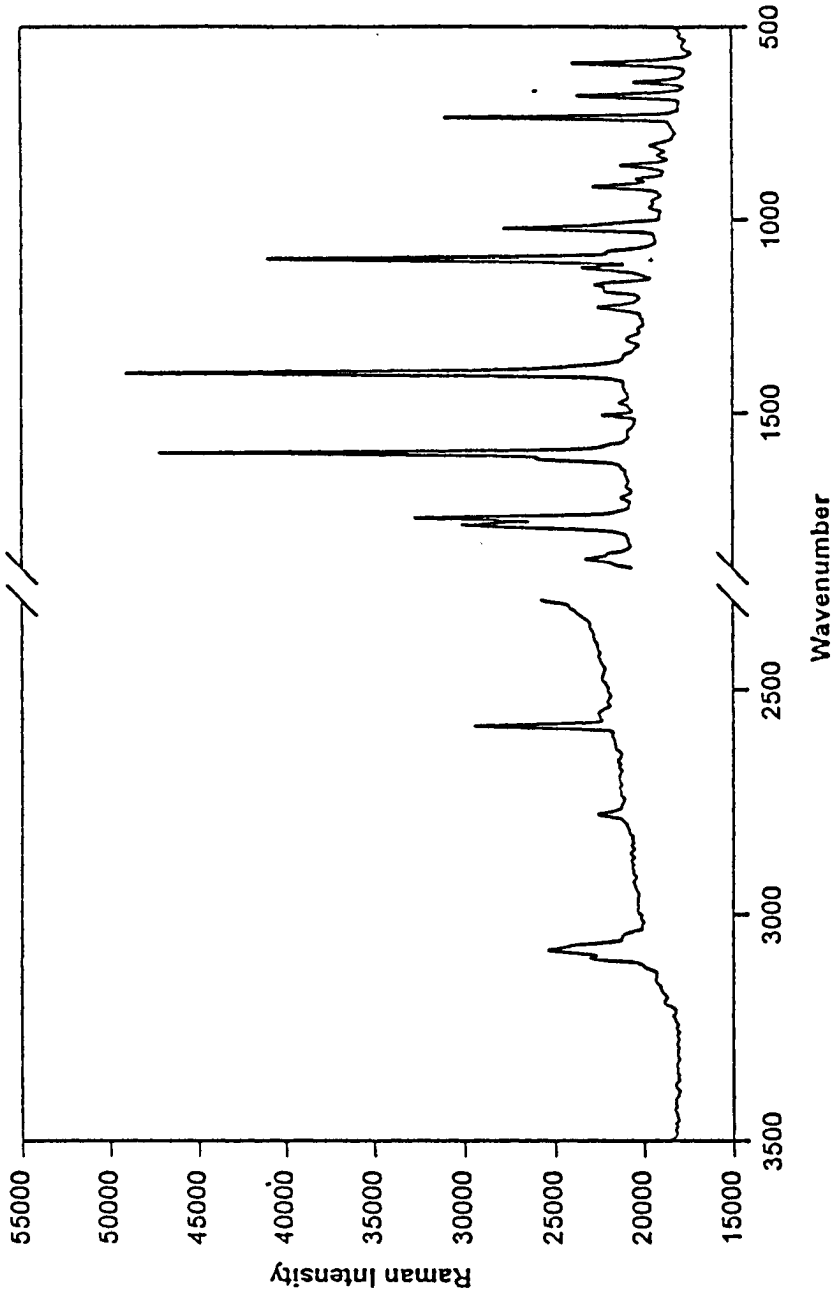

Figure 4. The normal Raman spectrum of neat 4-MPP.

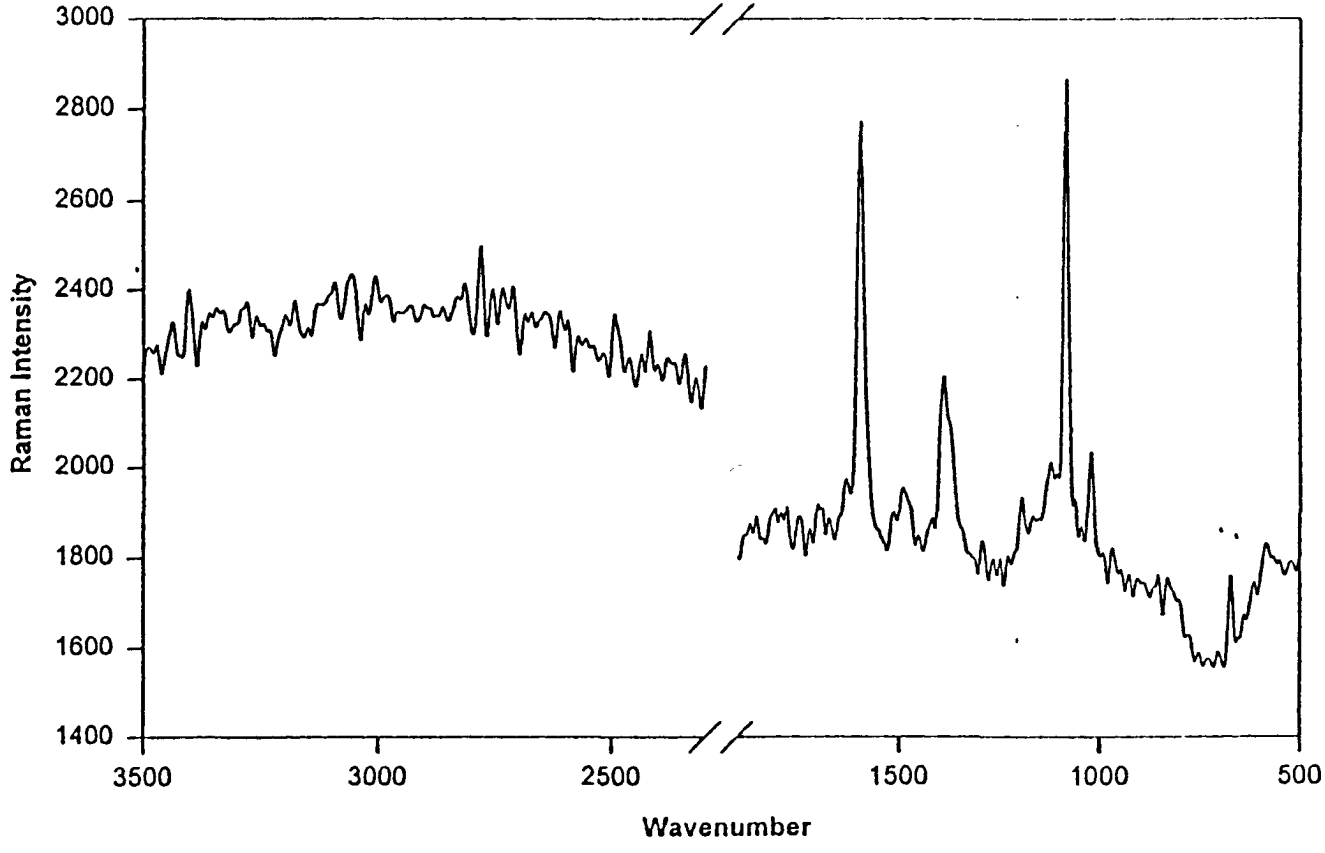

Figure 5. The SERS spectrum of a 4-MPP monolayer on gold island films.

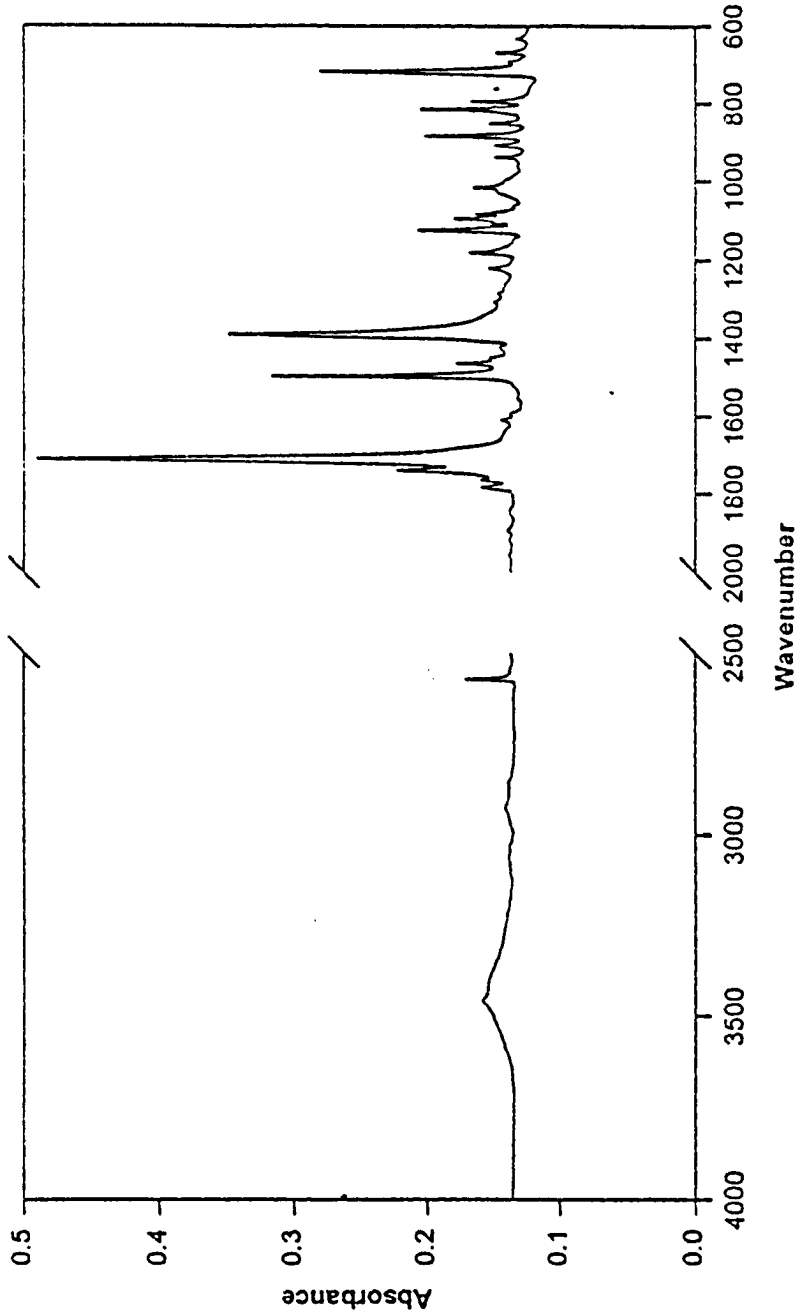

Figure 6. Transmission infrared spectrum of neat 4-MPP.

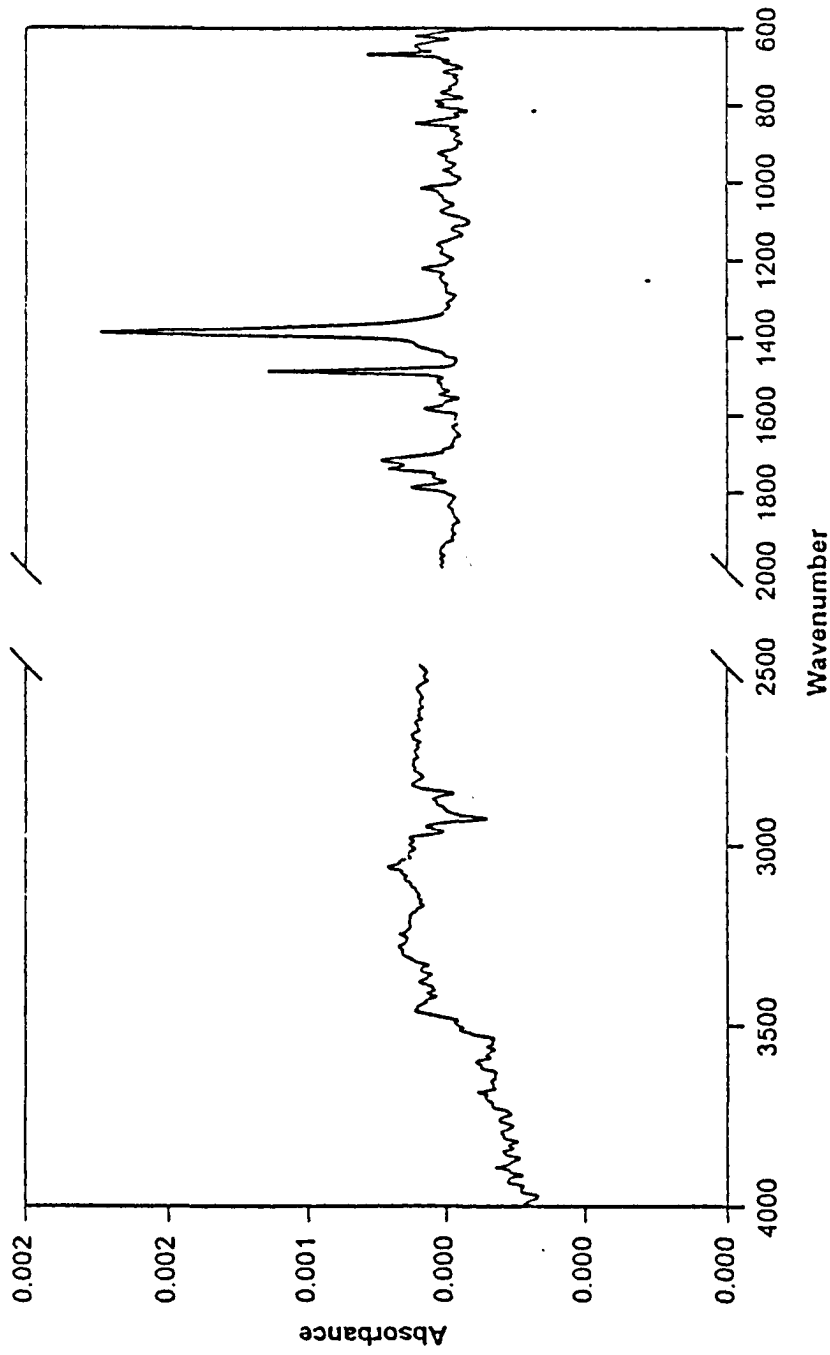

Figure 7. RAIR spectrum of a 4-MPP monolayer on gold.

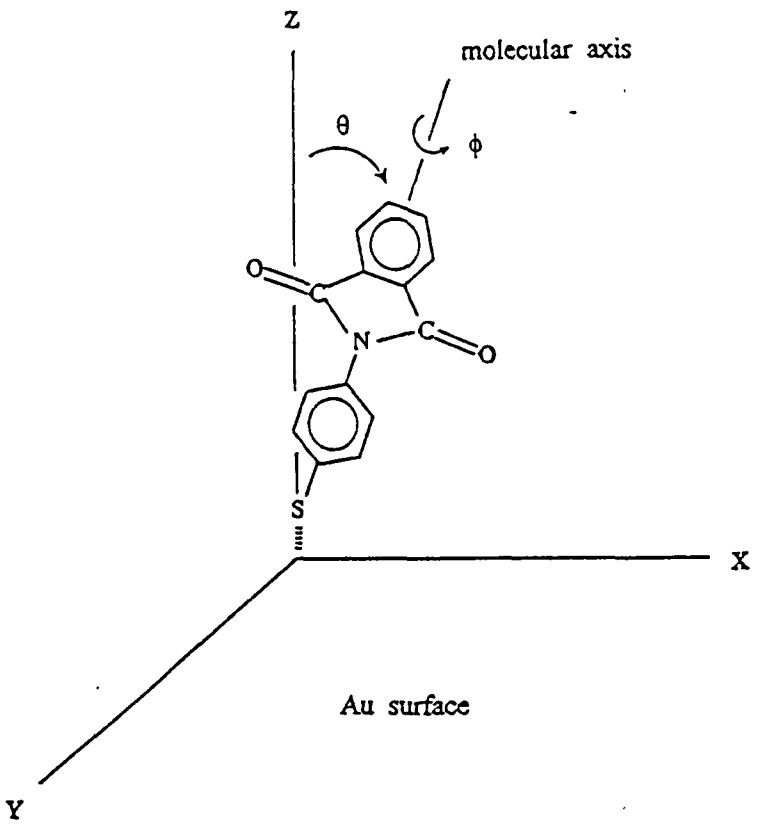

Figure 8. The definition of tilt angle θ and rotation angle ϕ of 4-MPP adsorbed onto the gold surface.

References

[1]H. Gerischer and C. W. Tobias, *Advances in Electrochemical Science and Engineering*, VCH Verlagsgesellschaft mbH, D-6940 Weinheim, 1990.

[2]K. S. Goto, *Solid State Electrochemistry and Its Applications to Sensors and Electronic Devices*, Elsevier Science Publishing Company Inc., 1988.

[3]H. Yugami and M. Ishigame, Jpn. J. Appl. Phys. **32**, 853 (1993).

[4]P. G. Edleman and J. Wang, *Biosensors and Chemical Sensors*, ACS Symposium Series 487, 1992.

[5]R. P. Buck, W. E. Hatfield, M. Umana, and E. F. Bowden, *Biosensor Technology*, Marcel Dekker, Inc. New York and Basel, 1990.

[6]T. P. Bowden and D. Tabor, *The Friction and Lubrication of Solids*, Oxford Universty Press: London, 1968.

[7]D. H. Kaelble, *Physical Chemistry of Adhesion*, Wiley-Intersciencs: New York, 1971.

[8]C. Tubandt and E. Lorenz, Z. Physik **87**, 513 (1914).

[9]W. van Gool, *Fast Ion Transport in Solids*, North-Holland Publishing Co., 1972.

[10]G. D. Mahan, *Superionic Conductors*, Plenum Press, 1976.

[11]S. Chandra, *Superionic Solids*, North-Holland Publishing Co., 1981.

[12]M. B. Salamon, *Physics of Superionic Conductors*, Springer-Verlag Berlin Heidelberg, 1979.

[13]A. L. Laskar and S. Chandra, *Superionic Solids and Solid Electrolytes*, Academic Press, Inc., 1989.

[14]A. Ulman, *Characterization of organic thin films*, Butterworth-Heinemann, Boston., 1995.

[15]A. J. Dianoux, M. Tachez, R. Mercier, and J. P. Malugani, J. Non-Crystallline Soilds **131-133**, 973 (1991).

[16]M. Tachez, R. Mercier, J. P. Malugani, and A. J. Dianoux, Solid State Ionics **20**, 93 (1986).

[17]A. Fontana, F. Rocca, M. P. Fontana, B. Rosi, and A. J. Dianoux, Phys. Rev. B **41**, 3778 (1990).

[18]P. Rahlfs, Z. Phys. Chem. Abt. **B31**, 157 (1936).

[19]K. Funke, Adv. Solid state Phys. **20**, 1 (1980).

[20]K. Funke, Soild State Ionics **6**, 93 (1982).

[21]G. L. Chiarotti, G. Jacucci, and A. Rahman, Phys. Rev. Lett. **57**, 2395 (1986).

[22]A. Fontana, F. Rocca, and A. Tomasi, J. Non-Crystallline Soilds **123**, 230 (1990).

[23]T. Hayes and J. B. Boyce, J. Phys. C **13**, L731 (1980).

[24]R. J. Cava, F. Reidinger, and B. J. Wuensch, J. Soild State Chem. **31**, 69 (1980).

[25]A. Rahman, J. Chem. Phys. **65**, 4845 (1976).

[26]J. W. Perram, *The Physics of Superionic Conductors and Electrode Materials*, Plenum Press, 1983.

[27]J. P. Rino, Y. M. M. Hornos, G. A. Antonio, I. Ebbsjo, R. K. Kalia and P. Vashishta, J. Chem. Phys. **89**, 7542 (1988).

[28]K. O'Sullivan, G. Chiarotti, and P. A. Madden, Phys. Rev. B **43**, 13536 (1991).

[29]R. W. Murray, *Molecular Design of Electrode Surface*, John Wiley & Sons, Inc., 1992.

[30]J. M. Leidheiser Jr. and P. D. Deck, Science **241**, 1176 (1988).

[31]A. K. Chakraborty, H. T. Davis, and M. Tirrell, J. Polym. Sci. Polym. Chem. Ed. **28**, 3185 (1990).

[32]R. G. Nuzzo and D. L. Allara, J. Am. Chem. Soc. **105**, 4481 (1983).

[33]M. D. Porter, T. B. Bright, D. L. Allara, and C. E. D. Chidsey, J. Am. Chem. Soc. **109**, 3559 (1987).

[34]L. Strong and G. M. Whitesides, Langmuir **4**, 546 (1988).

[35]C. D. Bain, E. B. Troughton, Y-T. Tao, J. Evall, G. M. Whitesides and R. G. Nuzzo, J. Am. Chem. Soc. **111**, 321 (1989).

[36]W. S. V. Kwan, L. Atanasoska, and L. Miller, Langmuir **7**, 1419 (1991).

[37]J. Kawamura and S. Hiyama, Solid State Ionics **53-56**, 1227 (1992).

[38]J. Fan, R. F. Marzke, E. Sanchez, and C. A. Angell, Non-Crystalline Solids **172**, 1178 (1994).

[39]A. P. Owens, A. Pradel, M. Ribes, and S. R. Elliott, J. Non-Crystallline Soilds **131-133**, 1104 (1991).

[40]M. Tatsumisago, Y. Shinkuma, and T. Minami, Nature 354, 217 (1991).

[41]P. Vashishta, J. N. Mundy, and G. K. Shenoy, *Fast Ion Transport in Solids*, Elsevier North-Holland Publishing Co., 1979.

[42]H. L. Tuller and M. Balkanski, *Science and Technology of Fast Ion Conductors*, Plenum Press, 1989.

[43]C. R. A. Catlow, J. Chem. Soc. Faraday Trans 86, 1167 (1990).

[44]P. Vashishta and A. Rahman, Phys. Rev. Lett. 40, 1337 (1978).

[45]M. Parrinello, A. Rahman, and P. Vashishta, Phys. Rev. Lett. 50, 1073 (1983).

[46]P. Vashishta, I. Ebbsjo, R. Dejus, and K. Skold, J. Phys. C: Solid State Phys. 18, L291 (1985).

[47]J. R. Ray and P. Vashishta, J. Chem. Phys. 90, 6580 (1989).

[48]F. Shimojo and H. Okazaki, J. Phys. Soc. Japan 60, 3745 (1991).

[49]F. Shimojo and H. Okazaki, J. Phys. condens. Matter 5, 3405 (1993).

[50]A. K. Ivanov-Shitz, A. S. Buchstab, and H. H. Kohler, Appl. Phys. A 54, 251 (1992).

[51]P. J. Lindan and M. J. Gillan, J. Phys.: Condens. Matter 5, 1019 (1993).

[52]A. G. Abdullayev, V. K. Aliyev, T. G. Fufayeva, and L. I. Skugareva, J. Chem. Phys. 90, 6580 (1980).

[53]H. Okazaki, J. Phys. Soc. Japan 43, 355 (1967).

[54]J. P. Rose and R. S. Berry, J. Chem. Phys. 98, 3262 (1993).

[55]J. P. Rose and R. S. Berry, J. Chem. Phys. 98, 3246 (1993).

[56]T. P. Martin, Phys. Rep. 95, 169 (1983).

[57]F. H. Stillinger and T. A. Weber, Phys. Rev. A 25, 978 (1982).

[58]J. Lou and U. Landman, *Physics and Chemistry of Small Clusters*, volume 158, NATO ASI Series B, Plenum, New York, 1987.

[59]G. L. Gaines, *Insoluble Monolayers at Liquid Gas Interfaces*, Wiley, New York, 1966.

[60]A. Bibo and I. R. Peterson, Adv. Mater. 2, 309 (1990).

[61]R. Kenn, C. Böhm, A. Bibo, I. R. Peterson, H. Möhwald, J. Alse-Nielsen and K. Kjaer, J. Phys. Chem. 95, 2092 (1991).

[62]S. W. Barton, B. N. Thomas, E. B. Flom, S. A. Rice, B. Lin, J. B. Peng, J. B. Ketterson and P. Dutta, J. Chem. Phys. 89, 2257 (1988)

[63]M. Lundquist, Chem. Scr. 1, 195 (1971).

[64]V. M. Kaganer, M. A. Osipov, and I. R. Peterson, J. Chem. Phys. 98, 3512 (1993).

[65]Z. Cai and S. A. Rice, Faraday Dicuss. Chem. Soc. 89, 211 (1990).

[66]Z. Cai and S. A. Rice, J. Chem. Phys. 96, 6229 (1992).

[67]C. M. Knobler and R. C. Desai, Rev. Phys. Chem. 43, 207 (1992).

[68]J. Harris and S. A. Rice, J. Chem. Phys. 88, 1298 (1988).

[69]Z. Cai and S. A. Rice, J. Chem. Phys. 90, 6716 (1989).

[70]S. Shin and S. A. Rice, J. Chem. Phys. 93, 5247 (1990).

[71]S. Shin, N. Collazo, and S. A. Rice, J. Chem. Phys. 96, 1352 (1992).

[72]J. Gao, N. Collazo, and S. A. Rice, J. Chem. Phys. 99, 7020 (1993).

[73]S. Shin and S. A. Rice, Langmuir 10, 262 (1994).

[74]S. Karaborni, Langmuir 9, 1334 (1993).

[75]M. Scheringer, R. Hilfer, and K. Binder, J. Chem. Phys. 96, 2269 (1991).

[76]J. P. Bareman and M. L. Klein, J. Phys. Chem. 94, 5202 (1990).

[77]J. Hautman and M. L. Klein, J. Chem. Phys. 91, 4994 (1989).

[78]J. Hautman and M. L. Klein, J. Chem. Phys. 93, 7483 (1990).

[79]J. Hautman, J. P. Bareman, and M. L. Klein, J. Chem. Soc. Faraday Trans. 87, 2031 (1991).

[80]J. I. Siepmann and I. R. McDonald, Langmuir 9, 2351 (1993).

[81]J. I. Siepmann and I. R. McDonald, Molecular Physics 79, 457 (1993).

[82]J. I. Siepmann and I. R. McDonald, Molecular Physics 75, 255 (1992).

[83]M. P. Allen and D. J. Tildesley, *Computer Simulation of Liquids*, Clarendon Press, Oxford., 1987.

[84]D. Frenkel, Molecular Physics 60, 1 (1987).

[85]G. P. Crawford, R. Stannarius, and J. W. Doane, Physical Review A 44, 2558 (1991).

[86]A. M. Somoza and R. C. Desai, J. Phys. Chem. 96, 1401 (1992).

[87]C. A. Alves, E. L. Smith, and M. D. Porter, J. Am. Chem. Soc. **114**, 1222 (1992).

[88]N. Camillone III, C. E. D. Chidsey, P. Eisenberger, P. Fenter, J. Li, K. S. Liang, G. Y. Liu and G. Scoles, J. Chem. Phys. 99, 744 (1993).

[89]R. J. Baxter, *Exactly Solved Models in Statistical Mechanics*, Academic Press, New York., 1982.

[90]G. N. Hassold and E. A. Holm, Computer in Physics 7, 97 (1993).

[91]D. Kandel, E. Domany, D. Ron, A. Brandt, and J. E. Loh, Physical Review Letters 60, 1591 (1988).

[92]E. P. Stroll, J. Phys.: Condens. Matter 1, 6959 (1989).

[93]R. G. Nuzzo, L. H. Dubois, and D. L. Allara, J. Am. Chem. Soc. 112, 558 (1990).

[94]M. A. Bryant and J. E. Pemberton, J. Am. Chem. Soc. 113, 8284 (1991).

[95]M. A. Bryant and J. E. Pemberton, J. Am. Chem. Soc. 113, 3629 (1991).

[96]C. A. Alves and M. D. Porter, Langmuir 9, 3507 (1993).

[97]M. M. Walczak, C. Chung, S. M. Stole, C. A. Widrig, and M. D. Porter, J. Am. Chem. Soc. 113, 2370 (1991).

[98]J. T. Young, F. J. Boerio, and K. M. Jackson, J. Adhes. , in press.

[99]M. G. Samant, C. A. Brown, and J. G. G. II, Langmuir 8, 1615 (1992).

[100]C. D. Bain and G. M. Whitesides, J. Am. Chem. Soc. 111, 7164 (1989).

[101]P. E. Laibinis et al., J. Am. Chem. Soc. 113, 7152 (1991).

[102]M. G. Samant, C. A. Brown, and J. G. G. II, Langmuir **7**, 437 (1991).

[103]A. Ulman, J. E. Eilers, and N. Tillman, Langmuir **5**, 1147 (1989).

[104]G. E. Poirier and M. J. Tarlov, Langmuir **10**, 2853 (1994).

[105]H. Sellers, A. Ulman, Y. Shnidman, and J. E. Eilers, J. Am. Chem. Soc. **115**, 9389 (1993).

[106]Please contact TLB for explicit potential parameters if the relevant manuals are not available.

[107]K. F. Lau, H. E. Alper, T. S. Thacher, and T. R. Stouch, J. Phys. Chem. **98**, 8785 (1994).

[108]C. A. Widrig, C. Chung, and M. D. Porter, J. Electroanal. Chem. **310**, 335 (1991).

[109]Z. Zhang and T. L. Beck, in preparation.

[110]M. Bishop and J. H. R. Clarke, J. Chem. Phys. **95**, 540 (1991).

[111]P. Lautenschläger and J. Brickmann, Macromolecules **24**, 1284 (1991).

[112]E. Sabatani, J. Cohen-Boulakia, M. Bruening, and I. Rubinstein, Langmuir **9**, 2974 (1993).